# FREQUENCY DOMAIN ANALYSIS OF
# THE ULTRAWIDEBAND RADIOWAVE PROPAGATION CHANNEL

by

NI XIN

B.A.Sc., The University of British Columbia, 2004

A THESIS SUBMITTED IN PARTIAL FULFILMENT OF
THE REQUIREMENTS FOR THE DEGREE OF
MASTER OF APPLIED SCIENCE

in

THE FACULTY OF GRADUATE STUDIES
(Electrical and Computer Engineering)

THE UNIVERSITY OF BRITISH COLUMBIA

October 2007

# Abstract

The CM 1-8 channel impulse response (CIR) models developed by the IEEE 802.15.4a task group are widely used to fairly compare the performance of alternative UWB signaling schemes under representative line-of-sight and non-line-of-sight conditions in four different environments: residential, office, industrial and outdoor. However, with the advent of MB-OFDM and related schemes, channel frequency response (CFR) models are becoming more pertinent. Here, we show how statistical models of the autoregressive frequency domain (AR-FD) model parameters that estimate for CM 1-8 can be used to gain insights concerning the nature of the channels and efficiently simulate the frequency response of the channels. After generating several thousand instances of the channel response, estimating the AR-FD model parameters for each one, then applying the Akaike Information Criterion (AIC) to determine the appropriate model order, we determine the marginal distributions that best describe each of the AR-FD parameters and their mutual correlation for each of the eight scenarios. We find that the model parameters fall into two independent groups: (1) a set of initial condition parameters that are jointly Gaussian and therefore completely described by their means, variances, and mutual correlation coefficients and (2) a set of parameters that describe the amplitude and phase of the autoregressive poles and the variance of the driving noise and that are described by more exotic distributions. As a result, their mutual correlation is most conveniently described by a copula, a statistical method widely used in finance and finding increasing use in engineering. The result allows us to specify both: (1) a set of statistical parameters that define frequency domain versions of CM 1-8 and (2) a frequency domain channel response simulator. Comparison of the distribution of RMS delay spreads associated with the original training data and simulated channel responses shows good agreement. Further, we demonstrate the utility of the AR-FD approach by using it to interpret UWB channel response data collected within an aircraft passenger cabin and by using AR-FD model parameters as features in the comparison and classification of UWB channel responses collected in different environments.

# Table of Contents

# List of Tables

# List of Figures

# Acknowledgments

# Co-Authorship Statement

All the research work was initiated by Dr David. G. Michelson; he has helped greatly on revisions of first manuscript. For the second manuscript, he was the main contributor for acquiring access to the aircraft on BCIT campus. He also provided some useful comments for the third manuscript. The three manuscripts are:

[1] N. Xin and D. G. Michelson, "Frequency Domain Analysis of the Ultrawideband Radiowave Propagation Channel," to be submitted to IEEE Transaction on Wireless Communication

[2] N. Xin and D. G. Michelson, "Frequency Domain Analysis of the Ultrawideband Radiowave Propagation within the Passenger Cabin of a Boeing 737-200 Aircraft," to be submitted to IEEE Transaction on Wireless Communication

[3] N. Xin and D. G. Michelson, "Comparison and Classification of UWB Channel Models in the Frequency Domain," to be submitted to IEEE Transaction on Wireless Communication

# Chapter 1

# Introduction

## 1.1 General Background and Motivation

Since FCC released a ruling about unlicensed use UWB in 3.1-10.6GHz band in Feb 2002, UWB has emerged as the de facto basis for next generation of short range wireless communication technology. The large bandwidth, defined as bandwidth larger than 500MHz or 20% of the carrier frequency, is intended to provide efficient use of scarce radio bandwidth while enabling high speed short range data link and energy efficient sensor network. The strength of UWB radio lies in its advantages of providing i) high data capacity, ii) low probability of intercept and iii) high time resolution. These advantages will be exploited by future generations of Bluetooth personal area network technology with support for high speed data transfer, future generations of ZigBee sensor network technology with support for precise positioning, future generations of the WiMedia standard for high speed peripheral interconnections, and a wireless extension to the Universal Serial Bus(Wireless USB).

Our research presented here is to propose an autoregressive frequency domain channel (AR-FD) modeling technique that can be used to fairly compare alternative UWB signaling schemes from different sources by considering the model and model parameters. Specifically, we have derived the AR-FD model parameters from a vast database of channel impulse responses from a range of environments. The distributions of the AR-FD model parameters and correlations among the parameters are modeled and characterized statistically. On one hand, this AR channel modeling technique can be extended to characterize channels in unfamiliar environment, like aircraft. On the other hand, the proposed model parameters can be used as feature sets of UWB channel classifier which recognizes or compares empirical UWB channel to existing channel

models. In what follows, we provide general background and motivation for the specific research work reported.

## 1.1.1 Autoregressive Frequency Domain Channel Model

Many proposals for UWB channel models have been made since FCC released a ruling about UWB unlicensed use in 2002. Some contributors are interested in different characteristics of channels that might arise UWB applications, such as cable replacement in home and offices. Others might be focused on a complete statistical description of large and small propagation characteristics in particular environment [1]. Fair comparison of alternative UWB signaling schemes designed for use in different applications requires a statistical channel model that fairly represents channel conditions in typical environments.

IEEE 802.15.3a task group were formed to develop standards for high data rate wireless personal area network (PAN). The subgroup identified a set of criteria that fairly compares channel models in typical indoor scenarios, like office and residential environment. The model adopted by the 3a task group was the "classic S-V" time domain model [5] which captures the tendency of multipath components to form clusters. This model appears to be a good fit for channel measurements; however, it has several limitations: i) the range considered was less than 10 meters, limiting the usability of the model ii) extraction of the cluster parameter in the S-V model was somewhat ambiguous. In particular, from the system design perspective whether to consider power delay profile (PDP) as a superposition of several closely spaced clusters or as a single cluster is arbitrary [4].

The 4a task group extended the standard channel models to some environments and applications which 3a did not cover or envision. The resulting model is a "mixed S-V" model with parameters defined for residential, office, industrial and outdoor (farm) environment in the 3-10GHz band [3]. The application focused by 4a group is low data

rate and geolocation capable sensor network. Like 3a, 4a model is based on extensive measurement campaigns, except for outdoor environment (which based on simulation only). Even though several improvements have been made from 3a standard model, 4a has limitations of its own: i) some underlying measurements did not cover the 3-10GHz band, restricting the validity range of the models, ii) more parameters are used to model the shape of PDPs, adding complexity of existing model .

Overall, 3a and 4a's channel impulse responses (CIRs) models are the preferred channel representations for assessing the performance of signaling scheme such as direct sequence ultrawideband(DS-UWB). However with the advent of multi-band orthogonal frequency division multiplexing (MB-OFDM) and related schemes, channel frequency responses (CFR) models are becoming more pertinent. Moreover, CFR model offer three significant advantages over CIR models: (1) compared to CIR models, CFR models are often much simpler and can often be characterized in a more compact form [12]. (2) Most UWB measurements are collected as channel frequency responses using a vector network analyzer (VNA). Estimating CFR model parameters directly from CFR data avoids expensive operations such as the inverse Fourier transform and deconvolution. (3) CFR model does not require subjective input, namely number of clusters.

CFR modeling has been done over the years [8]-[10], some do not have a complete statistical description of the channel model; others used too many parameters. Howard and Pahlavan pioneered statistical wide band FD modeling in office channel using autoregressive approach in the late 80s. They showed that characterizing wideband channel using AR approach was easy to set up. Moreover, fewer parameters are used in the AR than conventional time domain models. Ghassemzadeh *et al.* further proved AR applicability in the UWB context in residential environment. In his work, 30,000 power delay profiles were collected in 23 homes to derive the FD channel parameters. The common drawbacks of Howard and Ghassemzadeh's work are: (1) the modeling is done for a specific environment; thus, how autoregressive model parameters vary from one environment to the other is unknown. (2) For channel simulation, Howard proposed three different ways of generating frequency domain channel parameters, but eventually he

chose to stick to a simple assumption that the autoregressive poles are independent and Gaussian distributed. In Ghassemzadeh's work, he showed that the AR poles envelopes and phases were strongly correlated but correlations among other model parameters (i.e. correlation between observation noise and AR poles) were not fully exploited.

Motivated by the constraints of previous CIR and CFR models, we propose to study all 4a documented channel models using AR-FD methods, include

- CM1 Residential LOS
- CM2 Residential NLOS
- CM3 Office LOS
- CM4 Office NLOS
- CM5 Outdoor LOS
- CM6 Outdoor NLOS
- CM7 Industrial LOS
- CM8 Industrial NLOS

Through the study of standard channel models, we want to determine the order of the AR-FD model most appropriate to each channel model, to use distribution of the poles from AR-FD model to interpret physical significance and diversity of poles in each case, to determine statistical distributions that best describes AR-FD model parameters and to assess the suitability of the AR-FD approach in each of the eight cases by comparing channel condition parameters like RMS delay spread.

## 1.1.2  Aircraft Frequency Domain Channel Model

Most UWB channel modeling efforts have emphasized on characterizing time domain model parameters for conventional indoor environments, including residential, office, industrial and outdoor [1]-[7]. Aircrafts seem to be the last remaining environment where mobile communications and Internet access are not available. Some comparisons can be drawn between aircraft channel and existing underground subway channel model [15] because they are both tunnel-like. However, the physical dimension, scattering environment and presence of human activity make aircraft environment quite different from any of the previous modeled environments. A variety of studies have been conducted on wireless communication and multimedia data networks inside aircraft cabins. Previous studies [16]-[19] have emphasized i) field trials for passenger-carried electronic devices (i.e. cell phones), wireless LAN, and Bluetooth wireless technology ii) using simulation tools such as shooting and bouncing ray method to predict power propagation within aircraft cabin or using commercial off-the-shelf simulation tools "Site Planner" and "Wireless Insite" to emulate an aircraft cabin propagation environment in the absence of internal components (i.e. windows and overhead cargo bins) iii) measurement of RF coverage using client devices. In one instance, a measurement based in-flight channel characterization was done in the UMTS downlink band [14]. Overall, studies of measurement based channel characterization on aircraft cabin are scarce.

With an increase demand for in-flight services that provide passenger entertainment or business experience on board, it is very important to have a valid in-cabin channel characterization. In this work, we propose using the AR-FD technique to analyze aircraft channel in the 3.1 to 10.6 GHz. We derive the AR-FD channel parameters. The model can be used by system deployment of multimedia streaming or sensor network onboard. We use the AR-FD parameters to compare characteristics of aircraft channels with those

5

of conventional channels. Finally, we present accurate analysis of the channel condition parameters including RMS delay spread and coherence bandwidth.

## 1.1.3  AR-FD based Channel Classifier

A rich set of measurement data is often desirable from a modeling perspective; however, size and variety of database pose some serious challenges. The existing mixed S-V model incorporates detailed structures of multipath components (MPCs) as a function of time delay. To complete describe a new channel (from new environment or from new experiment setup) statistically, system designers need to characterize a set of time domain parameters, namely inter cluster arrival rate, ray arrival rate, cluster decay factor and etc, of over 10 parameters. Regardless that it takes considerable time and efforts to characterize S-V model parameters, they do not vary significantly from one environment to the other. Thus, there is no easy way to comment on different channel conditions based on the mixed S-V model parameters.

Some efforts have been devoted to use $4^{th}$ order statistics kurtosis, mean excess delay and rms-delay spread to identify NLOS channels from aggregated UWB channels for localization applications [20]. The method only gives us information about existence of obstacles between transmitter and receiver. No comparison can be drawn between new channel and existing channel models. In particular, whether it makes sense to add newly collected database to existing channel or to a new model remains unanswered.

Autoregressive model parameters is widely used as features for characterizing different classes of music, EEG signals and sensor array processing . In this work, we show that using statistically characterized AR-FD model parameters can classify UWB channel into different classes. The classes are environment dependent. This estimation and classification of channel parameters belonging to a particular modeled environment will allow better understanding of channel propagation in that particular environment. This work will also help system designers to make a fair comparison of channels in

6

extreme or new environment, such as aircraft cabins or underground mines, with conventional channels.

## 1.2 Thesis Outline

The thesis is organized as follows. Chapter 2 proposes autoregressive frequency domain equivalent model for all 4a documented environments and chapter 3 demonstrates AR-FD model's applicability in aircraft channels with detail analysis of physical significance of channel parameters. In chapter 4, we propose an AR-FD parameter based classifier for distinguishing UWB channels from different environment. Finally, chapter 5 concludes the work and outlines future research interests and challenges.

# Bibliography

[1]  A. F. Molisch, J. R. Foerster, and M. Pendergrass "Channel Models for Ultrawideband Personal Area Networks," *IEEE Wireless Communication*, Dec 2003, pp. 11-21

[2]  J. Foerster, V. Somayazulu, S. Roy, E. Green, K. Tinsley, C. Brabenac, D. Leeper, and M. Ho, IEEE802.15-03/109r1, March 2003

[3]  A.F. Molisch, K. Balakrishnan, D. Cassioli, CC. Chong, S. Emanmi, A. Fort, F. Karedal, J. Kunisch, H. Schantz, U. Schuster, and K. Siwiak., "IEEE 802.15.4a channel model - final report," *IEEE P802. 15-04/662r0-SG4a*

[4]  A. F. Molisch, "Ultrawideband Propagation Channels-Theory, Measurement, and Modeling," *IEEE Transactions on Vehicular Technology*, vol. 54, no.5, pp 1528-1545, September 2005

[5]  A. A. M. Saleh, and R.A. Valenzuela, "Statistical Model for Indoor Multipath Propagation," *IEEE Journal on Selected Areas in Communication*, vol. 5, no. 2, pp. 128-137, February 1987

[6]  D. Cassioli, M. Z. Win, and A. F. Molisch," The UWB indoor channel: From statistical model to simulations," *IEEE Journal on Selected Areas of Communications*, vol. 20, no. 6, pp. 1247-1257, Aug, 2002

[7]  W. Ciccognani, A. Durantini and D. Cassioli, "Time Domain Propagation Measurements of the UWB Indoor Channel Using PN-Sequence in the FCC-Compliant Band 3.6-6GHz," *IEEE Transactions on Antennas and Propagation*, vol. 53, no. 4, April 2005.

[8]  A. Alvarez, G. Valera, M. Lobeira, R. Torres, and J. L. Garcia, " New Channel Impulse Response Model for UWB Indoor System Simulations," *IEEE Vehicular Technology Conference*, vol. 1. 22-25, pp.1-5, Spring 2003

[9]  J. Kunisch and J. Pamp, " Measurement Results and Modeling Aspects for the UWB Radio Channel," *IEEE Conference on Ultra Wideband Systems and Technologies*, pp.19-23, 2002

[10] G. Morrison, and M. Fattouche, "Super-Resolution Modeling of the Indoor Radio Propagation Channel," *IEEE Transactions on Vehicular Technology*, vol.47, no. 2, pp. 649-657, May 1998

[11] S. J. Howard, and K. Pahlavan, "Autoregressive Modeling of Wide-Band Indoor Propagation," *IEEE Transactions on Communications*, vol. 40, no. 9, pp. 1540-1552, Sep. 1992

[12] S. S. Ghassemzadeh, R. Jana, C.W. Rice, W. Turin, and V. Tarokh, "Measurement and Modeling of an Ultra-Wide Bandwidth Indoor Channel," *IEEE Transactions on Communications*, vol. 52, no. 10, pp. 1786-1796, Oct. 2004

[13] G. J. M. Jassen, P. A. Stigter and R. Prasad, "Wideband Indoor Channel Measurements and BER Analysis of Frequency Selective Multipath Channels at 2.4, 4.75 and 11.5GHz.," *IEEE Transactions on Communications*, VOL. 44, NO. 10, 1272-1288, Oct.1996

[14] M. A. Do and S. Sun, " Statistical Modeling of Broadband Wireless LAN Channels at 18 GHz Using Directive Antennas," *International Journal of Wireless Information Networks*, VOL. 4, No. 1, 1997

[15] M. Lienard, P. Degauque, j. Baudet and D. Degardin, "Investigation on MIMO Channels in Subway Tunnels," *IEEE Journal on Selected Areas in Communications*, vol. 21, no. 3, April 2003, pp. 332-339

[16] C.P. Niebla, "Topology and Capacity Planning for Wireless Heterogeneous Networks in Aircraft Cabins," 2005 IEEE PRMRC 2005, vol. 3, pp. 2088-2092, Sep. 2005

[17] M, Youssef, and L, Vahala, "Effects of Passengers and Internal Components on Electromagnetic Propagation Prediction inside Boeing Aircrafts," IEEE APS 2006, pp. 2161-2164, Jul. 2006

[18] G, Hankins, L Vahala and J. H. Beggs, "Electromagnetic Propagation Prediction Inside Aircraft Cabins," IEEE APS 2004, pp. 2227-2230, Jun. 2004

[19] N. R. Diaz, "Wideband Channel Characterization for Wireless Communications inside a Short Haul Aircraft," *IEEE VTC,* 2004, Spring, VOL. 1, pp. 223-228

[20] I. Guvenc, C. Chong, and F. Watanabe, "NLOS Identification and Mitigation for UWB Localization Systems," WCNC 2007 Proceedings, Hongkong, March

# Chapter 2

# Frequency Domain Analysis of the IEEE 802.15.4a UWB Channel Models

## 2.1 Introduction

[1]In just over four years, ultra wideband (UWB) signaling has emerged as the *de facto* basis for the next generation of short range wireless communications technology including high speed short range data links and energy efficient sensor networks. The extremely wide bandwidth of UWB signals offers several advantages including: (1) high data capacity, (2) low probability of intercept by and interference to conventional wide band receivers and (3) high temporal resolution. These advantages will be exploited by the WiMedia radio platform for high speed peripheral interconnection, future generations of Bluetooth personal area network technology with support for high speed data transfer, a UWB-based wireless extension to the Universal Serial Bus (Wireless USB) and future generations of ZigBee sensor network technology with support for precise positioning.

Fair comparison of alternative UWB signaling schemes designed for use in such applications requires a set of statistical channel models that fairly represent channel conditions in typical environments. The standard channel models for residential and office environments that were developed by the IEEE 802.15.3a task group and extended to industrial and outdoor environments by IEEE 802.15.4a are based upon statistical analysis of a vast database of channel impulse responses (CIRs) collected by a large group of researchers from industry and academia [1][2]. Eight CIR models, designated CM 1-8, capture the response of line-of-sight and non-line-of-sight channels in each of the four environments. Because the bandwidth of the UWB channel is so wide, the time

---

resolution of UWB CIRs is extremely fine. As a result, a great deal of structure, including the tendency for multipath components (MPCs) to form clusters in the manner first observed by Saleh and Valenzuela [3], can be observed in a typical UWB CIR. Estimation of the statistical distributions of the many parameters that define CIR-based UWB channel models is fairly difficult and requires considerable time and effort.

Channel impulse responses are the preferred channel representation for assessing the performance of signaling schemes such as direct sequence ultra-wideband (DS-UWB). However, with the advent of multi-band orthogonal frequency division multiplexing (MB-OFDM) and related schemes, channel frequency response (CFR) models are becoming more pertinent. An indirect approach to CFR modelling involves taking the Fourier transform of responses generated from a CIR-based channel model. However, "native" CFR models that are derived directly from measured frequency response data offer two potential advantages over those derived from CIR models. First, compared to CIR models, native CFR models are often much simpler and can often be characterized in a more compact form with fewer parameters. Second, most researchers collect UWB channel response data in the form of complex frequency responses using a vector network analyzer-based measurement system. Estimating CFR model parameters directly from CFR data avoids the need to convert the response to a CIR and apply a host of other processing steps with their attendant complications and subjectivity.

Various methods for realizing wide-band and UWB frequency domain channel models have been proposed in recent years including techniques based upon sampled finite-impulse response filters, minimum-norm estimators and autoregressive frequency domain (AR-FD) methods [4][5][6]. Previous work in [5] and [6] has focused on estimation of the AR-FD model parameters and investigation of some of their properties. Here, we take the next step and demonstrate how one can develop complete statistical models of the AR-FD model parameters and use them to represent and, importantly, simulate the frequency response of a UWB channel. For convenience, we have demonstrated the technique using the CM 1-8 channel models but our method is applicable to any set of frequency domain channel response data that one might collect in a given environment.

We take the following approach. First, in the manner of previous AR-FD channel modeling studies, we generate many instances of the channel response, estimate the AR-FD model parameters for each one, and then apply the Akaike Information Criterion (AIC) to determine the appropriate model order. We then determine the precise form of both the marginal distributions that best describe each of the AR-FD parameters and their mutual correlation. The result allows us to specify both: (1) a set of statistical parameters for the frequency-domain versions of CM 1-8 (that we refer to as CFR 1-8) and (2) a simulator that allows us to generate multiple sets of the AR-FD model parameters that we can apply to an AR-FD frequency response simulator. Finally, we confirm the fidelity of the CFR 1-8 models by generating thousands of frequency responses, converting each one to a channel impulse response, and then comparing the corresponding RMS delay spread distributions with those of the CM 1-8 CIRs upon which our model is based.

The remainder of this paper is organized as follows: In Section 2.2, we review the essential aspects of the AR-FD channel model. In Section 2.3, we use AR-FD techniques to analyze the CM 1-8 channel responses and determine the model order that best represents each of the eight scenarios. In Section 2.4, we present expressions for the marginal distributions of the AR-FD model parameters applicable to each scenario and our estimates for their mutual correlation in each case. In Section 2.5, we show how to generate the AR-FD model parameters applicable to a given scenario given their marginal and joint distributions and assess the fidelity of the results. In Section 2.6, we summarize our major contributions.

## 2.2 Essential Aspects of the AR-FD Channel Model

### 2.2.1 Form of the Model

Autoregressive methods allow us to express a complex frequency response of span $\Delta f$ that has been sampled at intervals $f_s$ at a location $x$ and time $t$ as

$$\widehat{H}(f_k, t; x) + \sum_{i=1}^{p} a_i \widehat{H}(f_{k-i}, t; x) = U(f_k, t; x) \qquad (2.1)$$

where $\widehat{H}(f_k, t; x)$ is the *kth* sample of the complex frequency response at location x, $a_i$ is the AR coefficient of the *(k-i)th* frequency taps and $U(f_k, t; x)$ is the white Gaussian noise added to the *kth* sample (as in Figure 2.1).
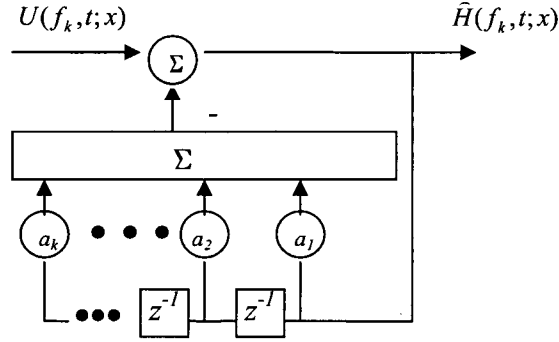


Figure 2.1 *k*th order AR Filter

Application of the autoregressive frequency domain (AR-FD) modeling approach is based upon the following assumptions: (1) the mean value of the response is flat across the span, (2) the sampling interval is sufficiently fine that the amplitude and phase of a given frequency component is correlated with those of the frequency components that precede it and (3) the coherence bandwidth (and the frequency autocorrelation function) remains constant across the entire frequency span.

The AR-FD approach allows us to synthesize a complex channel frequency response by representing the amplitude and phase of a given frequency component as the output of a filter of order $k$ that combines the weighted sum of the $k$ frequency components that immediately precede it with a white complex Gaussian random variable of specified variance, as depicted in Figure 2.2.
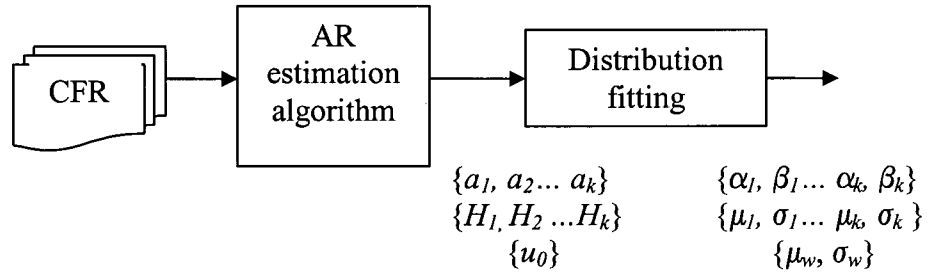
a) Parameter characterization
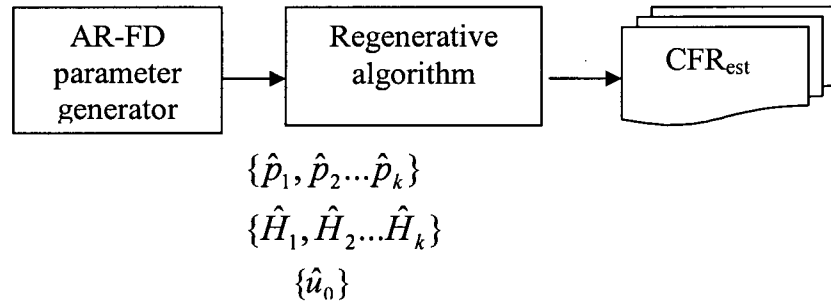


b) Channel emulation

Figure 2.2 AR-FD analysis and synthesis

The transfer function of such a filter $G(z)$ is given by

$$G(z) = \frac{1}{1 + \sum_{i=1}^{k} a_i z^{-i}}$$

(2.2)

or in terms of the poles of the response $\{p_i\}$, as

$$G(z) = \frac{1}{\prod_{i=1}^{k} (1 - p_i z^{-1})}$$

(2.3)

The two representations are equivalent, but the poles have greater physical significance because they can be interpreted as an indication of significant cluster arrivals.

An AR-FD channel model of order $k$ has $2k+1$ parameters: (1) the amplitude and phase of the $k$ poles (or the $k$ AR coefficients), (2) the real and imaginary parts of the $k$ initial conditions (*i.e.,* the values of the first $k$ components of the complex frequency response) and (3) the variance of the complex white Gaussian noise that drives the filter $G(z)$. The values of the AR coefficients and the variance of the driving noise are estimated from sample channel frequency responses or training data using the Yule-Walker equations. If the variance of the driving noise is otherwise set too high, the AR-FD-generated CFR will exhibit sharper peaks than the true CFR [8].

The requirement that the mean of the frequency response be flat with frequency is a limitation that must be addressed when AR-FD techniques are used to model the frequency response of UWB channels. In practice, the frequency dependence of path loss,

$$L(f) \propto f^{2\kappa} , \tag{2.4}$$

where $\kappa$ is the frequency dependent path loss exponent, must be removed before the AR-FD parameters are estimated and re-applied to UWB frequency responses that have been generated by an AR-FD-based frequency response simulator.

## 2.2.2 Estimation of the AR Model Parameters for CM 1-8

Our approach to estimation of the parameters of the AR-FD channel models that correspond to channel models CM 1-8 involves three steps. First, we used a simulator developed by the IEEE 802.15.4a channel modeling committee to generate 8320 independent realizations of the CIR for each of the eight scenarios captured by the models, and then we converted each of them to CFRs by applying a Fourier transform. Next, we used the Yule-Walker equations to estimate the AR coefficients and the variance of the driving noise for model orders of 1 through 7. Together with the initial

conditions, *i.e.*, independent estimates of the first $k$ frequency components of the CFR, they comprise the complete set of AR-FD model parameters that characterize the channel response. Finally, we applied the Akaike Information Criterion (AIC) to select the most appropriate model order for each scenario, as described in the next section.

The frequency sampling interval $f_s$ between the components of the CFR is determined by the length $\tau_{max}$ of the CIR. Ideally, $f_s$ would be identical for all cases considered but, in practice, this is generally not the case. Due to an idiosyncrasy of the IEEE 802.15.4a CIR generator, $\tau_{max}$ varies between different instances of the same scenario so we need to either zero pad or truncate the CIRs as required so that all of the CIRs have the same length. Here, we use the zero pad approach in order to preserve the integrity of the CIRs. Second, the $\tau_{max}$ of the CM 1-8 models vary over an order of magnitude between scenarios so it's impractical to use the same interval $f_s$ for all CIRs. This affects the scaling of the phase angle of the filter poles and must be accounted for when interpreting plots of the pole locations in the $z$-plane. The values of $\tau_{max}$ that we used for residential, office, outdoor and industrial environments are given in Table 2.1.

Table 2.1 Typical Maximum Excess Delays for CM1 to CM8

| $\tau_{max}$ (ns) | Residential | Office | Outdoor | Industrial |
|---|---|---|---|---|
| LOS | 331 | 994 | 657 | 212 |
| NLOS | 276 | 165 | 1093 | 841 |

## 2.3 AR-FD Model Parameters

## 2.3.1 Model Order Selection for CM 1-8

Selection of the appropriate model order represents a tradeoff between accuracy and complexity. The best value is not generally known *a priori* and must be determined by using the Akaike Information Criterion (AIC) to compare the frequency autocorrelation

function associated with the original data to the simplified representation associated with a given model order [7].

In [6], it was found that a second order AR process was the best choice for modeling the UWB channel response in residential environments. Applying the AIC criterion to select the appropriate model order for the other environments considered by IEEE 802.15.4a involves minimizing the information theoretic function

$$AIC = \log(V) + \frac{2k}{N} \tag{2.5}$$

with
$$V = \det(\frac{1}{N} \sum_{1}^{N} \varepsilon(f, a_N(k)) \varepsilon(f, a_N(k))^T) \tag{2.6}$$

and $V$ is the variance of prediction error, $k$ is the order of the process, $N$ is the number of data points in the CFR, and $\epsilon$ is the residual error between the estimated and actual autoregressive coefficients $a_N$ for a $k$ order process The term $2k/N$ penalizes the use of additional AR coefficients if they do not substantially reduce the prediction error.

The manner in which AIC values decrease as the model order increases for the eight scenarios captured by CM 1-8 is listed in Table 2.2 and depicted in Figure 2.3. In most cases, we find that channels in LOS environments tend to be much more accurately represented than those in the corresponding NLOS environments. However, while the difference is most striking in the office environment, and is less so in the residential and industrial environments, it is negligible for outdoor environments.

Table 2.2 AIC in Different Environments

| AR Order | Residential LOS | Residential NLOS | Office LOS | Office NLOS | Outdoor LOS | Outdoor NLOS | Industry LOS | Industry NLOS |
|---|---|---|---|---|---|---|---|---|
| 1st | -10.2074 | -9.6111 | -14.6264 | -8.8150 | -11.3972 | -10.9579 | -10.7101 | -9.9612 |
| 2nd | -11.4863 | -10.5161 | -16.7810 | -9.5682 | -13.0439 | -12.4160 | -12.2085 | -10.4001 |
| 3rd | -12.0984 | -10.9927 | -16.9462 | -9.9748 | -13.9809 | -13.5598 | -12.6770 | -10.6170 |
| 4th | -12.3437 | -11.2666 | -17.0323 | -10.2202 | -14.3278 | -14.2030 | -12.8308 | -10.7427 |
| 5th | -12.4696 | -11.4369 | -17.0878 | -10.3807 | -14.4785 | -14.5245 | -12.9089 | -10.8234 |
| 6th | -12.5491 | -11.5454 | -17.1247 | -10.4849 | -14.5784 | -14.7073 | -12.9575 | -10.8790 |
| 7th | -12.6017 | -11.6161 | -17.1505 | -10.5494 | -14.5676 | -14.8230 | -12.9910 | -10.9194 |

The relationship between prediction error and the model order is depicted in Figure 2.3. As expected, the prediction error diminishes with increasing model order, but the order required to minimize the prediction error is highest for outdoor environments, less so for residential, office NLOS and industrial LOS environments, and least for industrial NLOS and office LOS environments. In all cases, the prediction error is less than $10^{-4}$ as long as the model order is at least 2. For the remainder of this paper, we restrict ourselves to using second order AR-FD models to represent all eight CM models.
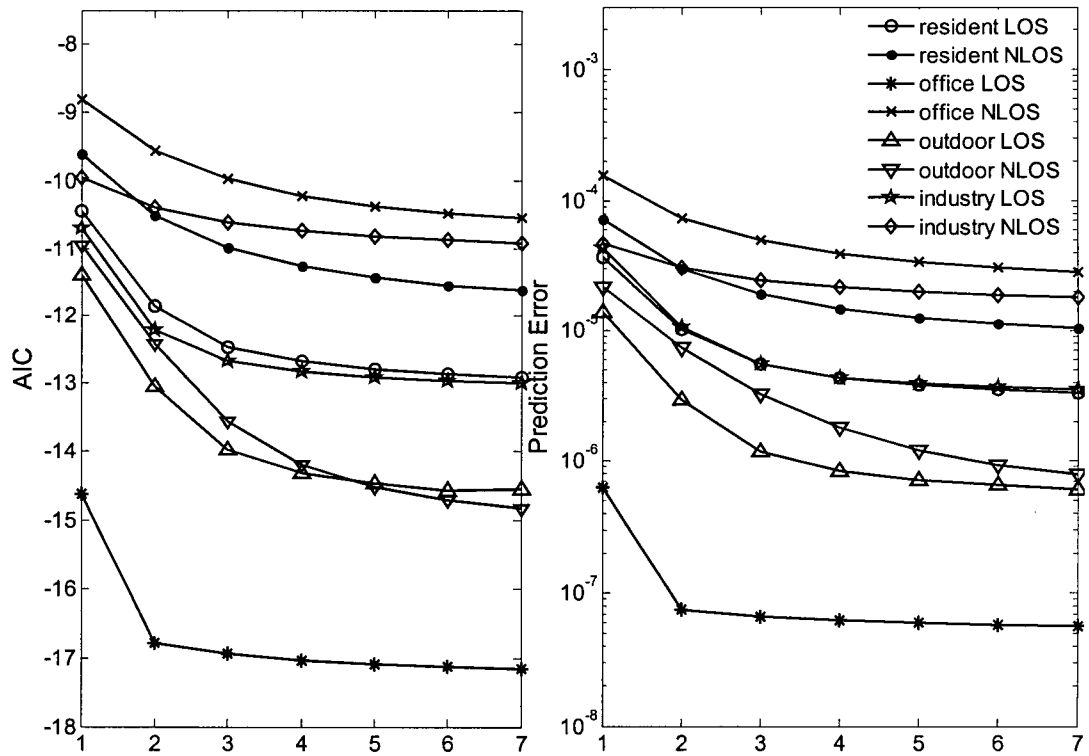


Figure 2.3 AIC and Prediction Error vs AR Order

## 2.3.2 Pole location, dispersion and physical interpretation

The locations of the autoregressive poles accounts for four of the nine parameters of a second-order AR-FD model. The eight autoregressive pole distributions plotted in Figure 2.4 and Figure 2.5 correspond to the LOS and NLOS scenarios in residential, office, outdoor, and industrial environments, *i.e.,* CM 1-8. As noted earlier, each is each based upon 8320 simulated UWB channel impulse responses that have been transformed to the frequency domain.

If the poles are close to the unit circle, the corresponding clusters carry significant energy. If the poles are close to the origin, the corresponding clusters carry lower energies. The positive real axis corresponds to a time delay of zero; from there, time delay increases clockwise. By the bilinear transform, the angle of a pole is

$$\arg(Z) = \Omega_s T = 2\pi f_s T \tag{2.7}$$

where $f_s$ is the interval between adjacent frequency components. The time delay at which the pole appears can be obtained from the pole phase

$$\tau_s = \frac{-\angle p}{\Omega_s} = \frac{-\angle p}{2\pi f_s} \tag{2.8}$$

Because $\tau_{max} = 1/f_s$ is different for each of the eight CM models, as explained in the previous section, the angular distribution of the poles must be interpreted carefully.

The results given in Figure 2.4 show that the pole distributions for the CM 1-4 models (residential and office environments) are similar to those observed by Howard and Pahlavan [4] and Ghassemzadeh *et al.* [6]. For residential LOS channels, the first pole magnitude falls in the range 0.76 and 0.99 while the magnitude of the second pole falls in the range of 0.32 to 0.97. For the office LOS environment, the magnitude of the first pole is usually greater than 0.93 and the magnitude of the second pole falls between 0.36 and 0.99. For the office NLOS scenario, the variances of the first and second poles are very similar. Otherwise, the second poles tend to have a larger variance than the first poles

with the difference being more apparent in the LOS case. This suggests a possible method for distinguishing LOS and NLOS channels based upon features derived from CFR data.

The results given in Figure 2.5 show the pole distributions for the CM 5-8 models (outdoor and industrial environments). In the outdoor environment, we observe similar pole distributions as in the indoor environment. The poles for the outdoor NLOS environment are mostly concentrated in the third quadrant. These poles, which occupy one third of the unit circle, are the result of scattering from distant objects. The distribution of the AR poles for the CM 8 Industrial NLOS model is very much narrower than that of the other seven models. The difference is so striking that it suggests that CM 8 may be based on too limited a sample of CIR data or that the data used may have been collected at too few locations. Further investigation of the Industrial NLOS scenario is therefore warranted.
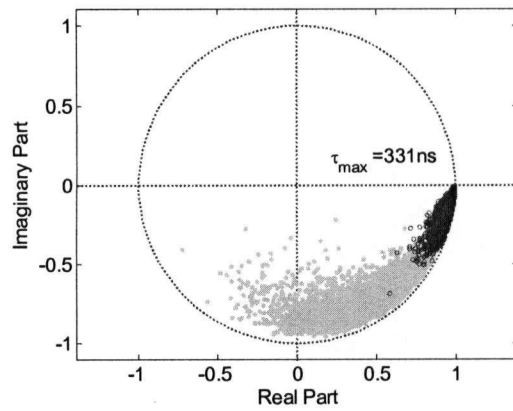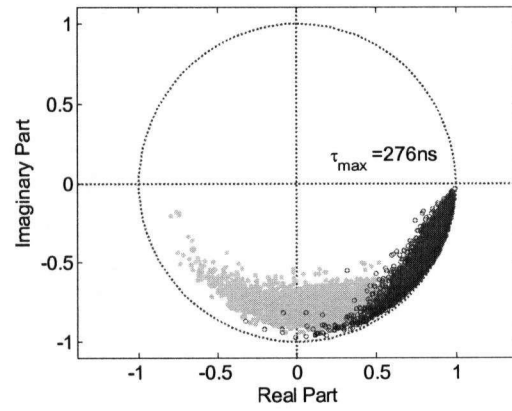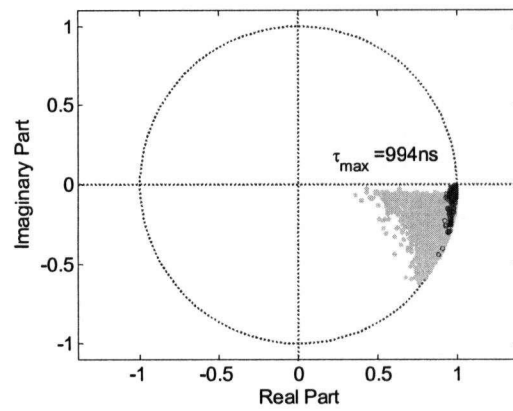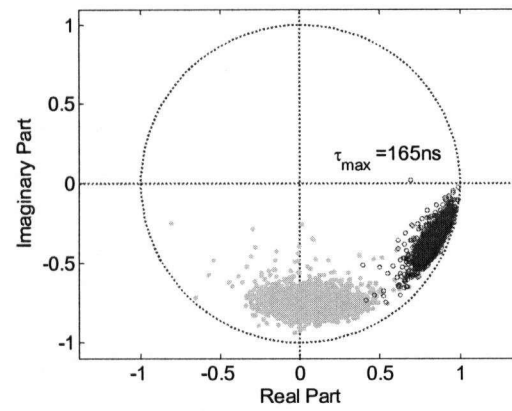
Figure 2.4. Distribution of AR-FD pole locations for LOS and NLOS cases of the residential and office environments. (Dark points – first pole locations, light point – second pole locations.)

a) CM 5 Outdoor LOS

b) CM 6 Outdoor NLOS

c) CM 7 Industrial LOS

d) CM 8 Industrial NLOS

Figure 2.5 Distribution of AR-FD pole locations for LOS and NLOS cases of the outdoor and industrial environments.

## 2.4 AR-FD Model Parameters Distribution

With thousands of instances of the AR-FD model parameters for each of the CM models on hand, our next step was to determine: (1) the marginal distributions that best describe each of the parameters and (2) the mutual correlations between the parameters. In each of the 72 cases (nine parameters times eight scenarios), we began by determining whether a given parameter in a given scenario followed a normal distribution. If it didn't, we conducted further tests to determine whether it followed a more exotic distribution. In each case, we used the Kolmogorov-Smirnov test to assess goodness-of-fit at a significance level of 0.01.AR-FD Poles.

## 2.4.1 Marginal Distribution of the AR-FD Poles

The results of our efforts to characterize the marginal distributions of the magnitude and phase of the autoregressive poles are presented in Table2.3. In all cases, we require two parameters to specify each of the distributions. Of the sixteen first and second pole magnitude distributions considered, two followed a normal distribution with a density function given by

$$f(x \mid \mu, \sigma) = \frac{1}{\sqrt{2\pi}\sigma} e^{-\frac{(x-\mu)^2}{2\sigma^2}} \tag{2.9}$$

where $\mu$ and $\sigma > 0$ are the mean and standard deviation, respectively. Two followed a Weibull distribution with a density function given by

$$f(x \mid k, \lambda) = \frac{k}{\lambda} \left( \frac{x}{\lambda} \right)^{k-1} e^{-(x/\lambda)^k} \tag{2.10}$$

where x ≥ 0 and $k > 0$ and $\lambda > 0$ are the scale and shape parameters, respectively. Five followed the log-Weibull distribution with a density function given by

$$f(|p_1| \mid \alpha, \beta) = \beta^{-1} \exp\left\{\frac{(\alpha - |p_1|)}{\beta} - \exp(\frac{(\alpha - |p|_1)}{\beta})\right\} \tag{2.11}$$

where $\alpha$ and $\beta > 0$ are the location and scale parameters respectively. Seven followed a beta distribution with a density function given by

$$f(|p_2| \mid \alpha, \beta) = \frac{(1 - |p_2|)^{\beta - 1} |p_2|^{\alpha - 1}}{B(\alpha, \beta)} \tag{2.12}$$

where $\alpha$ and $\beta$ are the shape factors and

$$B(\alpha, \beta) = \frac{\Gamma(\alpha)\Gamma(\beta)}{\Gamma(\alpha + \beta)} \cdot \tag{2.13}$$

Of the sixteen pole phase distributions considered, four followed a normal distribution, eight followed the log-Weibull distribution and four followed a logistic distribution given by

$$f(x \mid \mu, s) = \frac{1}{4s} \operatorname{sech}^2\left(\frac{x - \mu}{2s}\right) \tag{2.14}$$

where $\mu$ and $s > 0$ are the location and scale parameters, respectively.

24

Table2.3 AR-FD Model Parameters for CFR1 to CFR8

| Environment | Parameter | Distribution | $\alpha$ | $\beta$ |
|---|---|---|---|---|
| Residential | $|p_1|$ | E.V. | 0.97902 | 0.0126811 |
| LOS | $|p_2|$ | E.V. | 0.907689 | 0.0384309 |
|  | ANG($p_1$) | E.V. | -0.112781 | 0.0691762 |
|  | ANG($p_2$) | E.V. | -0.823681 | 0.200563 |
| Residential | $|p_1|$ | E.V. | 0.956557 | 0.0206694 |
| NLOS | $|p_2|$ | Weibull | 0.830912 | 20.1068 |
|  | ANG($p_1$) | E.V. | -0.334411 | 0.162197 |
|  | ANG($p_2$) | Logistic | -1.4209 | 0.143231 |
| Office | $|p_1|$ | Beta | 291.06 | 1.83643 |
| LOS | $|p_2|$ | Beta | 12.0806 | 1.13572 |
|  | ANG($p_1$) | E.V. | -0.0280643 | 0.0103262 |
|  | ANG($p_2$) | Logistic. | -0.198357 | 0.0825399 |
| Office | $|p_1|$ | E.V. | 0.937549 | 0.0187299 |
| NLOS | $|p_2|$ | Weibull | 0.798975 | 20.1621 |
|  | ANG($p_1$) | Logistic | -0.352289 | 0.0465455 |
|  | ANG($p_2$) | Logistic | -1.44995 | 0.0835703 |
| Outdoor | $|p_1|$ | Beta | 110.201 | 2.0347 |
| LOS | $|p_2|$ | E.V. | 0.924297 | 0.0424312 |
|  | ANG($p_1$) | E.V. | -0.080478 | 0.0406996 |
|  | ANG($p_2$) | Normal | -0.899339 | 0.219821 |
| Outdoor | $|p_1|$ | Beta | 34.8605 | 1.53616 |
| NLOS | $|p_2|$ | Beta | 8.07804 | 1.30163 |
|  | ANG($p_1$) | E.V. | -0.394444 | 0.135074 |
|  | ANG($p_2$) | Normal | -1.52237 | 0.467246 |
| Industrial | $|p_1|$ | Beta | 55.9055 | 0.92936 |
| LOS | $|p_2|$ | Beta | 11.7672 | 1.62909 |
|  | ANG($p_1$) | E.V. | -0.0402077 | 0.0348511 |
|  | ANG($p_2$) | E.V. | -1.00777 | 0.455724 |
| Industrial | $|p_1|$ | Normal | 0.883227 | 0.0054326 |
| NLOS | $|p_2|$ | Normal | 0.674853 | 0.0097030 |
|  | ANG($p_1$) | Normal | -0.504287 | 0.0155721 |
|  | ANG($p_2$) | Normal | -1.86243 | 0.0254698 |

## 2.4.2 Marginal Distribution of the Initial Conditions

The real and imaginary parts of the initial conditions for the eight scenarios all follow normal distributions. The mean and variance corresponding to each case are given in Table 2.4. In all cases, the means are two orders of magnitude less than the corresponding standard deviations and are therefore well approximated by zero. For a particular environment, the standard deviations of the real and imaginary parts of the initial conditions are essentially identical. This reduces the number of unique parameters required to specify the marginal distributions of the initial conditions in a given scenario to just one.

Table 2.4 Marginal Distributions of the Initial Conditions

| Scenario | Parameter | $\mu$ | $\sigma$ |
|---|---|---|---|
| Residential LOS | Re$\{H_1\}$ | -3.56e-5 | 5.79e-3 |
| | Im$\{H_1\}$ | 7.58e-5 | 5.79e-3 |
| | Re$\{H_2\}$ | -1.49e-5 | 5.76e-3 |
| | Im$\{H_2\}$ | 2.93e-5 | 5.76e-3 |
| Residential NLOS | Re$\{H_1\}$ | -4.85e-5 | 2.73e-3 |
| | Im$\{H_1\}$ | -1.18e-5 | 2.75e-3 |
| | Re$\{H_2\}$ | -6.48e-5 | 2.71e-3 |
| | Im$\{H_2\}$ | 1.56e-5 | 2.75e-3 |
| Office LOS | Re$\{H_1\}$ | 1.69e-5 | 7.97e-3 |
| | Im$\{H_1\}$ | 6.22e-5 | 7.97e-3 |
| | Re$\{H_2\}$ | 1.55e-5 | 7.97e-3 |
| | Im$\{H_2\}$ | 5.34e-5 | 7.96e-3 |
| Office NLOS | Re$\{H_1\}$ | -1.35e-4 | 1.22e-2 |
| | Im$\{H_1\}$ | 2.49e-4 | 1.23e-2 |
| | Re$\{H_2\}$ | 8.36e-5 | 1.22e-2 |
| | Im$\{H_2\}$ | 2.79e-4 | 1.24e-2 |
| Outdoor LOS | Re$\{H_1\}$ | 2.53e-4 | 9.48e-3 |
| | Im$\{H_1\}$ | 1.51e-4 | 9.47e-3 |
| | Re$\{H_2\}$ | 3.59e-4 | 9.47e-3 |
| | Im$\{H_2\}$ | 1.01e-4 | 9.52e-3 |
| Outdoor NLOS | Re$\{H_1\}$ | -3.11e-5 | 7.33e-3 |
| | Im$\{H_1\}$ | 1.47e-4 | 7.51e-3 |
| | Re$\{H_2\}$ | 1.12e-4 | 7.37e-3 |
| | Im$\{H_2\}$ | 9.51e-5 | 7.51e-3 |
| Industrial LOS | Re$\{H_1\}$ | 6.86e-5 | 1.25e-2 |
| | Im$\{H_1\}$ | 1.77e-4 | 1.26e-2 |
| | Re$\{H_2\}$ | 1.15e-4 | 1.25e-2 |
| | Im$\{H_2\}$ | 1.42e-4 | 1.26e-2 |
| Industrial NLOS | Re$\{H_1\}$ | -4.32e-5 | 4.60e-3 |
| | Im$\{H_1\}$ | 3.77e-5 | 4.64e-3 |
| | Re$\{H_2\}$ | 1.94e-4 | 4.72e-3 |
| | Im$\{H_2\}$ | 2.41e-5 | 4.65e-3 |

## 2.4.3 Marginal Distribution of the Variance of the Driving Noise

In most scenarios, the variance of the driving noise is lognormally distributed. However, the exponential distribution provides a much better fit for the outdoor NLOS and industrial LOS environments. The distributions and the corresponding parameters that apply to each of the eight CM scenarios are given in Table 2.5.

Table 2.5 Marginal Distributions of the Varaince of Driving Noise

| Scenario | Distribution | $\mu$ | $\sigma$ |
|---|---|---|---|
| Residential LOS | logn | -11.6377 | 0.808253 |
| Residential NLOS | logn | -10.7521 | 0.440403 |
| Office LOS | logn | -16.8811 | 0.9636 |
| Office NLOS | logn | -9.6782 | 0.3712 |
| Outdoor LOS | logn | -13.2402 | 0.833459 |
| Outdoor NLOS | exp | 6.061e-6 | - |
| Industrial LOS | exp | 6.147e-6 | - |
| Industrial NLOS | logn | -10.5998 | 0.0346458 |

## 2.4.4 Dependency between Model Parameters

Knowledge of the marginal distributions of the model parameters is necessary but not sufficient for the purposes of simulating the parameters. We must also capture the dependencies of the parameters on one another. Previous work that was conducted in residential environments and reported in [6] has shown that: (1) the initial conditions and the variance of the input noise are uncorrelated, (2) the poles and initial conditions are uncorrelated, but (3) the pole magnitudes and phases are correlated. Here, we examine the mutual dependencies in greater detail and for all eight CM scenarios. First, we calculated the linear mutual correlation coefficients between all nine parameters of the AR-FD model for each of the eight scenarios. Although the linear correlation coefficient

is most descriptive when the parameters are normally distributed, it still conveys useful information when they are not, as we shall show in the next section.

The results presented in Table 2.6 for CM 1 are typical. In each case, we discovered that the real and imaginary parts of the initial conditions are correlated with each other but not with the other five parameters. Thus, the initial conditions form an independent set. Because they are all normally distributed, they are completely described by a four-element mean vector and a four-by-four covariance matrix. Given the results of the previous section, we conclude that the initial conditions are completely characterized by just seven parameters: six mutual correlation coefficients and one standard deviation.

The remaining five model parameters are correlated with each other but, in general, are not normally distributed. While this greatly complicates the matter of modeling their mutual dependencies, Sklar's theorem teaches us that given joint multivariate distribution functions and the relevant marginal distributions, there exists a copula function that relates them. The copula method that is based upon this theorem provides us with a method for capturing the mutual dependencies in a form useful in simulation. Although not yet widely used in science and engineering, it has become a mainstay of dependency analysis in finance and economics [9][10]. We describe this approach in more detail in Section 2.5.

Table 2.6 Correlation between AR-FD Model Parameters for CM1

| $\rho$ | $\|p_1\|$ | $\|p_2\|$ | $\angle p_1$ | $\angle p_2$ | $u_0$ | $\mathrm{Re}\{H_1\}$ | $\mathrm{Re}\{H_2\}$ | $\mathrm{Im}\{H_1\}$ | $\mathrm{Im}\{H_1\}$ |
|---|---|---|---|---|---|---|---|---|---|
| $\|p_1\|$ | | 0.2384 | 0.5595 | 0.2039 | -0.6622 | -0.0259 | -0.0307 | -0.0115 | -0.0031 |
| $\|p_2\|$ | 0.2384 | | 0.0902 | 0.4616 | -0.4756 | 0.0030 | 0.0021 | 0.0017 | 0.0001 |
| $\angle p_1$ | 0.5595 | 0.0902 | | -0.0924 | -0.3443 | -0.0254 | -0.0297 | -0.0174 | -0.0089 |
| $\angle p_2$ | 0.2039 | 0.4616 | -0.0924 | | -0.6859 | 0.0128 | 0.0078 | 0.0019 | 0.0086 |
| $u_0$ | -0.6622 | -0.4756 | -0.3443 | -0.6859 | | 0.0103 | 0.0175 | 0.0083 | -0.0025 |
| $\mathrm{Re}\{H_1\}$ | -0.0259 | 0.0030 | -0.0254 | 0.0128 | 0.0103 | | 0.9267 | 0.0060 | -0.1904 |
| $\mathrm{Re}\{H_2\}$ | -0.0307 | 0.0021 | -0.0297 | 0.0078 | 0.0175 | 0.9267 | | 0.2022 | 0.0065 |
| $\mathrm{Im}\{H_1\}$ | -0.0115 | 0.0017 | -0.0174 | 0.0019 | 0.0083 | 0.0060 | 0.2022 | | 0.9281 |
| $\mathrm{Im}\{H_1\}$ | -0.0031 | 0.0001 | -0.0089 | 0.0086 | -0.0025 | -0.1904 | 0.0065 | 0.9281 | |

## 2.5 AR-FD Parameter Simulator

The results of the preceding section provide us with a strategy for designing an AR-FD-based simulator for the frequency domain equivalent of the CM 1-8 models. First we use the standard techniques that apply to jointly Gaussian random variables to generate a random sequence of state vectors whose elements have the same first-order statistics as the initial conditions $\{H_i\}$. Next, we use the copula method to generate a random sequence of state vectors whose elements have the same first-order statistics as the variance of the driving noise and the locations of the autoregressive poles. The two halves of the AR-FD model parameter vector are then applied to an AR-FD frequency response generator that consists of a second order filter $G(z)$ that is driven by a complex Gaussian white noise source, as described in Section 2.2. The resulting set of channel frequency responses has the same first-order statistical properties as those of the original training data.

## 2.5.1 Simulation of the Initial Conditions

We begin by generating a random sequence of state vectors **H** whose elements have the same first-order statistics as the real and imaginary components of the initial conditions observed in the original training data. First, we generate a vector **U** that contains four independent sequences of Gaussian distributed random numbers with zero mean and unit variance. Applying the transformation

$$\mathbf{H} = \left[ C_{IC} \right]^{1/2} \mathbf{U} + \boldsymbol{\mu}_{IC} \tag{2.15}$$

where $\boldsymbol{\mu}_{IC}$ and $[C_{IC}]$ are the mean vector and covariance matrix, respectively, that describe the initial conditions, yields the desired result.

## 2.5.2 Simulation of the Pole Locations and the Variance of the Driving Noise

Our next step is generate a random sequence of state vectors **P** whose elements have the same first-order statistics as the magnitude and phase of the autoregressive poles and the variance of the driving noise associated with the original training data. First, we denote the magnitude and phase of the poles and the variance of the driving noise, $\{|p_1|, |p_2|, \angle p_1, \angle p_2, u_0\}$, as the random variables $\{s_1, \dots s_5\}$. According to Sklar's theorem, if $F(s_1, \dots, s_5)$ is an five-dimensional joint distribution function, and each random variable, $s_{i,\ i=1,\dots5}$ has a marginal distribution specified by $F_1(s_1), \dots, F_5(s_5)$, there exists an 5-copula $C$ such that for all $s_{i,\ i=1,\dots5}$ in $\bar{R}_5$

$$F(s_1, \dots s_5) = C(F_1(s_1), \dots F_5(s_5)) \tag{2.16}$$

If $F_1(s_1) \dots F_n(s_n)$ are continuous, then $C$ is uniquely defined. By a change of variables, the copula can be expressed as

31

$$C(u_1,...,u_5) = \Pr(F_1^{-1}(u_1),...F_n^{-1}(u_5)) \qquad (2.17)$$

for any $u$ [0 1]$^5$.

## 2.5.3 Gaussian copula and Spearman's Rho

The precise form of the copula function depends upon the form of the marginal distributions. If the marginal distributions are Gaussian, the Gaussian copula applies. Multivariate student-t distributions will lead to the t-copula. Other combinations of distributions will be characterized by their own copula functions. However, all copula functions behave identically in the limit as the correlation between the variables approaches either 1 or -1. Although the best results are obtained using the ideal copula function, acceptable results can often be obtained by using a simpler function.

Here, we used the Gaussian copula. A Gaussian copula with specified correlation matrix $K_s$ is defined by

$$C(u_1,...,u_5) = \phi_{K_s}^5 (\phi_1^{-1}(u_1),...\phi_5^{-1}(u_5)) \qquad (2.18)$$

The elements in the correlation matrix $K_s$ are the mutual linear correlation between the two random variables. The linear correlation $K_s$ fully specifies the dependency structure of elliptical distributions, such as the Gaussian and t-distributions. For copulas with non-elliptical distributions, one must generally use rank correlation instead. The most widely accepted rank correlation is Spearman's rho, which can be expressed via

$$\rho_{sp} = Corr(F_1(s_1),...F_5(s_5)) \qquad (2.19)$$

## 2.5.4 Simulation Steps

To generate correlated model parameters using a Gaussian copula, we followed the procedure described in [10] and [11]. Assume that the parameter simulator outputs $5$ dimension parameters $(s_1, \ldots s_5)$. Each $s_{i,i=1,\ldots5}$ has a predefined marginal distribution $F_i(s_i)$, and the underlying dependency is characterized by linear correlation matrix $K_s$. The steps for generating dependent random variables are as follows:

i) We start by generating white Gaussian random variables $R = (r_1, \ldots r_5)$. The white Gaussian random variables have cumulative density functions $(u_1, \ldots u_5)$. Each $u_{i,i=1,\ldots5}$ is independent and uniformly distributed in $[0, 1]$. $\Pr(u_i, {}_{i=1,..5}) = 1/N$, where N is the number of empirical data points.

ii) The next step is to transform the Gaussian random variables to the eigenspace defined by the correlation matrix. Applying decomposition to the covariance matrix $K_s$, we obtain a diagonal matrix $D$ with eigenvalues on the main diagonal plus a matrix $V$ with corresponding eigenvectors as column vectors.

$$K_s = VDV^{-1} \tag{2.20}$$

$$T = V(D^{\frac{1}{2}}) \tag{2.21}$$

$$\begin{bmatrix} r_{Ks}^1 \\ \vdots \\ r_{Ks}^5 \end{bmatrix} = T \begin{bmatrix} r_1 \\ \vdots \\ r_5 \end{bmatrix} \tag{2.22}$$

iii) By transforming Gaussian random variables $(r_1, \ldots r_5)$ to the eigenspace specified by matrix $V$, we get multivariate Gaussian $(r_{Ks}^1, \ldots r_{Ks}^5)$ with dependency specified by correlation $K_s$. During the transformation, the linear correlation is preserved. The multivarite Gaussian random variables have marginal cumulative density functions $(u_{Ks}^1, \ldots u_{Ks}^5)$, which are also uniformly distributed.

iv) Applying inverse transform to ($u_{Ks}^1, \ldots u_{Ks}^5$) with previously specified marginal parameter (as presented in Section 2.4.1, 2.4.2 and 2.4.3), we get random variables ($\hat{s}_1, \ldots \hat{s}_5$). For example, if the specified marginal is an extreme value distributed random variable EV($\alpha_1$, $\beta_1$), then $\hat{s}_1$ can be generated by

$$\hat{s}_1 = \beta_1 \ln\left\{-\ln(1 - u_{Ks}^1)\right\} + \alpha_1 \tag{2.23}$$

The variables ($\hat{s}_1, \ldots \hat{s}_5$) have the same marginal distributions as the modeled parameters and they have the specified correlation in $K_s$.

## 2.5.5 Goodness-of-fit Test for Poles

Copula is one way of modeling dependency between multivariate data. Finding a type of copula that best resemble empirical data is an active area of research [13]. Our objective is to verify that the Gaussian copula generated poles and the AR-FD modeled poles have the same statistical distribution. In the univariate case, the null hypothesis $H_0$, the simulated pole magnitudes are statistical the same as the modeled poles, can be tested by the Kolmogorov –Smirnov (K-S) statistic [11]

$$D_n = \sup_{|p_1| \in [0,1]} \left| F(|\hat{p}_1|) - F(|p_1|) \right| \tag{2.24}$$

where $F(|\hat{p}_1|)$ is the distribution function of copula generated poles and $F(|p_1|)$ is the distribution function of the modeled poles. Some more or less satisfying techniques are available for testing good-of-fit for multivariate data: i) Justel et al [12] used Rosenblatt's transform before testing a simple GOF assumption ii) Pollard et al [14] recommended to form disjoint cells and use $x^2$ test for testing goodness of fit in each cell. For the first approach, it is very computational intensive to do the Rosenblatt's transform as dimension grows. For the chi-square test, it is hard to justify what is the best way of setting the cell boundaries. Here, we compare the results of copula-simulated poles and

34

original poles by: i) the pole plots of CM1-8 vs CFR 1-8 (Figure 2.6 and Figure 2.7)) and ii) the RMS delay spread derived from 4a and AR-FD model (Figure 2.8 and Figure 2.9).
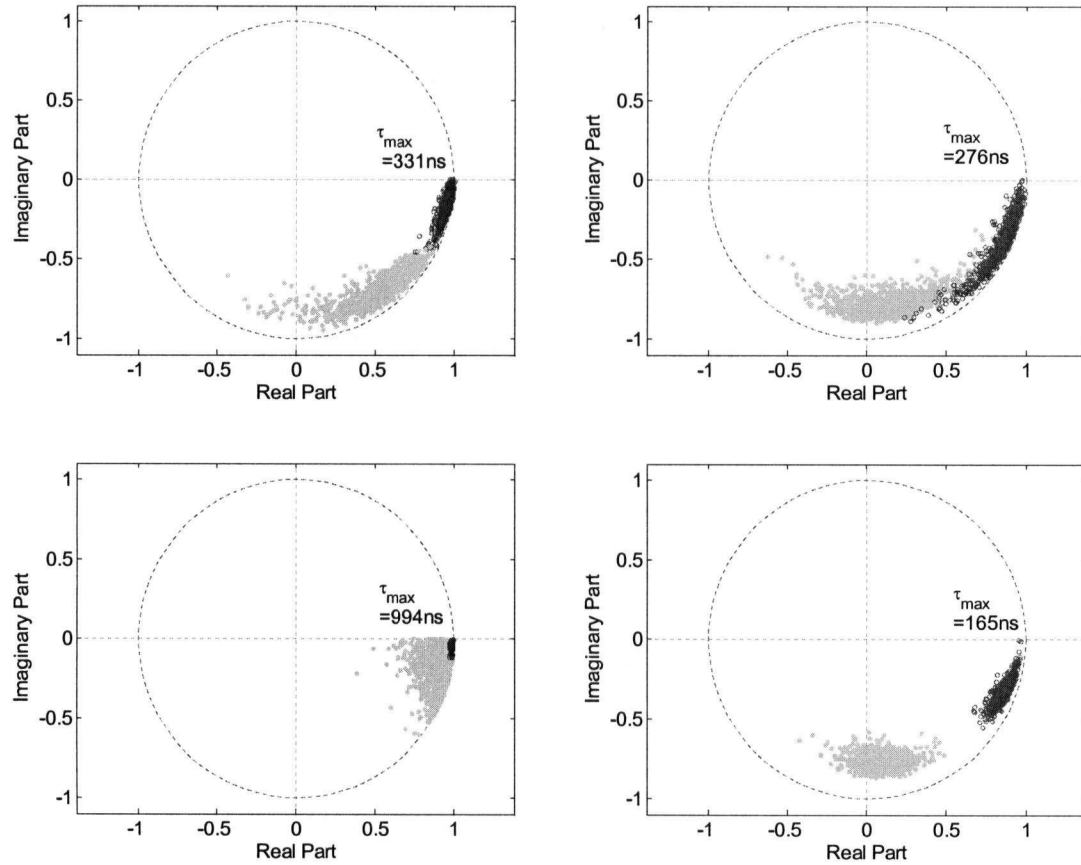


Figure 2.6 Copula generated AR-FD pole locations for LOS and NLOS cases of the residential and office environments. (Dark points – first pole locations, light point – second pole locations.)
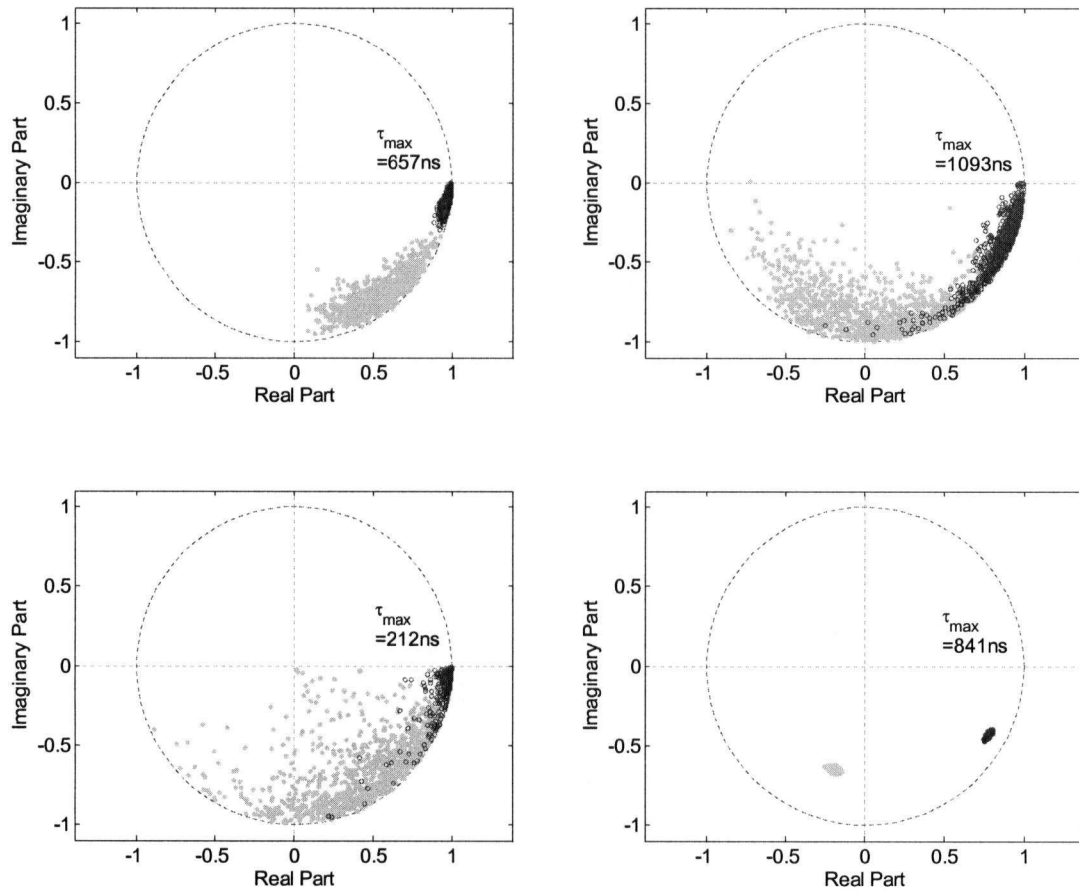
Figure 2.7 Copula generated AR-FD pole locations for LOS and NLOS cases of the outdoor and industrial environments. (Dark points – first pole locations, light point – second pole locations.)
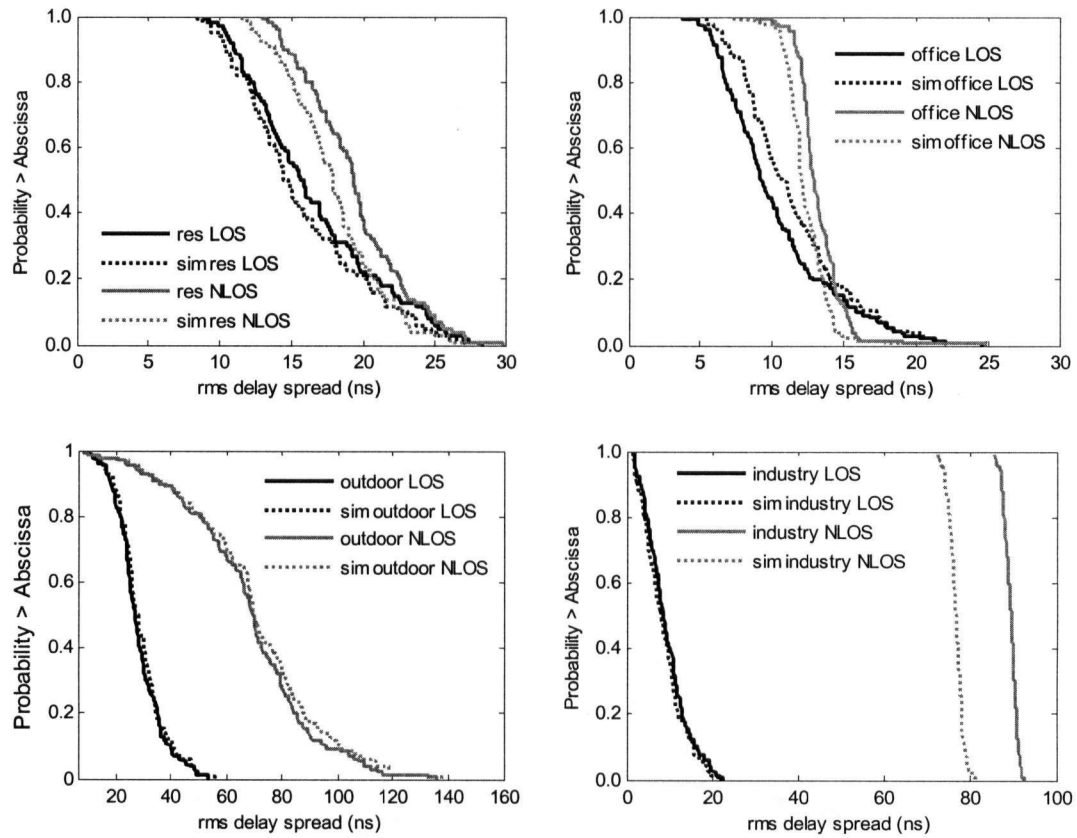
Figure 2.8 Comparison of RMS Delay Spreads for obtained from the estimated AR-FD and S-V models (CM 1-8)
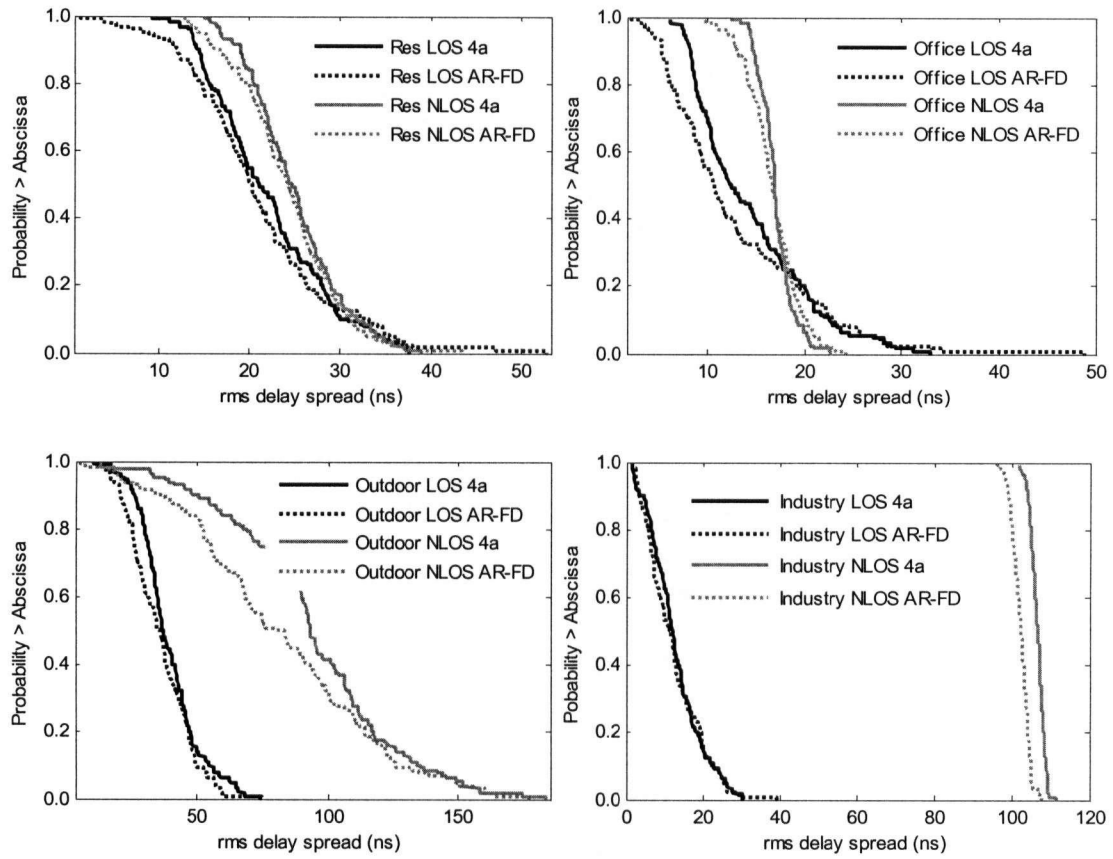
Figure 2.9 Comparison of RMS Delay Spreads for obtained from the copula-regenrated AR-FD and S-V models (CM 1-8)

## 2.6 Conclusion

We have determined that the eight CM channel models developed by the IEEE 802.15.4a task group can all be represented with reasonable fidelity by second-order autoregressive frequency domain channel models. LOS environments tend to be much more accurately represented than the corresponding NLOS environments, but the difference depends upon the environment with office environments displaying the greatest difference and outdoor environments the least. The distribution of the AR poles for the CM8 Industrial NLOS model is very much narrower than that of the other seven models. The difference is so striking that it suggests that CM 8 may be based on too limited a sample of CIR data or that the data used may have been collected at too few locations. Further investigation of the Industrial NLOS scenario is therefore warranted.

We have also determined the marginal distributions and mutual correlation for each of the nine model parameters that apply to each of the eight scenarios captured by CM 1-8. We have shown that the parameters divide into two independent sets: the initial conditions form a joint multivariate normal distribution on one hand and the variance of the driving noise and the magnitudes and phases of the autoregressive poles form a more general joint multivariate distribution on the other. Using a scheme based upon copulas allows us generate random sequences of AR-FD model parameters that have the same first-order statistics as the original training data.

Our technique for reducing the AR-FD model parameters to a statistical model useful in simulation can also be applied to reduction of frequency response data measured in new environments. Moreover, unlike schemes used to reduce channel impulse response data, it can likely be automated with relative ease. Although we obtained good results using a Gaussian copula, it would be useful to compare the performance that can be achieved using more sophisticated copula functions. This is a task for future studies.

# Bibliography

[1]  A. F. Molisch et al., "IEEE 802.15.4a Channel Model - Final Report," Tech. Rep., IEEE P802. 15-04/662r0-SG4a, Sep. 2004

[2]  A. F. Molisch, "Ultrawideband propagation channels- Theory, measurement, and modeling," *IEEE Trans. Veh. Technol.*, vol. 54, no.5, pp. 1528-1545, Sep. 2005.

[3]  A. A. M. Saleh, and R. A. Valenzuela, "Statistical model for indoor multipath propagation," *IEEE J. Sel. Areas Commun.*, vol. SAC-5, no. 2, pp. 128-137, Feb. 1987

[4]  S. J. Howard, and K. Pahlavan, "Autoregressive modeling of wide-band indoor propagation," *IEEE Trans. Commun.*, vol. 40, no. 9, pp. 1540-1552, Sep. 1992.

[5]  G. Morrison, and M. Fattouche, "Super-resolution modeling of the indoor radio propagation channel," *IEEE Trans. Veh. Technol.*, vol.47, no. 2, pp. 649-657, May 1998.

[6]  S. S. Ghassemzadeh, R. Jana, C.W. Rice, W. Turin, and V. Tarokh, "Measurement and modeling of an ultra-wide bandwidth indoor channel," *IEEE Trans. Commun.*, vol. 52, no. 10, pp. 1786-1796, Oct. 2004

[7]  N. Xin and D. G. Michelson, "AR frequency domain analysis of the IEEE 802.15.4a standard channel models," *Proc. IEEE WCNC 2007*, pp. 2058-2062, Mar. 2007.

[8]  S. L. Marple Jr., Digital Spectral Analysis with Applications, Prentice-Hall, 1987, pp. 229.

[9]  R. B. Nelsen, An Introduction to Copulas, 2nd ed., Springer, 2006, pp. 51-108.

[10]  T. Schmidt, "Coping with Copulas" in Copulas: From theory to application in finance, J. Rank, Ed., London: Risk Books, 2007, pp. 3-34.

[11]  Simulating Dependent Random Variables Using Copulas. The Mathworks. [Online]. Available: http://www.mathworks.com/products/statistics/demos.html

[12]  A. Justel, D. Pena and R. Zamar, "A multivariate Kolmogorov-Smirnov test of goodness of fit," *Statist. Prob. Lett.*, vol. 35, pp. 251-259, 1997.

[13]  J-D, Fermanian, "Goodness-of-fit tests for copulas," *J. Multivariate Anal.*, vol. 95, no. 1, Jul. 2005, pp. 119-152

[14]  D. Pollard, "General chi-square goodness-of-fit tests with data-dependent-cells," *J. Probability Theory and Related Fields*, vol. 50. No. 3, Jan. 1979, pp. 317-331.

# Chapter 3

# Frequency Domain Analysis of UWB Radiowave Propagation within the Passenger Cabin of a Boeing 737-200 Aircraft

## 3.1 Introduction

[2]With an increase demand for in-flight services that provide passengers entertainment or business experience on board, it is very important to have a valid in-cabin channel characterization. Aircraft environment is intrinsically different from conventional environments in the following sense: (1) geometry of the aircraft cabin is tunnel like, enclosed by metallic reflectors [5] (2)high density of obstacles (seats) in a conventional commercial aircraft suggests severe propagation conditions in such environment (3)high density of human presence is anticipated to introduce excess losses on the propagation channel. A variety of studies have been conducted on wireless communication and multimedia data networks inside aircraft cabins. Previous studies [8][9][14] have emphasized: (1) field trials for passenger-carried electronic devices (i.e. cell phones), wireless LAN, and Bluetooth wireless technology (2) using ray tracing simulation tools such as "Site Planner" and "WirelessInsite" to predict power propagation within aircraft cabin or to emulate an aircraft cabin propagation environment in the absence of internal components (i.e. windows, overhead cargo bins) (3) measurement of RF coverage using client devices. In one instance, a measurement based in-flight channel characterization was done in the UMTS downlink band [14]. Overall, studies of measurement based channel characterization on aircraft cabin are limited to existing narrowband technologies except for [14].

---

streaming as well as network access services within aircraft passenger cabin (2) facilitating operations and maintenance through deployment of sensor networks, emergency communication and precise positioning system. However, to the best of our knowledge, no measurement based frequency domain channel characterization has ever been done in the 3.1 to 10.6 GHz band. Past efforts by dedicated task groups, such as IEEE 802.15.3a and 4a, to develop UWB propagation models focused only on time domain models like the Saleh-Valenzuela (S-V) model, and their corresponding time domain model parameters for conventional environments such as residential, office, outdoor, and industrial [6]. Because aircraft cabin is a very specific environment hosting numerous functionalities and UWB is well known for its low interference with existing systems, in this paper we propose to characterize UWB channel onboard statistically in frequency domain using autoregressive frequency domain (AR-FD) approach. In AR-FD, we first estimate the autoregressive coefficients and the residual error between true and estimated spectra. Then, we use the characterized coefficients to find autoregressive poles of the system. These pole locations are discussed in detail and compared with those found in conventional environments documented by 802.15.4a [11]. From the AR-FD analysis, we derive the auxiliary channel parameters, such as RMS delay spread and coherence bandwidth. We show that these auxiliary parameters are statistically similar to those derived from measured channel responses.

The remainder of the paper is organized in the following way: Section 3.2 gives an overview of the considered aircraft environment, as well as the measurement setup that was used to collect data. Section 3.3 describes the AR-FD model and the parameterization of such model. Section 3.4 describes the derived system parameters such as RMS delay spread and coherence bandwidth. Section 3.5 concludes the paper.

## 3.2 Measurement Setup and Locations

### 3.2.1 Measurement Setup and Calibration

UWB frequency domain measurements were performed in the aircraft using an Agilent E8362B vector network analyzer (VNA). For point-to-multipoint(p-to-mp) setup, port A of the vector network analyzer was connected to the transmitting antenna through a short coaxial cable(as shown in Figure 3.1a). Transmitter height was fixed. Port B of the VNA was connected to the receiving antenna through a 15m coaxial cable. At both the transmitting and the receiving end, we used an Electro-Metrics EM-6865 omnidirectional bicone antenna, which has a gain of 0 dBi typically. These antennae are chosen because they have a large bandwidth and constant impedance over a large frequency. For the peer-to-peer (p-to-p) setup, both the transmitting and receiving antenna are connected to the VNA ports by 15m double-shielded coaxial cables. Before measurements were performed, calibration with cables is carried out in the 3.0 to 10.6 GHz band using through-line calibration. The calibration procedure is meant to compensate for the effect of amplitude and phase variations caused by long cables and VNA. As a result, the UWB channel measurements contain the effect of the channel as well as transmitting and receiving antenna.

The source power level is set to 5dB and at receiver side IF bandwidth is set to 3 kHz. In each sweep, the VNA takes in 6401 sample points, corresponding to 1.18 MHz spacing between each sampled points. The time resolution at the receiver is the inverse of the center frequency 0.147 ns and the maximum excess delay of the system is 842 ns. Investigations on maximum excess delay of indoor channels to be 70ns have been reported by other researchers [3].

## 3.2.2 Description of Measurement Location

Measurements were carried out in a mid-size Boeing 737 airliner. The main cabin of the aircraft is 21 m in length, 3.54 m in width, and 2.2 m in height. The cabin has 21 rows with 6 passenger seats in each row (seats A to C on one side, and seats D to F on the other side). A full aircraft can take more than 100 passengers. As mentioned previously, the measurement campaign has two configurations: (1) point-to-multipoint (p-to-mp) and (2) peer-to-peer (p-to-p). For the p-to-mp configuration, transmit antenna is mounted at the ceiling height at row 2 (approximately 2.2 m above floor) and receiving antenna is placed at 50 different seat locations throughout the cabin from row 4 to row 18. In addition, the receiving antenna is mounted at different heights to represent how a wireless device is likely to be deployed, include headrest, armrest and footrest positions. The second configuration, p-to-p, investigates the effects of different transmitting antenna locations have on the channel. The transmitter is placed at headrest, armrest and footrest positions instead. These configurations allow us to study effects of receivers at different heights as well as AR-FD channel model parameter as a function of distance.

## 3.2.3 Sampling Strategy

The measurement is taken from row 4 to row 19 of a commercial aircraft; the last three rows were not considered due to limitation in cable length; but the result for the last rows can be derived because of the parameters' dependency on distance. Symmetry of the aircraft allows us to perform measurements on right half of the airplane, i.e., from seat A to C. To reduce the time and effort needed to sample the aircraft, measurements were only taken at every other seat (as shown in Figure 3.2).
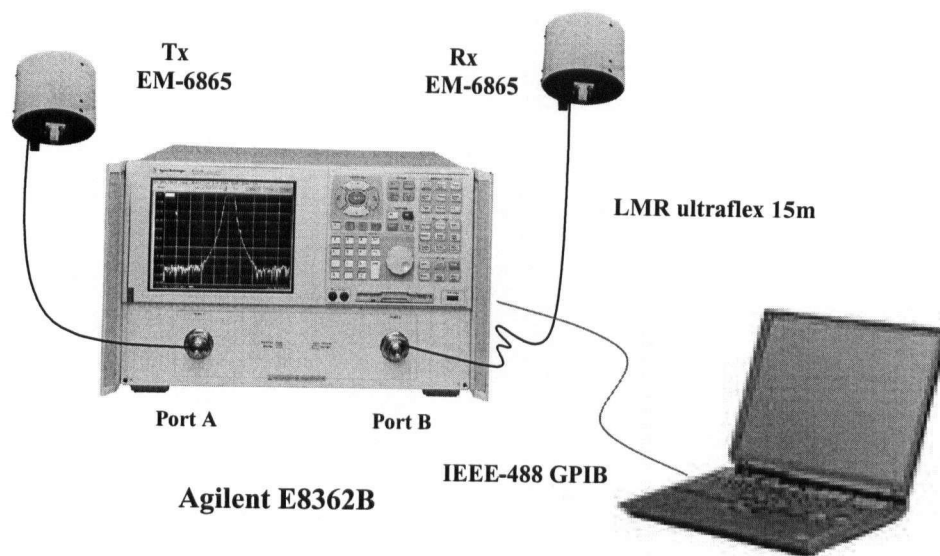
a)



b)

Figure 3.1 a) measurement setup b) typical location of receiving antenna

(a)



(b)
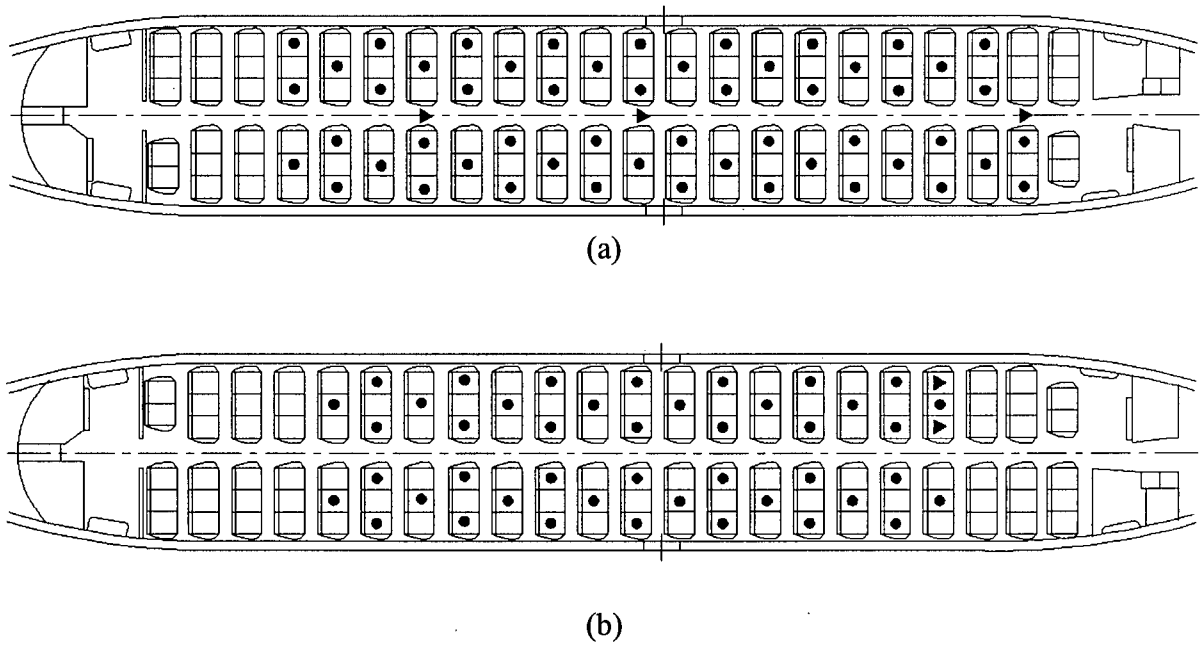
Figure 3.2 Location of the transmitting and receiving antennas within a Boeing 737-200 aircraft for (a) point-to-multipoint and (b) peer-to-peer configurations during the development runs. In production runs, only one side of the aircraft and one transmitting antenna

## 3.3 Autoregressive Frequency Domain Model

The autoregressive frequency domain (AR-FD) model has been demonstrated to be promising for characterizing and simulating indoor UWB channels [2][11]. In particular, indoor office LOS, outdoor LOS and NLOS channels are more accurately presented by AR-FD model due to existence of dominant cluster [11]. The AR-FD model has several advantages over time domain S-V model. Firstly, in the process of characterizing model parameters, AR-FD model requires less subjective user input, namely order of the AR model rather than number of cluster in a particular environment. Secondly, with most channel measurements done using a VNA, characterizing frequency domain model avoids expensive operations such as inverse Fourier transform and deconvolution that might introduce more errors into the measurement, e.g. finite bandwidth effects. As a result, frequency domain channel characterization becomes attractive for modeling propagation channels in an unfamiliar environment, like aircraft.

## 3.3.1 Background

AR-FD approach estimates the complex channel frequency response based on the complex autocorrelation between frequency taps assuming that each frequency tap is sum of the previous taps plus some observation noise. By taking the z-transform, the channel frequency responses are treated as the output of an all-pole filter in the form of

$$G(z) = \frac{1}{1 + \sum_{i=1}^{k} a_i z^{-i}}$$

$$G(z) = \frac{1}{\prod_{i=1}^{k} (1 - p_i z^{-1})} \tag{3.1}$$

To find the filter function G(z) that model complex channel response as desired output, we apply a well known AR parameter estimation algorithm Yule Walker to over 1000 snapshots of channel frequency response taken in aircraft cabin (as shown Figure 3.3a). The AR order $k$ must be chosen with special care. The order determines tradeoff between spectrum resolution and model complexity. We show in the next session an information criterion which is often used to determine appropriate AR order.

The AR-FD model parameters include AR coefficients $\{a_i\}$, initial conditions $\{H_i\}$, and variance of driving noise $\sigma$. A simple flow chart showing the extraction process of AR-FD model parameters is shown in Figure 3.3a. The AR coefficients completely characterize the filter function G(z). For channel emulation process, we take the characterized autoregressive poles $\{p_i\}$, initial conditions and variance of driving noise as inputs. The frequency taps are generated recursively as in Figure 3.3 b) by

$$\hat{H}(f_k,t;x) + \sum_{i=1}^{p} a_i \hat{H}(f_{k-i},t;x) = U(f_k,t;x) \qquad (3.2)$$

where $U(f_k, t; x)$ is white Gaussian noise with variance $\sigma$.



(a)



(b)
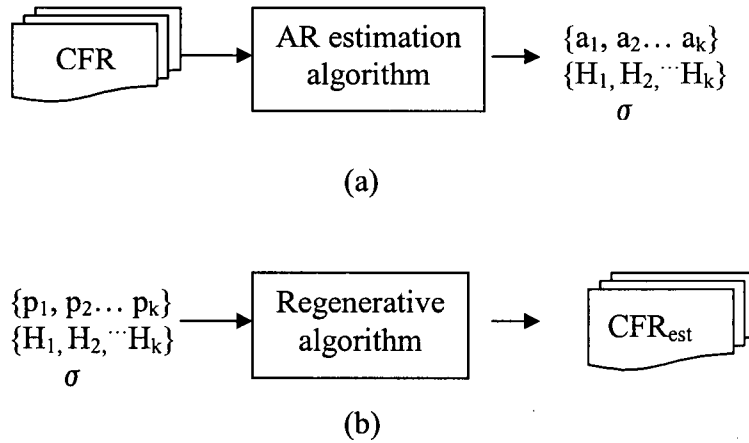
Figure 3.3 a) AR-FD parameter characterization, b) AR-FD aircraft channel emulation

## 3.3.2 AIC

In practice, the best choice of filter order is not generally known *a priori*. Higher order gives better resolution and finer details to the estimated frequency response but increases system complexity. If the order is too low, resulting frequency response will be too smooth. With empirical data, the prediction error variance alone is often not sufficient to indicate which order is most appropriate, unless there is some definitive order after which the rate of change in error variance reduction suddenly decreases [11] (Figure 3.4). A selection criterion named the Akaike information criterion (AIC) chooses the model order by minimizing the following information theoretic function

$$AIC = \log(V) + \frac{2k}{N} \tag{3.3}$$

$$V = \det(\frac{1}{N} \sum_{j=1+k}^{N} \varepsilon(f,\hat{\theta}_j)\varepsilon(f,\hat{\theta}_j)^T) \tag{3.4}$$

where $V$ is the loss function (also known as the variance of residual error between true and estimated spectrum), $k$ is the number of estimated parameters, $N$ is the number of data used for estimation and $\hat{\theta}_N$ is the estimated AR coefficients. The term $2k/N$ is a penalty for use of extra AR coefficients that do not substantially reduce prediction error.

From Table 3.1, the AIC value drops from -10.9826 to -12.7135 as the AR order increases from 1 to 7. These AIC values are most close to what was found in characterizing industrial LOS channels using different orders of AR estimation

**Table 3.1 AIC in Aircraft Environment**

| AR Order | AIC | Prediction Error |
|---|---|---|
| $1^{st}$ | -10.9826 | 1.9619e-5 |
| $2^{nd}$ | -11.9241 | 8.2170e-6 |
| $3^{rd}$ | -12.3522 | 5.5097e-6 |
| $4^{th}$ | -12.5371 | 4.6267e-6 |
| $5^{th}$ | -12.6284 | 4.2529e-6 |
| $6^{th}$ | -12.6807 | 4.0589e-6 |
| $7^{th}$ | -12.7135 | 3.9443e-6 |
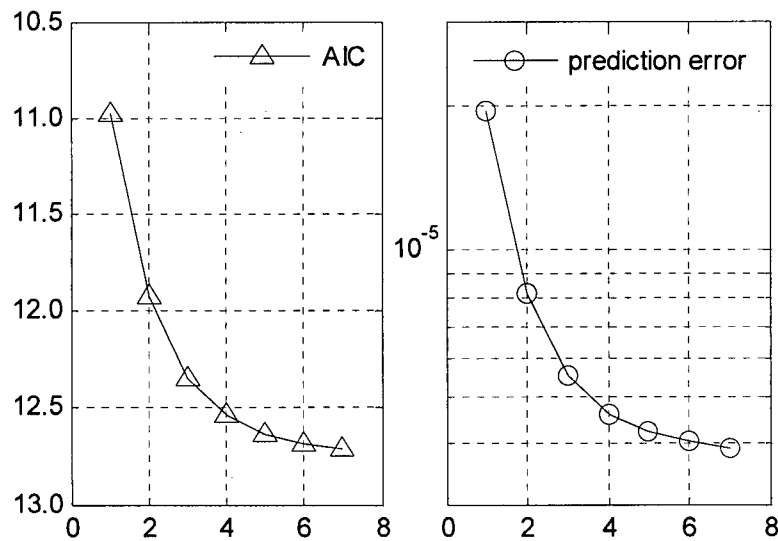


Figure 3.4 AIC and Prediction Error vs AR Order

## 3.3.3 Autoregressive Coefficients and Poles of the System

The AIC analysis shows that a second order autoregressive model can estimate the aircraft channel response quite accurately. To characterize autoregressive poles, AR-FD model order is set to 2 and 500 measured UWB channel response in an empty aircraft is input to the estimation algorithm to yield complex coefficients $a_1$ and $a_2$. The poles $p_1$

and $p_2$ are found by solving the denominator of G(z). Figure 3.5 is the pole plot of the second order AR-FD model; the pole locations for aircraft channel is closest to those found in office NLOS.
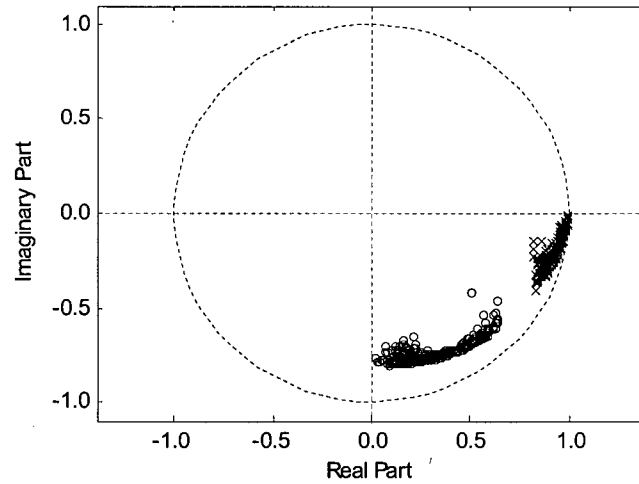


Figure 3.5 Second Order Autoregressive Poles of Channels in Empty Aircraft

### 3.3.3.1 Pole Magnitude

First order poles are located near the unit circle. Their magnitudes fall in the range of 0.8034 to 0.9981. From spectral estimation, poles close to unit circle suggest the spectrum has significant energy at certain delays [11]. These delays can be modeled by pole phase. In our context, large pole magnitudes also suggest existence of dominant cluster in the impulse response [11]. Magnitudes of second order pole fall in the range of 0.6556 to 0.8769. Second order poles that have magnitudes greater than 0.5 suggest energy of corresponding channels is not significantly attenuated [1]. Given the pole plots in Figure 3.5, we observe that the variance in angle spread of first pole and second pole are not significantly different; thus, we can conclude snapshots of the aircraft channels are made of mostly NLOS channels, where no dominant cluster exists. The channel energy in such environment spreads over time; thus, RMS delay spread is anticipated to be quite large.

### 3.3.3.2 Pole Phase

The time delay corresponding to a pole is modeled by

$$\tau = \frac{-\angle p}{\Omega_s} = \frac{-\angle p}{2\pi f_s} \tag{3.5}$$

The frequency step $f_s$ in our context is 2.375MHz. Starting from the positive real axis which corresponds to time delay of zero, time delay increases in clockwise direction. Delay derived from phase of 1st order pole falls in the range of 0.4934 ns to 54.20ns, which correspond to unambiguous distance of 0.15m and 16.2585m. The 0.15m is the distance between Tx at armrest and Rx at armrest in the same row. The 16.2585 m is the distance between Tx at front row and Rx at row 18. Time delay corresponds to 2nd order pole falls in the range of 41.7612ns and 124.3992ns. This range suggests propagation distance from 12.5294m to 41.7612m. The relationship shown in (5) implies a pole's dependency on propagation distance through time delay. This relationship will be exploited in the analysis of pole and auxiliary parameters in the next section.

In time domain analysis, the arrival time of the first path in the power delay profile $t_0$ models the distance between transmit and receiver if LOS exists. This parameter is often taken into account and power delay profile is often shifted by $t_0$ in order to obtain more accurate analysis of mean excess delay. In AR-FD approach, the pole phase and time delay is modeled by (3.5). The $t_0$ effect can be compensated by multiplying the frequency response with $e^{j\omega t0}$. In our modeled mid-size aircraft environment, $t_0$ falls in the range of 1 to 39ns. The change of phase in pole plot is not observable. In other environment with larger dimension (e.g. distance between transmitter and receiver are greater than 50m), this $t_0$ effect need to be removed in order to obtain more accurate pole locations.

### 3.3.3.3 Pole Statistics

The autoregressive poles can be characterized statistically by finding a good fit of its magnitude and phase through Kolmogorov-Smirnov test. The K-S tests accepts hypothesis of an AR-FD model based on testing the vertical distance between estimated CDF and empirical CDF, the level of significance is set at 0.01. Figure 3.6 shows the distribution fitting of pole parameter and pole phase. Magnitudes of first order and second order pole both follow extreme value distribution (in Figure 3.6 a and b). Extreme value distribution is the log of a Weibull distribution. The density function of an extreme value distributed variable $|p_1|$ is given by

$$f(|p_1| \mid \alpha, \beta) = \beta^{-1} \exp\left\{ \frac{(\alpha - |p_1|)}{\beta} - \exp(\frac{(\alpha - |p_1|)}{\beta}) \right\} \tag{3.6}$$

E.V. distribution was used for fitting pole magnitude in some indoor environments. Researchers in [2] have taken similar approach to model pole statistics in residential environment. The first order and second order pole phase follow Gaussian distributions (as shown in Figure 3.6 c and d). A complete list of distributions and distribution parameters is shown in Table 3.2
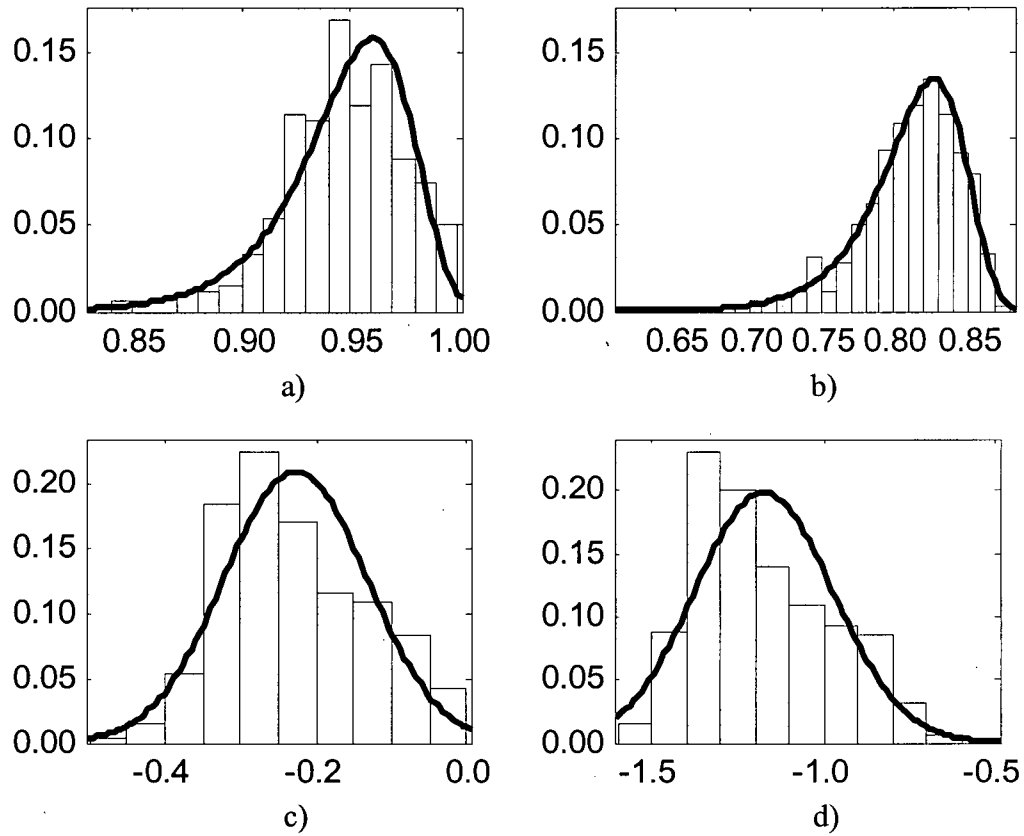
Figure 3.6 Pole Magnitude and Phase Histogram with Best Fit Distribution a) first order pole magnitude with extreme value fit; b) second order pole magnitude with extreme value fit; c) first order pole phase with normal fit; d) second order pole phase with normal fit

**Table 3.2** Poles of AR-FD Model

| Parameter | Distribution | $\alpha$ | $\beta$ |
|-----------|--------------|----------|---------|
| $|p_1|$ | E.V. | 0.9608 | 0.0244 |
| $|p_2|$ | E.V. | 0.8312 | 0.0287 |
| $Ang(p_1)$ | Normal | -0.2275 | 0.0949 |
| $Ang(p_2)$ | Normal | -1.1761 | 0.2037 |

### 3.3.3.4    Initial Conditions of AR-FD Model

First and second autoregressive poles in aircraft environment are important parameters to characterize because they determine the filter transfer function G(z). Other AR-FD model parameters include initial conditions of the channel frequency responses and variance of the driving noise. Study in [2] shows initial conditions varies in different indoor and outdoor environment, but they tend to follow normal distribution with empirical mean close to zero. Here, we found the characterized second order initial conditions for aircraft channels also follow normal distributions. Table 3.3 shows the first and second order statistics of characterized initial conditions.

Table 3.3 Initial Conditions of AR-FD Model

|   | $Re\{H_1\}$ | $Im\{H_1\}$ | $Re\{H_2\}$ | $Im\{H_2\}$ |
|---|---|---|---|---|
| $\mu$ | -8.4474e-4 | -8.4695e-4 | -1.3661e-3 | -5.9173e-4 |
| $\sigma$ | 1.3924e-2 | 1.4597e-2 | 1.3282e-2 | 1.4265e-2 |

From Table 3.3, it is concluded that real and imaginary part of initial conditions characterized for aircraft channel have a mean close to zero as anticipated. The variance of initial condition is in the order of 10e-2. The real part of first order initial condition is highly correlated with the real part of second order initial condition. Same applies to the imaginary parts. Their correlation coefficients are shown in Table 3.4.

Table 3.4 Correlation Coefficients between Initial Conditions

| $\rho$ | $Re\{H_1\}$ | $Re\{H_2\}$ | $Im\{H_1\}$ | $Im\{H_2\}$ |
|---|---|---|---|---|
| $Re\{H_1\}$ | 1 | 0.8734 | -0.0559 | -0.4017 |
| $Re\{H_2\}$ | 0.8734 | 1 | 0.3564 | 0.0136 |
| $Im\{H_1\}$ | -0.0559 | 0.3564 | 1 | 0.9040 |
| $Im\{H_2\}$ | -0.4017 | 0.0136 | 0.9040 | 1 |

### 3.3.3.5 Variance of Driving Noise for AR-FD Model

Previous work in [2] shows variance of driving noise $u_0$ follows a lognormal distribution. Figure 3.7 shows the histogram of the characterized initial condition in aircraft environment and a best fitted distribution; the parameter is found to be normal distributed with mean at 3.22e-5 and standard deviation at 1.08e-5. It is correlated with the second order autoregressive poles, but uncorrelated with initial conditions. Table 3.5 lists the normalized covariance matrix of $u_0$ and autoregressive poles.
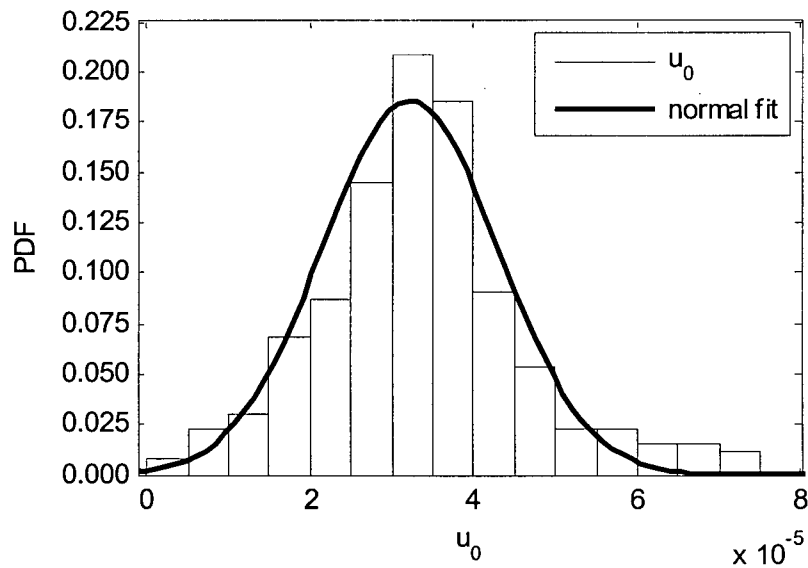


Figure 3.7 Distribution of variance of driving noise with normal fit

Table 3.5 Correlation Coefficient between Variance of Driving Noise and Autoregressive Poles

| $\rho$ | $u_0$ | $|p_1|$ | $|p_2|$ | $\text{ang}(p_1)$ | $\text{ang}(p_2)$ |
|---|---|---|---|---|---|
| $u_0$ | 1 | -0.9609 | 0.7733 | -0.6921 | -0.7152 |
| $|p_1|$ | -0.9609 | 1 | 0.8336 | 0.7603 | 0.8526 |
| $|p_2|$ | -0.7733 | 0.8336 | 1 | 0.4837 | 0.6786 |
| $\text{ang}(p_1)$ | -0.6921 | 0.7603 | 0.4837 | 1 | 0.8609 |
| $\text{ang}(p_2)$ | -0.7152 | 0.8526 | 0.6786 | 0.8609 | 1 |

## 3.4 Result and Discussion

In this session, we investigate how pole locations alter with different receiver positions and different density of passengers. We study auxiliary parameters like excess attenuation introduced by passengers; RMS delay spread $\tau_{RMS}$ and coherence bandwidth $B_c$ of the aircraft channel.

## 3.4.1 Pole Dependency on Distance

In an empty aircraft (January data), pole location changes with receiving antenna's mounting positions in two ways i) the projected distance to horizontal plane (from row 4 to row 18) ii) in the vertical direction (headrest, armrest and footrest). To relate measurement distance with the location of characterized poles, we study correlation between pole and distance. Figure 3.8 shows pole magnitudes are inverse proportional to distance. As receiver moves towards the back of passenger cabin, the first order and second order poles magnitude decreases (as Figure 3.8 a). This decrease in magnitude is seen in pole plot as that first and second order poles move farther away from the unit circle. Decrease in pole magnitude is very often accompanied by decrease in pole phase (as Figure 3.8 a and b). When modeling channels that correspond to a relatively large propagation distances (i.e. at the back of a cabin), the second pole is anticipated to have a large negative phase. Analytically, the pole magnitudes and phases can be modeled by distance as follows

$$\begin{aligned} |p_1| &= -0.0076d + 0.9883 \\ |p_2| &= -0.0098d + 0.8697 \end{aligned} \tag{3.7}$$

$$\begin{aligned} \angle p_1 &= -0.0192d - 0.1347 \\ \angle p_2 &= -0.0556d - 0.8802 \end{aligned} \tag{3.8}$$

The above relationship is by fitting pole magnitude and phase with respect to distance linearly in a least square sense. The work in [2] uses a similar approach.

58
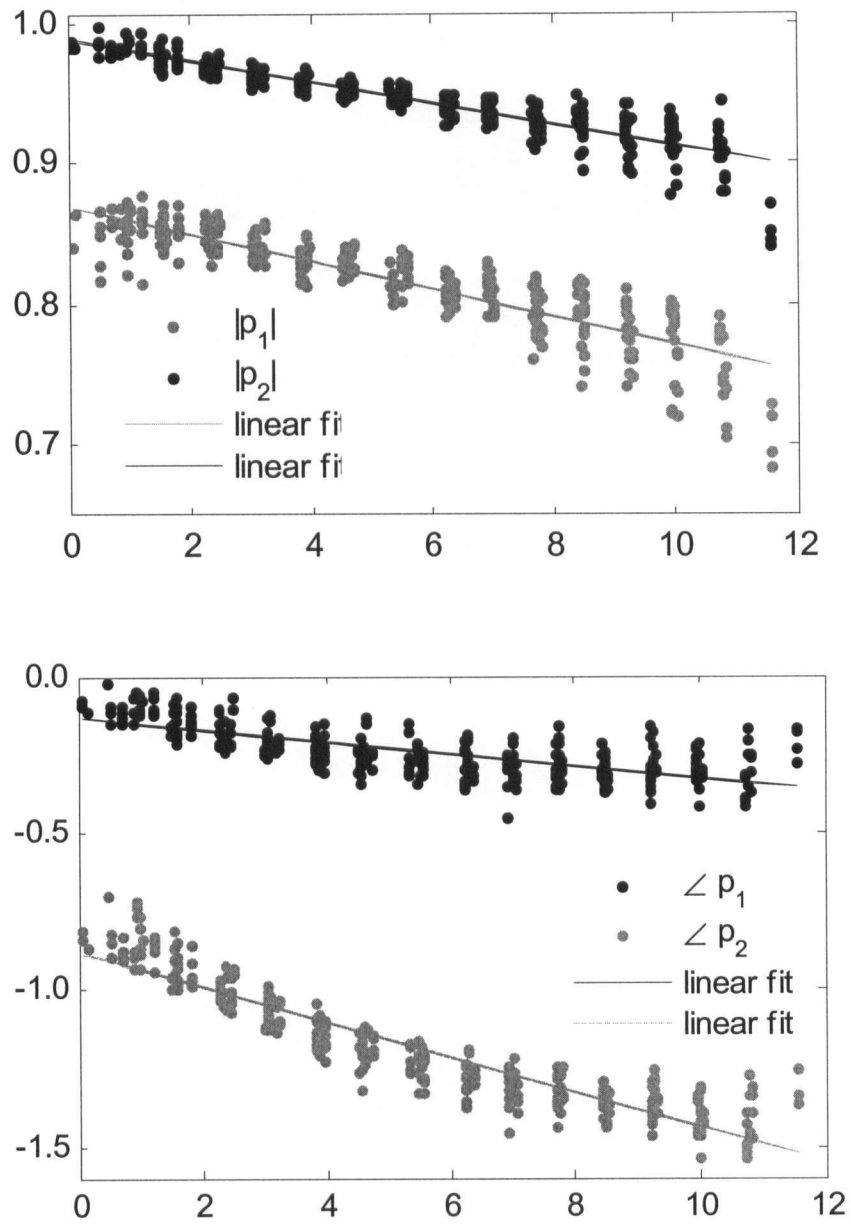
Figure 3.8 a) Pole Magnitude vs Distance b) Pole Phase vs Distance

## 3.4.2 Pole's Dependency on Receiver's Mounting Positions

Applications on demand in aircraft cabin require receiving antenna placed at different locations. For configuration where receiving antenna is placed at headrests, first order poles are found near the unit circle and the magnitudes fall are greater than 0.94(as seen in Figure 3.9a); variance of first poles is relatively small compared to armrest and footrest case. This result is anticipated because receivers placed at headrests enjoy LOS paths most of the time. Dominant cluster can be found in those headrest channels and the channel energy is concentrated at delays when significant multipaths arrive. The delay that models dominant cluster arrival is obtained by first order pole phase. From the cumulative density function in Figure 3.9 c, it is observed that the first pole phase fall in the range of -0.4458 to -0.0856, equivalent to propagation delay of 11.4ns and 59.7ns. For receiver placed armrest positions, transmitter enjoys LOS on aisle seats; for middle and window seats, LOS are obstructed. In comparison with headrest case, the first order pole for armrest placed receiver tilt more towards origin because i) not all the channel has dominant cluster (strong poles with large magnitude) ii) channel energy spread more over time due to NLOS paths (Figure 3.9a). For receiver placed at footrest positions, LOS paths are completely obstructed. The first order pole magnitude thus has lower magnitudes and larger angular spreads compared with the previous scenarios. The second order pole has similar properties as the first pole (Figure 3.9b and d). Overall, pole with large magnitude and small phases are found in positions when LOS exists, including headrests positions and aisle seat armrests and footrests. Small poles with more negative phases are found in NLOS cases, including armrest and footrest at middle and window seats.
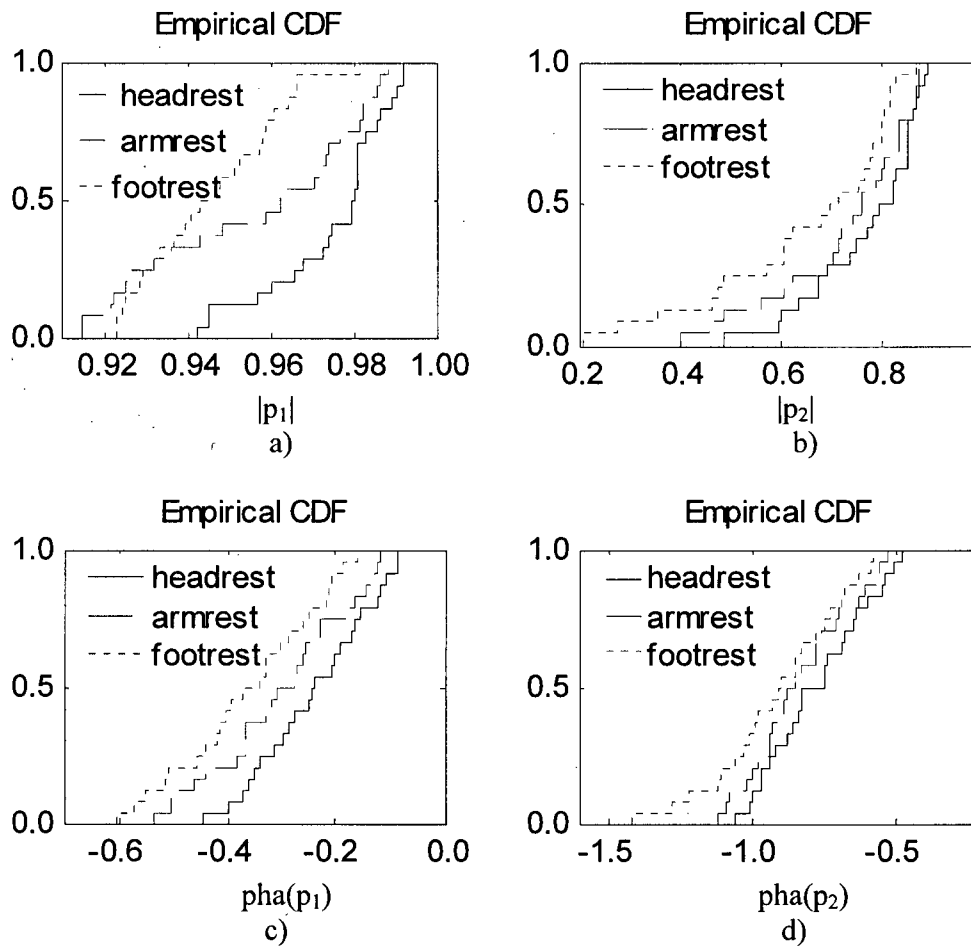
Figure 3.9 a) CDF for first order pole magnitude; b) CDF for second order pole magnitude; c) CDF for first order pole phase; d) CDF for second order pole phase

## 3.4.3 Influence of People

Measurements have been conducted in an aircraft passenger cabin to investigate influence of passengers on the radio channel. The measurement configuration was divided into three scenarios: i) within an empty aircraft ii) with every other seat occupied by passengers from row 4 to row 16; iii) with all seats occupied by passengers from row 4 to row 10. Figure 3.10a shows pole locations for empty, half full and full aircraft. Figure 3.10b and c show pole locations based on data from 10 locations with receivers placed at headrest and armrest positions respectively. The first order pole does not show a significant variation with change of number of passengers. The second order poles however show a decrease in pole magnitude as passenger increases. The effect is more obvious when receiver is placed at armrest. The excess attenuation at location x is found by examining pole energy in an empty aircraft with those in aircraft with 50% of the seats occupied, and every seat occupied aircraft (as in Figure 3.6).

$$\widetilde{X}_{atten}(x) = \sum_{i=1}^{k} p_{i\_empty}(x) p_{i\_empty}^{*}(x) - p_{i\_full}(x) p_{i\_full}^{*}(x) \qquad (3.9)$$

We conclude more influence is introduced by people when receiver is placed at armrests than headrests. This is opposite to what has been found in indoor laboratory environment where people have more influence on LOS channel. This difference is due to the fact that in aircraft environment all passengers are assumed to be remaining in their seats for most of the time and transmit antenna is mounted on the ceiling level, passengers do not completely block the LOS when receiver is placed at the headrest. For armrest positions which consist of both LOS and NLOS, passengers are part of the scattering environment; they introduce excess attenuation to the channel.

Table 3.6 Attenuation of Passengers on Poles

| Rx | $E\{P_{empty}\} - E\{P_{full}\}$ | var | $E\{P_{empty}\} - E\{P_{half}\}$ | var |
|---|---|---|---|---|
| armrest | 1.7030dB | 0.0832dB | 1.4610dB | 0.0050dB |
| headrest | 1.4903dB | 0.0098dB | 1.4107dB | 0.0012dB |
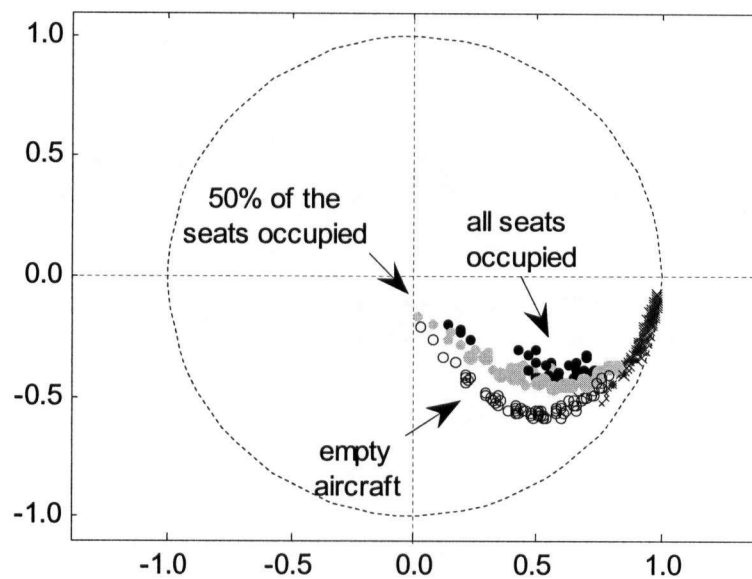


(a)
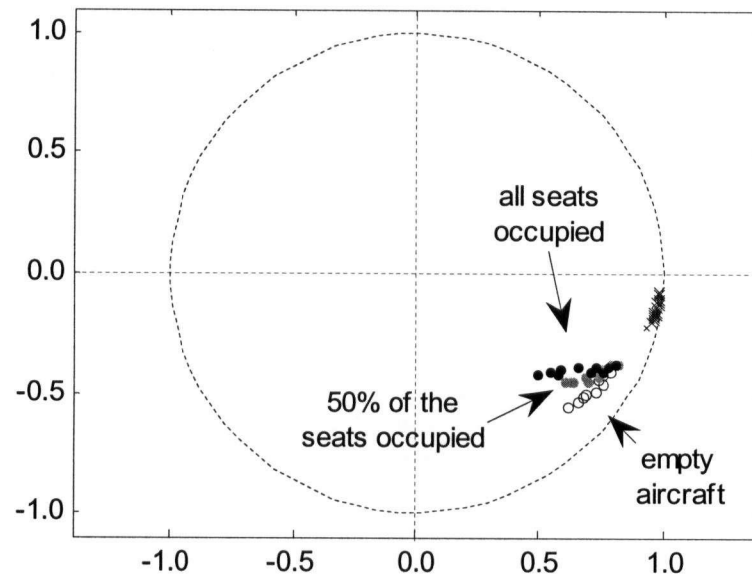
(b)
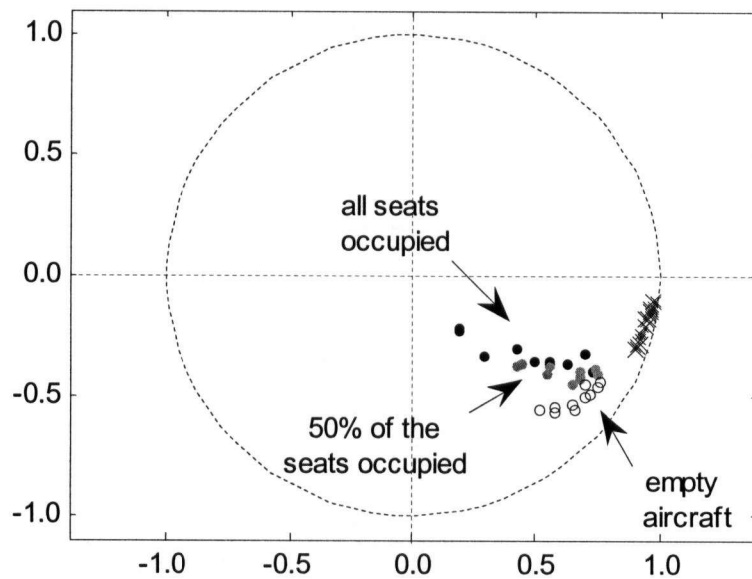


(c)

Figure 3.10 Pole Plots for Receivers Placed at (a) all positions; (b) headrest; (c) armrest within empty, half-full, and full aircraft

## 3.4.4 RMS Delay Spread

The RMS delay spread is the square root of the second central moment of the power delay profile. It is an important parameter for system design because it measures the dispersion of radio channel, and consequently the inter-symbol interference. When no equalization or diversity technique is applied to the channel, the RMS maximum reliable data rate $R_{max}$ is given by [12]

$$R_{max} = 1/4\tau_{rms} \qquad (3.10)$$

In previous indoor channel studies, many researchers have found RMS delay spread follows a normal distribution. For point to multipoint setup, the average values and standard deviation of RMS delay spread in an empty aircraft is studied and shown in Table 3.7.

Table 3.7 RMS Delay Spread for Different Receiver Locations

| Rx | Aisle seat $\overline{\tau}_{rms}$ | Aisle seat $\sigma$ | Middle seat $\overline{\tau}_{rms}$ | Middle seat $\sigma$ | Window seat $\overline{\tau}_{rms}$ | Window seat $\sigma$ |
|---|---|---|---|---|---|---|
| Head | 4.07 | 1.64 | 7.83 | 2.96 | 13.81 | 4.27 |
| Arm | 8.89 | 1.90 | 20.98 | 6.91 | 21.71 | 6.39 |
| Foot | 18.71 | 3.82 | 22.75 | 4.22 | 23.92 | 3.48 |

From the results it is concluded that the $\overline{\tau}_{rms}$ is minimum when receiver is mounted at headrests. This is true for all seating positions. Receivers at headrest positions enjoy the LOS views of transmitter and thus values of $\overline{\tau}_{rms}$ are low at these positions, typically between 4ns and 14ns. Armrest and part of the footrest at aisle seats also have unobstructed path to the transmitter; therefore, values of RMS delay spread at these positions are smaller than those found at other seats. Larger RMS delay spread is found when path is obstructed, typically in armrest and footrest positions of middle and window seats.

RMS delay spread increases with distance as shown in Figure 3.12a. Using previously characterized AR-FD parameters, channel impulse responses are regenerated. The RMS delay spread from characterized CIR and from original CIR are compared in Figure 3.12b. The result shows AR-FD model can characterize the aircraft channel reasonably well. With passengers introduced to the aircraft cabin, RMS delay spread decreases. Passengers block some paths and introduce excess attenuation approximately 1 to 3dB across the channel. The RMS delay spread is reduced by10ns.
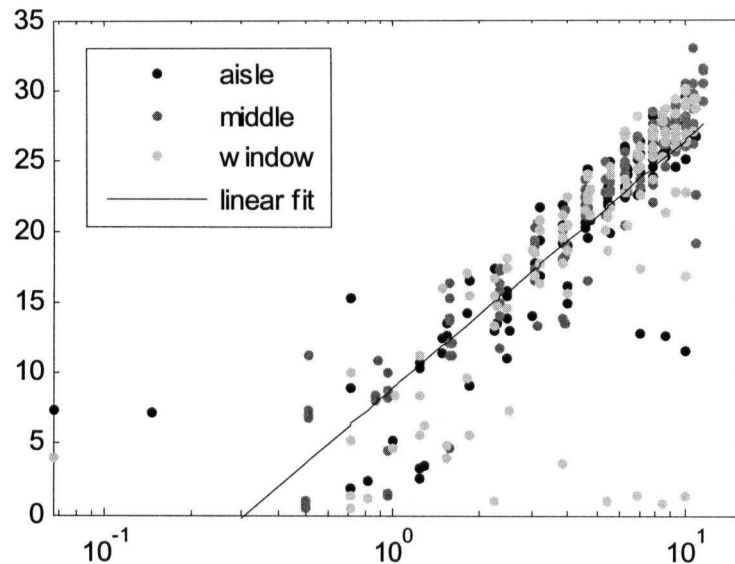


(a)
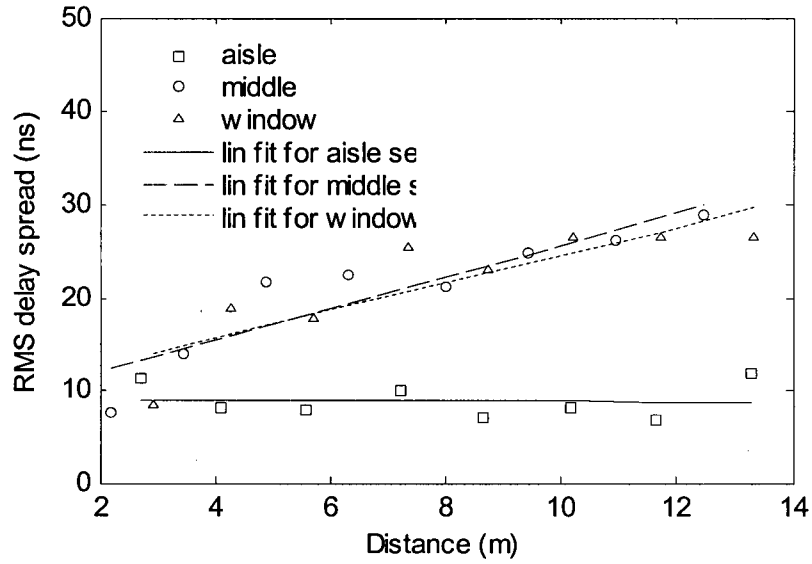
(b)
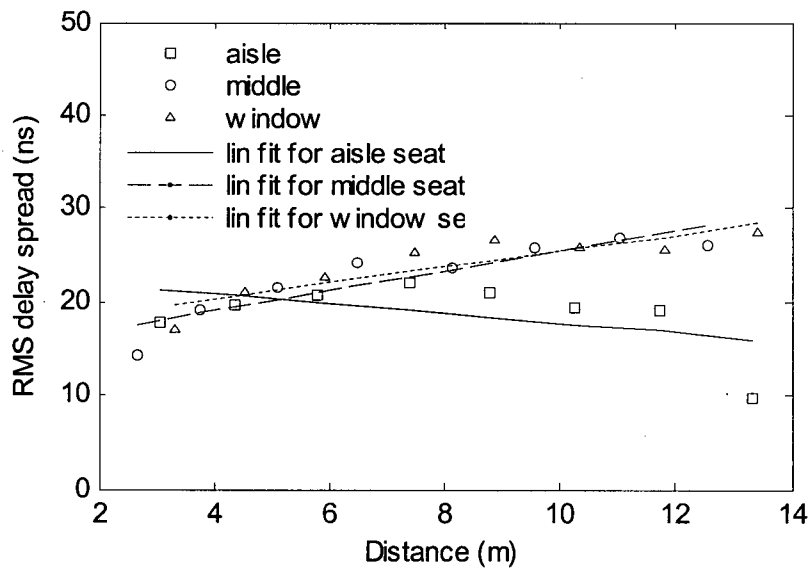


(c)

Figure 3.11 RMS delay spread for aisle/middle/window seats at a) headrest b) armrest c) footrest

For point-to-multipoint configuration, LOS exists for some receiving antenna mounting location; for peer-to-peer configuration, we found that NLOS dominates and

RMS delay spread increases with distance as shown in Figure 3.12a. Using previously characterized AR-FD parameters, channel impulse responses are regenerated. The RMS delay spread from characterized CIR and from original CIR are compared in Figure 3.12b. The result shows AR-FD model can characterize the aircraft channel reasonably well. With passengers introduced to the aircraft cabin, RMS delay spread decreases. Passengers block some paths and introduce excess attenuation approximately 1 to 3dB across the channel. The RMS delay spread is reduced by10ns.



(a)
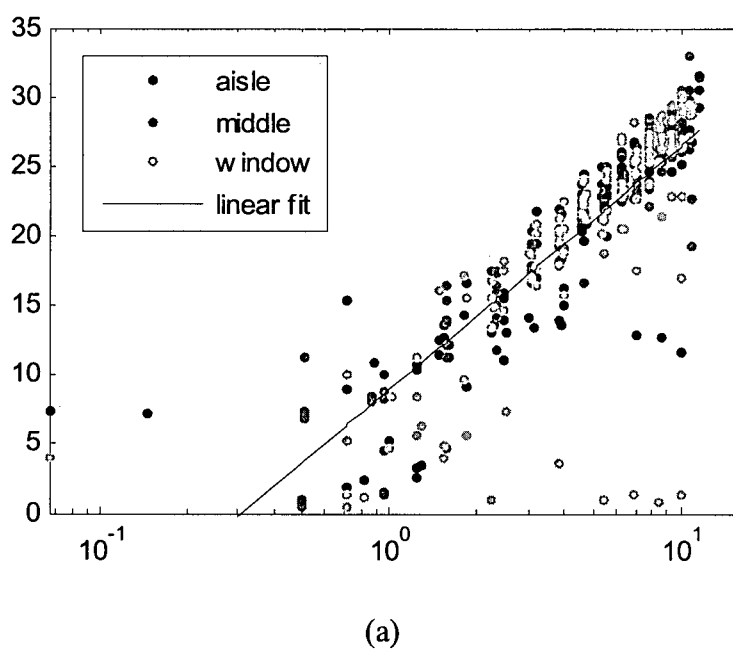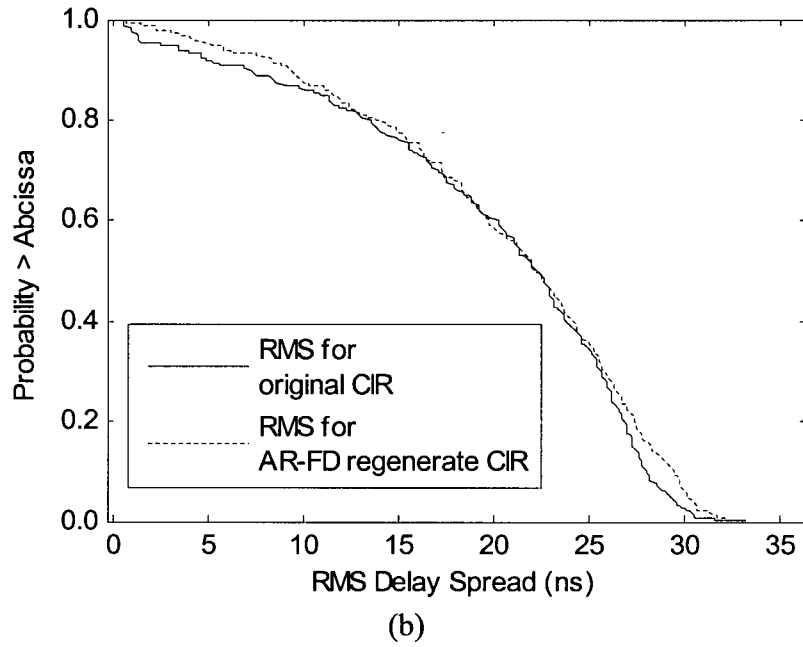
Figure 3.12 (a) RMS delay spread for peer-to-peer configuration (b) CDF for RMS derived from 4a simulated CIRs vs RMS derived from AR-FD simulated CIRs.

## 3.4.5 Coherence Bandwidth

Coherence bandwidth is the statistical average bandwidth of the channel, over which signal propagation characteristics are correlated. It is defined on basis of the complex autocorrelation

$$\phi_{HH}[f_n, f_{n+m}] = \sum_{k=-N}^{N} H(f_n)H^*(f_{n+m-k}) \qquad (3.11)$$

The coherence bandwidth is defined as the value where $\phi_{HH}$ decreases by 3dB from the maximum. The value of coherence bandwidth is determined by the fading statistics of the channel at a particular location. At locations where a channel does not experience deep fade and channel is very flat, the channel will have a larger coherence bandwidth. Examining more than 500 complex responses in an empty aircraft environment, we found 90% of channel measurements have coherence bandwidth falls between 4.75MHz to 25

69

MHz, with the mean of coherence bandwidth equal to 7.125MHz. For some LOS locations where the distance between transmitter and location are placed very close together (< 0.5m), the coherence bandwidth becomes very large; no deep fades can be seen in such channel. For the locations where large coherence bandwidth is found, the value for coherence bandwidth over 350 MHz that can be considered flat (as seen in Figure 3.13); less than 10% of data falls in this category and is excluded from data set.
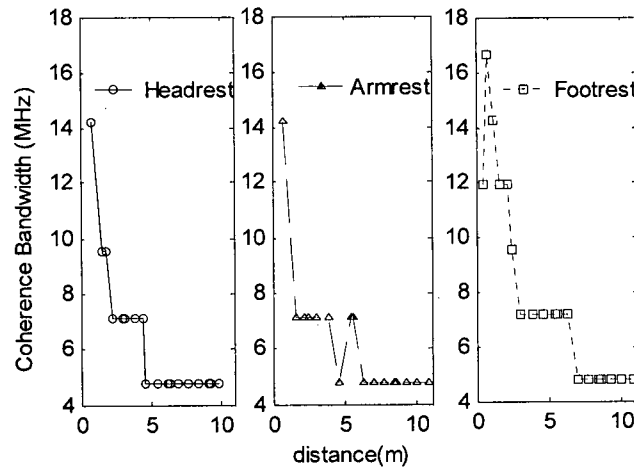


Figure 3.13 Coherence Bandwidth vs Distance for Empty Aircraft

The coherence bandwidth in Figure 3.13 shows when transmitter is placed at a fixed location (row 4 and window seat), and receiver is placed at headrest, armrest, footrest locations through row 4 to row 18. As the receiver moves father away from the transmitter, the coherence bandwidth decreases. This is as expected because coherence bandwidth is inverse proportional to RMS delay spread. RMS delay spread increases with distance. Coherence bandwidth thus decreases with distance. Another observation is coherence bandwidth does not change significantly with change in receiver's vertical locations. Generally the coherence bandwidth is reverse proportional to the RMS delay spread in terms of [12].

$$BW_{coh} = \frac{1}{\alpha_o \tau_{RMS}}$$
(3.12)

$$BW_{coh} = \frac{1}{\alpha_o \tau_{RMS}} \qquad (3.12)$$

The parameter $\alpha_o$ of the inverse proportional relation for coherence bandwidth and RMS delay spread for the UWB aircraft channel is characterized in the LMS sense, and for aircraft channel $\alpha_o$ is found to be 7.3125 (as in Figure 3.14) Thus, we have

$$BW_{coh} = \frac{1}{7.3125 \tau_{RMS}} \qquad (3.13)$$
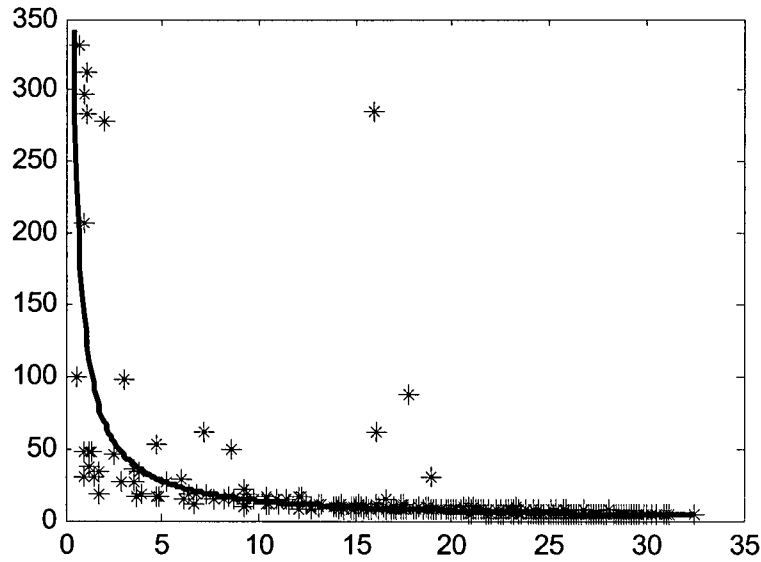


Figure 3.14 Coherence Bandwidth vs. RMS delay spread

## 3.5 Conclusion

Our results show that a second order AR-FD model can perform reasonably well for estimating UWB aircraft channel. Second order pole locations are most close to those found in indoor NLOS environment. Passengers introduce 1-3 dB excess attenuation across the channel, and the autoregressive second poles show decrease amplitude as the

density of passenger increases. We show that regardless of receiving antenna's vertical positions (headrest/armrest/footrest), receiver placed at aisle seats has smaller RMS delay spread. The RMS delay spread for LOS channels doesn't increase with distance; for NLOS case, RMS delay spread increase with distance.

# Bibliography

[1] Howard, S. J. and Pahlavan, "Autoregressive Modeling of Wide-Band Indoor Radio Propagation," IEEE Trans. Commun., vol. 40, no. 9, pp. 1540-1552, Sep. 1992

[2] Ghassemzadeh, S. S, Jana R., Rice, C. W., Turin W., and Tarokh, V., "Measurement and Modeling of an Ultra-Wide Bandwidth Indoor Channel," IEEE Trans. Commun., vol. 52, no. 10., pp. 1786-1796, Oct. 2004

[3] G. J. M. Jassen, P. A. Stigter and R. Prasad, "Wideband Indoor Channel Measurements and BER Analysis of Frequency Selective Multipath Channels at 2.4, 4.75 and 11.5GHz," IEEE Trans. Commun., vol. 44, no. 10, pp. 1272-1288, Oct. 1996

[4] M. A. Do and S. Sun, "Statistical Modeling of Broadband Wireless LAN Channels at 18 GHz Using Directive Antennas," International J. Wireless Inf. Networks, vol. 4, no. 1, Jan. 1997

[5] C.P. Niebla, "Topology and Capacity Planning for Wireless Heterogeneous Networks in Aircraft Cabins," IEEE PIMRC 2005, vol 3, pp 2088-2092, Sep. 2005

[6] A.F. Molisch et al., "IEEE 802.15.4a channel model - final report," Tech. Rep., IEEE P802. 15-04/662r0-SG4a, Sep. 2004

[7] A, Jahn, M, Holzbock, J. Muller, R, Kebel, A, Rogoyski, O, Franzrahe, M. Werner, and F. Hu, "Evolution of Aeronautical Communications for Personal and Multimedia Services," IEEE Commun. Mag., vol. 41, no. 7, pp. 36-43, Jul. 2003

[8] M, Youssef, and L, Vahala, "Effects of Passengers and Internal Components on Electromagnetic Propagation Prediction inside Boeing Aircrafts," IEEE APS 2006, pp. 2161-2164, Jul. 2006

[9] G, Hankins, L Vahala and J. H. Beggs, "Electromagnetic Propagation Prediction Inside Aircraft Cabins," IEEE APS 2004, pp 2227-2230, Jun. 2004

[10] J. Chuang, N. Xin, H. Huang, S Chiu, and David G. Michelson, "UWB Radiowave Propagation within the Passenger Cabin of a Boeing 737-200 Aircraft," IEEE VTC 2007-Spring, pp. 496-500, Apr. 2007

[11] N. Xin and D. G Michelson, "AR Frequency Domain Representation of the IEEE 802.15.4a Standard Chanel Models," IEEE WCNC 2007, pp. 2058-2062, Mar. 2007

[12] Rappaport, T. S., "Wireless Communications Principles and Practice", Second Edition, 2002, Chapter 5, pp. 202

[13] S. L. Marple Jr., "Digital Spectral Analysis with Applications" Prentice-Hall, pp. 229, 1987

[14] N. R. Diaz, "Wideband Channel Characterization for Wireless Communications inside a Short Haul Aircraft," IEEE VTC 2004-spring, vol. 1, pp. 223-228, May. 2004

# Chapter 4

# Comparison and Classification of UWB Channel Models in the Frequency Domain

## 4.1 Introduction

[3]Ultrawide band (UWB) has emerged as a promising technology for next generation multimedia data streaming within short ranges. Its two anticipated major applications include wireless interconnections throughout digital home and office and low maintenance sensor networks. Deployment of UWB devices requires a reliable channel model and model parameters that are suitable for the evaluation of system performance. Currently, UWB propagation is modeled using time-domain models based on the well-known Saleh-Valenzuela (S-V) model. The existing (S-V) model parameters are characterized as constant parameters for eight types of channels, namely CM 1-8. It is difficult to access and compare channel performance based on constant model parameters. On the other hand, if system designers were to use the S-V model in a new environment, like aircraft or underground mine, the model parameters have to be re-characterized. There is no existing scheme that allows us to compare UWB channels in different environment automatically and efficiently using S-V model parameters.

For channel propagation problems, very often the environment to be characterized is unconventional or unfamiliar. Comparison and similarities drawn between the new environment and existing channel models would help system designers deploying wireless system in unfamiliar environment.

---

[3]A version of this chapter will be submitted for publication: N. Xin and D. G. Michelson, "Comparison and Classification of UWB Channel Models in the Frequency Domain," to *IEEE Transaction on Wireless Communication*, Oct. 28, 2007

Identifying the type of channel the device is operating in has been recognized as a crucial step for optimizing system performance. For instance, Guevenc et. al have used kurtosis, mean excess delay, and RMS delay spread to identify LOS channels from aggregated LOS and NLOS channels in localization applications [9]. The possibility of recognizing a channel response from unidentified source, where the measurement site and setup are unknown, as a sample of a particular standard channel model has not exploited. The challenge thus lies in searching a set of channel parameters which i) compares how similar CM 1-8 to each other in a statistical sense and ii) provides us with some information on how similar a new set of channel impulse responses (CIRs) is to existing models.

Several researchers have proposed to characterize UWB channels in frequency domain using autoregressive approach (AR) [1][2][3]. The autoregressive model uses parameters such as autoregressive coefficients, driving noise and initial conditions. In [1][2], the researchers show statistics of second order autoregressive poles in office and residential environment can be used to characterize complex channel frequency response. In particular, the work in [3] demonstrated autoregressive poles characterized in each of the 4a documented channel models follow standard distributions.

Autoregressive model parameters is widely used as features for characterizing different classes of music, EEG signals and sensor array processings [20][21]. In this paper, we propose using statistically characterized AR-FD model parameters to classify UWB channels from diverse environment. A reliable estimation and classification of channel parameters belonging to a modeled environment will allow a better understanding of channel propagation and AR-FD model parameters in that particular environment. This classification will also help system designers make a fair comparison of UWB channel conditions in different environments and deploy UWB devices in new or extreme environment, like aircraft cabins and underground mines.

The reminder of the paper is organized as follow: Section 4.2 presents general background of AR-FD model and provides a complete statistical description of model parameters. Two novel parameters, first and second moment of pole, are introduced and

characterized statistically in this section. Together with AR-FD parameters, these two new parameters serve as attributes of our proposed classifier. Section 4.3 presents a supervised Bayesian classifier with Naïve Bayesian assumption. The final decision of the classifier is based upon evaluating joint probabilities of good attributes using maximum likelihood criterion. Section 4.4 shows simulated classification results for untrained data from each standard channel model. Applicability of the proposed classifier for complex channel response from an unfamiliar source is demonstrated using channel responses collected in aircraft environment. Section 4.5 concludes the paper.

## 4.2 AR-FD Model Features Extraction

Some success has been demonstrated in characterizing wideband office and residential UWB channels using AR technique [1][2]. Our work in [3] in particular shows AR-FD model is appealing for modeling UWB channels in a range of indoor environments. Since the AR-FD model gives a statistical representation of the different types of channel frequency responses with reasonable accuracy, we can use the model parameters as attributes for a UWB channel classifier.

Multivariate AR-FD model and determination of appropriate order for the AR-FD model are briefly reviewed here. We show that the accuracy of estimating UWB channels response using AR technique depends on existence of dominant clusters in a power delay profile.

### 4.2.1  AR-FD Model General Description

To apply AR analysis to the complex UWB frequency response, we assume that the current frequency tap can be expressed as a cumulative sum of previous frequency taps. The memory of previous frequency taps is determined by order of the model. In the context of our study, we assume that the UWB channel frequency responses are

stationary with respect to time. The complex channel frequency response (CFR) is governed by,

$$\hat{H}(f_k,t;x) + \sum_{i=1}^{p} a_i \hat{H}(f_{k-i},t;x) = U(f_k,t;x) \tag{4.1}$$

where $\hat{H}(f_k,t,x)$ is the kth sample of the complex frequency response at location x, $a_i$ is the AR coefficient of the (k-i)th frequency taps and $U(f_k,t;x)$ is the white Gaussian noise added to the kth sample. This assumption is valid if the spacing between correlated neighboring frequency taps is equal or less than coherence bandwidth (in terms of MHz). With this assumption, we can treat the complex channel frequency response as the output of a linear filter with order k, which takes the form of

$$G(z) = \frac{1}{1 + \sum_{i=1}^{k} a_i z^{-i}} \qquad \text{or}$$

$$G(z) = \frac{1}{\prod_{i=1}^{k} (1 - p_i z^{-1})} \tag{4.2}$$

where $\{p_i\}$ are a collection of poles. The above all-pole filter is fed by complex Gaussian noise with variance determined by energy of the output $R_{HH}(0,x)$ over energy of the filter $R_{GG}(0,x)$. The autoregressive coefficient representation and the poles representation of the filter are interchangeable, but the poles have more physical meanings: they can be seen as an indication of significant cluster arrivals.

## 4.2.2 Data Acquisition and Preprocessing

AR-FD model parameters are obtained through Fourier transform of a large collection of channel impulse responses generated using the CIR generation code in the 802.15.4a final report [10]. Each set of AR-FD model parameter is derived from 8320 snapshots of unambiguously identified channel frequency responses from a particular environment as

shown in Figure 4.1. Before estimating AR-FD parameters, an information criterion is used to determine order of the model. Given a selected model order, snapshots of independent channel response are fed into an AR estimation algorithm [18] and yield multiple copies of model parameters. The AR-FD model parameters include $k$th order complex poles $\{p_1,...p_k\}$, $k$th order initial conditions $\{H_1,...H_k\}$, and variance of the input white noise, $\sigma_w$. All the parameters have their own distributions and a thorough discussion will be presented in later section.
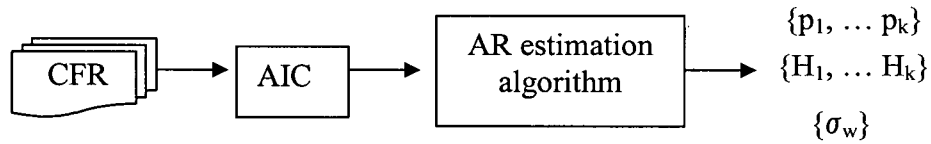


Figure 4.1 AR-FD Model Acquisition and Preprocessing

## 4.2.3 Akaike Information Criterion

In practice, an appropriate model order is selected by information theoretic function [18]. The Akaike information criterion (*AIC*) is a measure of goodness fit of an estimated model. It trades off between complexities (the order of an estimated model) against how well the data fits an estimated model, in terms of prediction error. A possible solution of the model order maybe derived by minimizing the following theoretic function [8][18]

$$AIC = \log(V) + \frac{2k}{N} \tag{4.3}$$

$$V = \det(\frac{1}{N} \sum_{j=1}^{N} \varepsilon(t, \hat{\theta}_j) \varepsilon(t, \hat{\theta}_j)^T) \tag{4.4}$$

where $V$ is the loss function (also known as the variance of the estimated parameters), $k$ is the number of estimated parameters, $N$ is the number of data used for estimation and $\hat{\theta}_N$ is the estimated AR coefficients. The term $2k/N$ is a penalty for use of extra AR coefficients that do not substantially reduce prediction error.

In previous work [3], we have showed that most of channels frequency responses (CFRs) from indoor environments can be modeled by second order AR-FD model based on the rate of change in AIC values. In particular, office LOS, outdoor LOS and NLOS channels are more accurately represented by second order AR-FD model. For outdoor channels, a higher-order model might be more appropriate to obtain less prediction error. For the scope of this study, we focus on classification of the second order AR-FD model.

## 4.2.4 AR-FD Parameters Statistics

### 4.2.4.1  AR Poles

From classical parameter estimation, pole close to unit circle implies the corresponding spectra has significant energy at a particular delay [1][3]

$$\tau = \frac{\angle 1 - \angle p}{\Omega_s} = \frac{\angle 1 - \angle p}{2\pi f_s} = \frac{-\angle p}{2\pi f_s} \qquad (4.5)$$

Poles locate near the origin implies the corresponding spectra are significantly attenuated. In UWB channel characterization, the magnitude of pole affects the shape of the power delay profile.

If a second order AR model is to be used and the first order poles are found close to the unit circle, the corresponding power delay profiles have a dominant cluster. This is mostly found in channels with LOS paths. On the other side, if the first order pole is farther away from the unit circle, the related channel impulse response does not experience a strong cluster arrival and envelope of power delay profile is anticipated to be Rayleigh distributed. Pole phase can be directly related to distance through (4.5). Poles derived from a particular set of channel frequency responses varies because i) the dimension of each environment varies; if the sampling frequency $f_s$ and the number of sampling points $N$ are fixed, the pole locations, especially the difference between pole phases, suggest the dimension of the modeled environment ii) For some environment, such as industrial environment, part of second order poles are found near origin (Figure 4.3c). The energy in the corresponding channel is very spread out. Thus, we can utilize poles magnitudes and pole phases as features to classify channels from different environments. Figure 4.2 and 4.3 show the AR-FD second order pole locations for 4a documented environments. In previous work, the autoregressive poles are found to be dependent on distance [2]. Magnitudes and phases of higher order poles are functional dependent because they are functions of distance.

## 4.2.4.2 Initial Conditions and Variance of Driving Noise

Initial conditions of the AR-FD model do not affect stability of the system. They were previously characterized as distance dependent parameter with a Gaussian random part in residential indoor environment. Variance of driving noise was characterized as a lognormal distributed variable which also appeared to be dependent on distance in [2].

Distributions of initial conditions and variance of driving noise in other indoor environments and outdoor will be exploited in the next section.

## 4.2.4.3  Moments of Poles

We introduce two parameters which are first and second moment of pole magnitude. The parameters are defined as follows

$$\hat{m}_1 = \frac{\sum_{i=1}^{2} \angle p_i \, | p_i |}{\sum_{i=1}^{2} | p_i |} \tag{4.6}$$

$$\hat{m}_2 = \frac{\sum_{i=1}^{2} | p_i | (\angle p_i)^2}{\sum_{i=1}^{2} | p_i |} - \hat{m}_1 \tag{4.7}$$

First and second moments of poles, derived from AR-FD model poles, are analogous quantities of mean excess delay and rms delay spread since the poles as described before can be used to represent where the significant energy is located in a channel impulse response. We have incorporated these two parameters into our classifier since it is well known that these two parameters are derived from the geometrical properties of the channel; specifically, they describe the relative locations of the scatterers in the environment with respect to the receiver. Furthermore, as an example, mean excess delay and rms delay spread were used as features to separate LOS and NLOS channels in [9] for localization applications.  Note that since the moments of the poles are derived from the magnitude and phase of poles themselves, they are considered as to be totally functional dependent on the pole parameters.
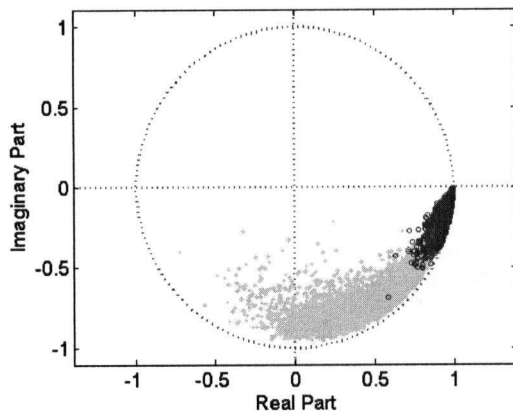
a) CM 3 Residential LOS
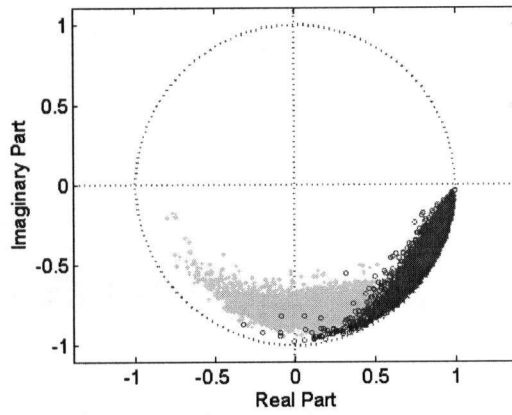
b) CM 4 Residential NLOS
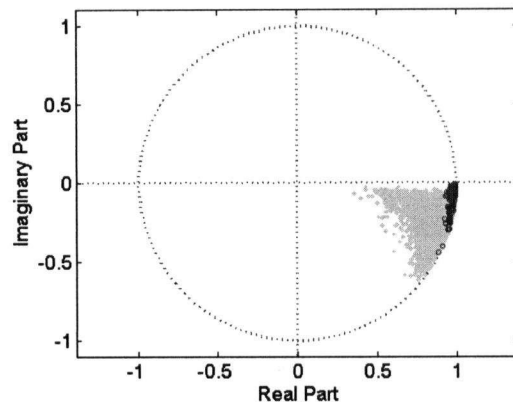
c) CM 3 Office LOS
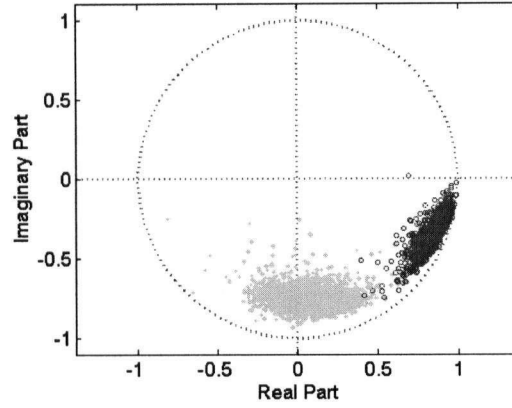
d) CM 4 Office NLOS

Figure 4.2. Distribution of AR-FD pole locations for LOS and NLOS cases of the residential and office environments. (Dark points – first pole locations, light point – second pole locations.)
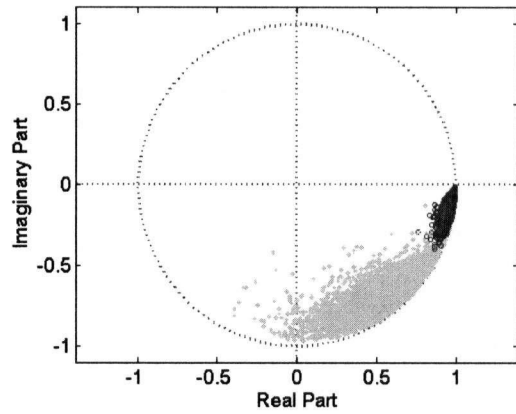
a) CM 5 Outdoor LOS
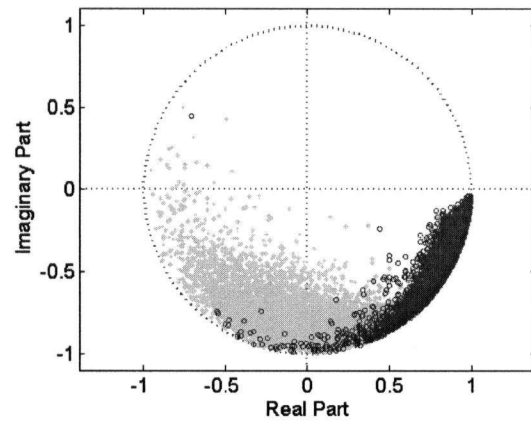
b) CM 6 Outdoor NLOS
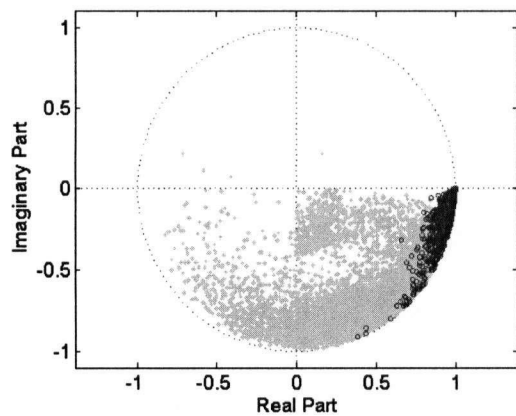
c) CM 7 Industrial LOS
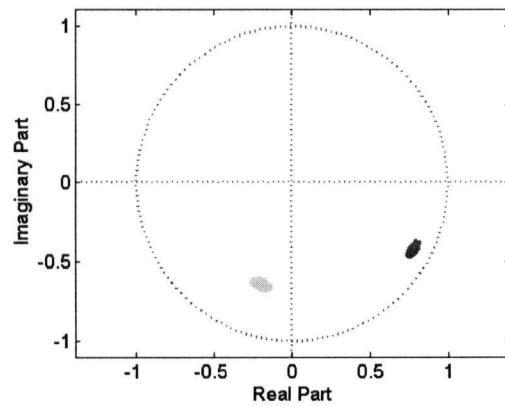
d) CM 8 Industrial NLOS

Figure 4.3 Distribution of AR-FD pole locations for LOS and NLOS cases of the outdoor and industrial environment

## 4.2.5 Characterization of AR-FD Features as Prior Knowledge

Given a predefined channel model from a specific environment, the AR-FD model parameters can be characterized statistically. The approach is based on previous work in [3]. To choose an appropriate distribution for an AR-FD model parameter, several candidate distributions are compared using the Kolmogorov-Smirnov (K-S) goodness of fit test. The distributions under test include extreme value, beta, logistic, normal and weibull. Given a channel model from a particular environment (i.e. Office LOS), conditional probability density functions of AR-FD pole statistics are characterized as depicted in Figure 4.4. It is found that most of the first order pole magnitudes can be modeled by an extreme value distribution, with a PDF given as follows

$$P(|p_1| \mid \alpha, \beta) = \beta^{-1} \exp\left\{ \frac{(\alpha - |p_1|)}{\beta} - \exp(\frac{(\alpha - |p_1|)}{\beta}) \right\} \tag{4.8}$$

or a beta distribution which takes the form of

$$P(|p_2| \mid \alpha, \beta) = \frac{(1 - |p_2|)^{\beta-1}|p_2|^{\alpha-1}}{B(\alpha, \beta)} \tag{4.9}$$

with
$$B(\alpha, \beta) = \frac{(\alpha - 1)!(\beta - 1)!}{(\alpha + \beta - 1)!} \tag{4.10}$$

The second order pole magnitude can be modeled by a Beta, extreme value, Normal or Weibull distribution depending on the modeled environment. A complete list of AR-FD pole statistics is provided in Table 4.1. From the characterization results, it is observed that the first and second order pole magnitudes very often follow the same distribution. In other words, $|p_1|$ and $|p_2|$ are not only found correlated, but also can be identified as functional dependent variables as shown in [2]. Angle($p_1$) and angle($p_2$) are functional dependent as well . These correlations are characterized in Table 4.2.

For a second order AR-FD model, initial conditions $H_1$ and $H_2$ need to be characterized; both the real and imaginary parts of initial conditions follow a normal

distribution (see Table 4.3). Real part of the $H_1$ is strongly correlated with real part of $H_2$, and imaginary part of $H_1$ and $H_2$ are strongly correlated as well. Marginal distributions for initial conditions are found to be normal. Variances of input noise for AR-FD model are characterized as lognormal distributions for all indoor environments; exponential distribution has a better fit for outdoor channels. We choose a distribution based on values of the log likelihood.

Table 4.1 AR-FD Model Parameters for CFR1 to CFR8

| Channel Model | Parameter | Distribution | $\alpha$ | $\beta$ |
|---|---|---|---|---|
| Residential LOS | $|p_1|$ | E.V. | 0.97902 | 0.0126811 |
| | $|p_2|$ | E.V. | 0.907689 | 0.0384309 |
| | ANG($p_1$) | E.V. | -0.112781 | 0.0691762 |
| | ANG($p_2$) | E.V. | -0.823681 | 0.200563 |
| Residential NLOS | $|p_1|$ | E.V. | 0.956557 | 0.0206694 |
| | $|p_2|$ | Weibull | 0.830912 | 20.1068 |
| | ANG($p_1$) | E.V. | -0.334411 | 0.162197 |
| | ANG($p_2$) | Logistic | -1.4209 | 0.143231 |
| Office LOS | $|p_1|$ | Beta | 291.06 | 1.83643 |
| | $|p_2|$ | Beta | 12.0806 | 1.13572 |
| | ANG($p_1$) | E.V. | -0.0280643 | 0.0103262 |
| | ANG($p_2$) | Logistic | -0.198357 | 0.0825399 |
| Office NLOS | $|p_1|$ | E.V. | 0.937549 | 0.0187299 |
| | $|p_2|$ | Weibull | 0.798975 | 20.1621 |
| | ANG($p_1$) | Logistic | -0.352289 | 0.0465455 |
| | ANG($p_2$) | Logistic | -1.44995 | 0.0835703 |
| Outdoor LOS | $|p_1|$ | Beta | 110.201 | 2.0347 |
| | $|p_2|$ | E.V. | 0.924297 | 0.0424312 |
| | ANG($p_1$) | E.V. | -0.080478 | 0.0406996 |
| | ANG($p_2$) | Normal | -0.899339 | 0.219821 |
| Outdoor NLOS | $|p_1|$ | Beta | 34.8605 | 1.53616 |
| | $|p_2|$ | Beta | 8.07804 | 1.30163 |
| | ANG($p_1$) | E.V. | -0.394444 | 0.135074 |
| | ANG($p_2$) | Normal | -1.52237 | 0.467246 |
| Industrial LOS | $|p_1|$ | Beta | 55.9055 | 0.92936 |
| | $|p_2|$ | Beta | 11.7672 | 1.62909 |
| | ANG($p_1$) | E.V. | -0.0402077 | 0.0348511 |
| | ANG($p_2$) | E.V. | -1.00777 | 0.455724 |
| Industrial NLOS | $|p_1|$ | Normal | 0.883227 | 0.0054326 |
| | $|p_2|$ | Normal | 0.674853 | 0.0097030 |
| | ANG($p_1$) | Normal | -0.504287 | 0.0155721 |
| | ANG($p_2$) | Normal | -1.86243 | 0.0254698 |
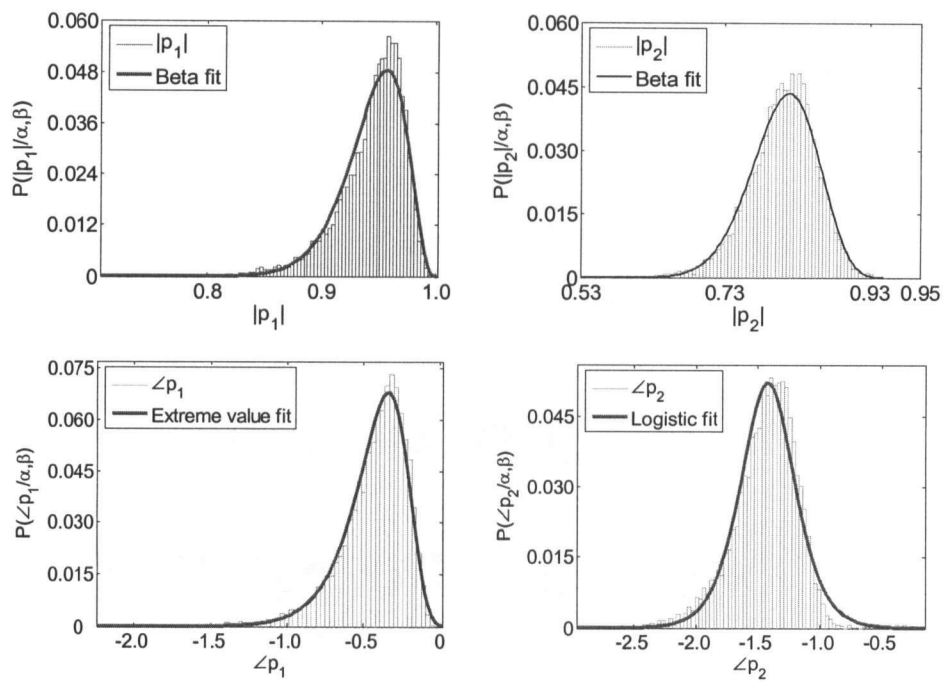
Figure 4.4 Conditional Probability Density Function of AR-FD Parameters for CFR3
Office LOS Channel

Table 4.2 Correlation of AR Pole Magnitudes and Phases

| CM | $\rho_{|p1|, |p2|}$ | $\rho_{pha(p1), pha(p2)}$ |
|----|----------|----------|
| 1 | 0.2384 | -0.0924 |
| 2 | 0.1706 | 0.5656 |
| 3 | 0.0949 | -0.0248 |
| 4 | 0.1752 | 0.0951 |
| 5 | 0.1664 | -0.0159 |
| 6 | 0.4977 | 0.3925 |
| 7 | -0.1364 | 0.0817 |
| 8 | 0.1695 | 0.2756 |

Table 4.3 Initial Conditions for CFR 1-8

| CM | | $Re\{H_1\}$ | $Im\{H_1\}$ | $Re\{H_2\}$ | $Im\{H_2\}$ |
|----|----|----------|----------|----------|----------|
| 1 | $\mu$ | -3.56e-5 | 7.58e-5 | -1.49e-5 | 2.93e-5 |
|   | $\sigma$ | 5.79e-3 | 5.79e-3 | 5.76e-3 | 5.76e-3 |
| 2 | $\mu$ | -4.85e5 | -1.18e-5 | -6.48e-5 | 1.56e-5 |
|   | $\sigma$ | 2.73e-3 | 2.75e-3 | 2.71e-3 | 2.75e-3 |
| 3 | $\mu$ | 1.69e-5 | 6.22e-5 | 1.55e-5 | 5.34e-5 |
|   | $\sigma$ | 7.97e-3 | 7.97e-3 | 7.98e-3 | 7.96e-3 |
| 4 | $\mu$ | -1.35e-4 | 2.49e-4 | 8.36e-5 | 2.79e-4 |
|   | $\sigma$ | 1.22e-2 | 1.23e-2 | 1.22e-2 | 1.24e-2 |
| 5 | $\mu$ | 2.53e-4 | 1.51e-4 | 3.59e-4 | 1.01e-4 |
|   | $\sigma$ | 9.48e-3 | 9.47e-3 | 9.47e-3 | 9.52e-3 |
| 6 | $\mu$ | -3.11e-5 | 1.47e-4 | 1.12e-4 | 9.51e-5 |
|   | $\sigma$ | 7.33e-3 | 7.51e-3 | 7.37e-3 | 7.51e-3 |
| 7 | $\mu$ | 6.86e-5 | 1.77e-4 | 1.15e-4 | 1.42e-4 |
|   | $\sigma$ | 1.25e-2 | 1.26e-2 | 1.25e-2 | 1.26e-2 |
| 8 | $\mu$ | -4.32e-5 | 3.77e-5 | 1.94e-4 | 2.41e-5 |
|   | $\sigma$ | 4.60e-3 | 4.64e-3 | 4.72e-3 | 4.65e-3 |

Table 4.4 Variance of Input Noise for CFR 1-8

| Distribution | Residential Logn($\mu,\sigma$) | Office Logn($\mu,\sigma$) | Outdoor Exp($\mu$) | Industrial Logn($\mu,\sigma$) |
|----|----|----|----|----|
| LOS | -11.6377 0.808253 | -16.8811 0.9636 | 5.6595e-6 | -12.367 1.37264 |
| NLOS | -10.7521 0.440403 | -9.6782 0.3712 | 5.6895e-3 | -10.5998 0.0346458 |

## 4.3 AR-FD Based Channel Classification

The main purpose of our classification algorithm is to decide whether a new measured channel frequency response (from a new environment or a new measurement from known environment) belongs to a particular channel model $c_i, i = 1,...8$, with $c_i \in C$. The conditional probability densities of AR-FD parameters are characterized in previous session as prior.

In the first part of the classifying algorithm, Bayes decision rule finds the conditional probability for a single attribute. Then, conditional probabilities of all the attributes are considered using Naïve Bayesian assumption. Finally the most probable channel model is selected based on maximum likelihood criterion

## 4.3.1 One Attribute Classifier Using Bayesian Learning

In previous section, snapshots of channel frequency response are characterized to yield attributes (features) of the AR-FD model. The probabilistic model shown in Table 4.1, Table 4.3 and Table 4.4 (poles, initial conditions and variances of noise respectively) become our prior. The posterior probability that we seek for is the hypothesis (likelihood) of unclassified complex channel responses belong to a particular modeled environment $P(c_i \mid a_1,...a_t)$, where $a_j$, $j = 1,...t$ is probability of attribute obtained from data training. For a single attribute, Baye's rule states

$$P(C_i \mid a_i) = \frac{P(a_i \mid C_i)P(C_i)}{P(a_i)} \tag{4.11}$$

where $P(a_j \mid c_i)$ in the numerator is the likelihood of an attribute equal to a fixed value if the hypothesis of channel model $c_i$ is true. For example, $P(|p_1| = x \mid c_1)$ is the likelihood of the first order pole envelope equal to $x$ given the channel response is measured in a

residential LOS environment. If $|p_1|$ is characterized as an extreme value distributed variable in Table 4.1, then

$$
\begin{aligned}
P(a_i \mid C_i) &= P(|p_1| = x \mid \alpha, \beta) \\
&= \beta^{-1} \exp\{(\alpha - |p_1|)/\beta - \exp(\alpha - |p_1|)/\beta\}
\end{aligned}
\tag{4.12}
$$

On the other hand, $P(c_i)$ in the numerator is the prior brief, also known as the probability of hypothesized class $c_i$ before seeing any data. In the context of this study, we assume that data under test are multiple snapshots of complex channel response from an unknown environment; therefore, it is equal probable that the CFRs are to be classified as any of the eight channel models. The prior brief is thus $P(c_i) = 1/8$. The denominator can be expanded as

$$
P(a_i) = \sum_{j=1}^{8} P(a_i \mid C_j) P(C_j)
\tag{4.13}
$$

The term $P(a_j \mid c_i) P(c_i)$ is the joint probability and can be denoted as $P(a_j, c_i)$. The sum of all the joint probability yields $P(a_i)$, the marginal probability of an attribute. It is the data evidence of a feature belonging to all channel models. We choose the most probable hypothesis, $P(c_i \mid a_j)$, known as maximum a posteriori hypothesis.

## 4.3.2 Maximum Likelihood Criterion

The Maximum likelihood classifier choose the maximum of posterior probability based on

$$
h_{MAP} = \arg \max P(C_i \mid a_i)
\tag{4.14}
$$

A useful observation is that $P(C_i \mid a_i)$ does not depend on denominator $P(a_i)$ in the classification computation since $P(a_i)$ will be the same for all classifying channel

models. In addition, the prior brief $P(C_i)$ is equal probable. The hypothesis then reduces to the form

$$h_{ML} = \arg\max P(a_i \mid C_i) \qquad (4.15)$$

This is a well known maximum likelihood criterion, which only depends on conditional probability of attribute given a hypothesis of a certain model is true.

## 4.3.3 Naïve Bayes Assumption for Combining Multiple Bayesian Classifiers

The AR-FD model that we considered has multiple attributes; including magnitude of first order pole, magnitude of second order pole, phase of first order pole, phase of second order pole, real part of first order initial condition, imaginary part of first order initial condition, real part of second order initial condition, imaginary part of second order initial condition, and variance of white noise, in total of 9 dimensions. We need to introduce an assumption that deals with multiple attributes. The Naïve Bayes assumption allows us to deal with multiple attributes by considering independency of each attribute, as shown in

$$P(A \mid C_i) = P(a_1,...a_C \mid C_i) = \prod_{i=1}^{c} P(a_i \mid C_i) \qquad (4.16)$$

where $A$ is collection of all the attributes $\{a_1,...a_t\}$. Although independency is a poor assumption and often violated in reality, Naïve Bayes often yields surprisingly good results with nearly functional dependencies [5][6]. With naïve Bayes assumption in (4.16), the maximum likelihood becomes

$$h_{MAP} = \arg\max \prod_{i=1}^{c} P(a_i \mid C_i) \qquad (4.17)$$

Each term of the product in (4.17) is a Bayesian classifier result for a single attribute. The test channel response is then assigned to class $c_i$ by selecting the maxima of the above criterion.

## 4.4 Simulation and Results

An eight class channel model classification problem is considered in this section by using i) simulated data from 4a CIR simulator ii) experiment data collected from a 737-200 mid-size airliner environment. With the simulated data, the channel model $C_i$ is known as a prior, we thus considered a variety of attributes to study sensitivity of our classification algorithm and validate completeness of our characterized attributes. For the measured aircraft data, we would like to compare the channel from an unfamiliar environment with existing channel models, and comment on the channel behavior of the unfamiliar environment based on our classification result.

### 4.4.1 Classification with Simulated Data

In feature extraction procedure of channel frequency response, a second order AR-FD model can represent diverse UWB channels with reasonable accuracy, with variance of prediction error ranging from 7.556e-8 to 7.380e-5, depending on modeled environment [3]. For lower AIC values, higher order poles and initial conditions are required. As the model order increases, dimensions of classifier increase. In practice, we would like to keep the dimension of classifier as low as possible [7].

In previous section, we show pole magnitude controls the shapes of channel impulse response, and the pole phase determines time arrival of spectrum with significant energy. Since pole information directly contributes to shape of power delay profile, type I classifier considers first and second order pole magnitudes and pole phases (4 dimensions). Initial condition is another parameter depending on selected model order.

Type II classifier considers pole statistics with initial conditions (8 dimensions all together). Attributes for type III classifier include pole, initial conditions and variance of driving noise (9 dimensions). Input for all three types of classifiers is 100 samples of attributes derived from untrained complex channel responses from each class. The result in Table 4.5 shows the correct classification rate for all three types of classifier

Table 4.5 Type I, Type II and Type III Classifier

| $C_i$ | Correct Classification Rate (/100 samples) | | |
| --- | --- | --- | --- |
| | Type I | Type II | Type III |
| | Poles (%) | Poles + Initial Conditions (%) | Poles + Initial Conditions + variance of driving noise (%) |
| 1. Res LOS | 47 | 62 | 64 |
| 2. Res NLOS | 55 | 95 | 97 |
| 3. Office LOS | 94 | 92[*] | 96 |
| 4. Office NLOS | 68 | 88 | 89 |
| 5. Outdoor LOS | 48 | 46[*] | 55 |
| 6. Outdoor NLOS | 65 | 68 | 30[*] |
| 7. Industrial LOS | 53 | 68 | 69 |
| 8. Industrial NLOS | 100 | 100 | 100 |
| correct classification rate | 66.25 | 77.38 | 75 |

With only pole statistics as classifier attributes, more than 47% of the channels are accurately classified for each channel model. In particular, office LOS, and industrial NLOS channels are recognized by type I classifier with classification rate as high as 94% and 100% respectively. Residential LOS is the worst identified class given the pole statistics. For type II classifier, initial conditions are added as classifier attributes. The average recognition percentage increased by 11.13% from 66.25% to 77.38%. For residential and office environment, the initial conditions help to increase correct classification rate by 15-40%. Type II classifier has higher classification rate than type I classifier for most of the channel classes, with exception for recognizing office LOS and outdoor LOS, where classification rates slightly decline by 2 %. Type III classifier with driving noise considers 9 dimension attributes. It outperforms the type II classifier by 1 – 9 %, except for outdoor NLOS. When classifying outdoor NLOS channels, the performance degrades by 31%. This large degree decline suggests type III classifier which incorporates variance of driving noise as attribute has difficulty distinguishing outdoor NLOS from other classes. Because the outdoor NLOS is poorly identified, the average classification rate of type III classifier is not as high as type II and drops slightly to 75%. In comparison to the first classifier, the third classifier improves correct classification rate by 9.375%, with only outdoor NLOS channels that the classification rate is lower. Overall, no single classifier from Table 4.5 is best for all channel models, the second classifier has the best average performance. However, classification rate for outdoor LOS is below 50%. Table 4.7 shows the classification rate of type II and type III classifier with its major competitor. Type II classifier has difficulty distinguish outdoor LOS with its major competitor Res LOS. Type III classifier has difficulty distinguish outdoor NLOS and Res NLOS.

The confusion matrix in Table 4.6 shows detailed classifying result of type III classifier with 9 dimension attributes. For four cases, residential NLOS, office LOS, office NLOS and industrial NLOS, the third classifier is able to recognize the true channel model at rate 97%, 96%, 89% and 100% respectively. For residential LOS class, the classifier labeled it incorrectly to residential NLOS 13% of the time and outdoor LOS

15% of the time. The reason is that residential LOS and outdoor LOS channels have clearly overlaps in pole locations; residential LOS and residential NLOS have similar second pole location. With outdoor LOS, the classifier gets a bit confused between residential, industrial and outdoor LOS. For outdoor NLOS, because the pole locations are very close to those found in residential LOS and NLOS, the correct classification rate reduces to 30%.

Table 4.6 Confusion Matrices for the 9 Dimension Classifier for $C_{1-8}$ with Untrained Data

| Classified as | Residential LOS (%) | Residential NLOS (%) | Office LOS (%) | Office NLOS (%) | Outdoor LOS (%) | Outdoor NLOS (%) | Industrial LOS (%) | Industrial NLOS (%) |
|---|---|---|---|---|---|---|---|---|
| Residential LOS | 64 | 13 | 0 | 2 | 15 | 2 | 4 | 0 |
| Residential NLOS | 2 | 97 | 0 | 1 | 0 | 0 | 0 | 0 |
| Office LOS | 0 | 0 | 96 | 0 | 1 | 1 | 2 | 0 |
| Office NLOS | 2 | 7 | 0 | 89 | 0 | 1 | 1 | 0 |
| Outdoor LOS | 24 | 0 | 1 | 0 | 55* | 0 | 20 | 0 |
| Outdoor NLOS | 24 | 25 | 1 | 3 | 12 | 30* | 5 | 0 |
| Industrial LOS | 8 | 0 | 3 | 3 | 13 | 4 | 69 | 0 |
| Industrial NLOS | 0 | 0 | 0 | 0 | 0 | 0 | 0 | 100 |

Table 4.7 Distribution of Auxiliary Parameters $m_1$ and $m_2$ for $C_{1-8}$

|  | $C_1$ | $C_2$ | $C_3$ | $C_4$ | $C_5$ | $C_6$ | $C_7$ | $C_8$ |
|---|---|---|---|---|---|---|---|---|
| $m_1$ | Lognormal | Lognormal | Lognormal | Log-logistic | Normal | Log-logistic | Nakagami | Normal |
| $\mu$ | -0.678869 | -0.138212 | -2.06455 | -0.160159 | 0.483066 | -0.1073 | 1.39967 | 1.09251 |
| $\sigma$ | 0.258124 | 0.22916 | 0.377277 | 0.0602481 | 0.103582 | 0.186159 | 0.291511 | 0.0151633 |
| $m_2$ | Lognormal | Lognormal | Nakagami | Log-logistic | Nakagami | Logistic | Nakagami | Normal |
| $\mu$ | -0.964123 | -0.691945 | 1.27766 | -0.613933 | 3.27233 | 0.545094 | 1.1933 | 0.672948 |
| $\sigma$ | 0.290753 | 0.15656 | 0.013846 | 0.0679616 | 0.170053 | 0.111516 | 0.26258 | 0.0127937 |

Table 4.8 Winning Class and Its Major Competitor for Type II and Type III Classifier

| $C_i$ | Type II<br>Poles + Initial Conditions<br>(%) | Type III<br>Poles + Initial Conditions + variance of driving noise<br>(%) |
|---|---|---|
| 1. Res LOS | 62 / 16 | 64 / 15 |
| 2. Res NLOS | 95 / 3 | 97 / 2 |
| 3. Off LOS | 92 / 6 | 96 / 2 |
| 4. Off NLOS | 88 / 8 | 89 / 7 |
| 5. Out LOS | **46 / 33** | 55 / 24 |
| 6. Out NLOS | 68 / 11 | **30 / 25** |
| 7. Ind LOS | 68 / 11 | 69 / 13 |
| 8. Ind NLOS | 100 / 0 | 100 / 0 |

## 4.4.2 Feature Selection and Classifier with Auxiliary Parameters

We want to obtain better classification result with larger distance between a winning class and its major competing class. Since pole phase is proportional to propagation delay by (4.5) and pole magnitude suggest the peak amplitude. To improve classification rate of the classifier, we introduce two parameters which are first moment and second moment of pole. First and second moments of poles are analogous quantities of mean excess delay and rms delay spread. Mean excess delay and rms delay spread were used as features to separate LOS and NLOS channels in [9]. Statistical distribution of $\hat{m}_1$ and $\hat{m}_2$ are listed in Table 4.7. The classification result is shown in Table 4.9. With auxiliary parameters m1, the average classification rate is 75.63%. The improvement on outdoor NLOS is 12% (compared with 30% of type III classifier). With m1 and m2 combined, the correct classification rate for outdoor NLOS increased from 30% to 52%. The results in column 3 and 4 of Table 4.8 show that with variance of driving noise removed, the classification rate for outdoor NLOS improved by almost 20% compared to type V classifier in column

2. The tradeoff of tuning the classifier to better recognize worse identified case outdoor NLOS channel is that the correct classification rate in other classes drops. For type IV classifier, the classification rate of outdoor LOS drops by 13% and for residential NLOS, the classification rate drops 7%. The classifier considering poles, initial conditions, first and second moment of poles as attributes is chosen based on an average classification rate of 76.25% and for the worst identified case outdoor NLOS, the winning class and the major competitor are differ by 35%. We recommend type II and type V classifier. Type II classifier has the maximum average classification rate. Type V classifier's has better winning class to major competitor class ratio for the worst identified case.

Table 4.9 Classification with Different Combination of Attributes

|  | Rate of correction classification (/100 samples) | | | |
|---|---|---|---|---|
|  | Type IV | Type V | Type VI | Type VII |
| $C_i$ | Poles + Initial conditions + Variances + m1 10 dimensions (%) | Poles + Initial Conditions +variance of driving noise m1 + m2 + (%) | Poles +Initial Conditioi ns+ m1 (%) | Poles + Initial Conditions +m1 +m2 (%) |
| 1. Res LOS | 62 | 60 | 61 | 57 |
| 2. Res NLOS | 95 | 96 | 89 | 92 |
| 3. Off LOS | 95 | 94 | 92 | 92 |
| 4. Off NLOS | 87 | 86 | 85 | 85 |
| 5. Out LOS | 61 | 61 | 48 | 50 |
| 6 Out NLOS | 42 | 52 | 71 | 72 |
| 7 Ind LOS | 63 | 61 | 59 | 59 |
| 8 Ind NLOS | 100 | 100 | 100 | 100 |
| CCR | 75.63 | 76.25 | 75.63 | 75.88 |

Table 4.10 Type II vs. Type V Classifier

|  | Type II | Type V |
|---|---|---|
| $C_i$ | Poles + Initial Conditions (%) | Poles + Initial Conditions +variance of driving noise m1 + m2 + (%) |
| 1. Res LOS | 62 / 16 | 60 / 16 |
| 2. Res NLOS | 95 / 3 | 96 / 2 |
| 3. Off LOS | 92 / 6 | 94 / 4 |
| 4. Off NLOS | 88 / 8 | 86 / 9 |
| 5. Out LOS | **46/ 33** | 61 / 23 |
| 6. Out NLOS | 68 / 11 | **52 / 17** |
| 7. Ind LOS | 68 / 11 | 61 / 21 |
| 8. Ind NLOS | 100 / 0 | 100 / 0 |
| CCR | 77.38 | 76.25 |

## 4.4.3 Classification based on time-domain parameters

Previous work in [9] uses RMS delay spread, mean excess delay and kurtosis to classify LOS and NLOS for channel realizations from a given environment. Here, we access the decency of our feature selection by comparing classifier based on AR-FD model features with that based on time domain model features. The result is shown in the following Table 4.11

From Table 4.10, RMS delay spread appears to be the best time domain model feature for obtaining the highest CCR. This is because RMS delay spread measures the temporal and spatial average of consecutive CIRs over a local area. In particular, RMS delay spread measures the spread of MPCs arrival over time. For outdoor environment, where scattering objects are farther apart, channels have larger delay spread in the range of 100ns. For indoor environments, where reflecting objects are denser in a given area, the RMS delay spreads are found to be under 50ns. Figure 4.5 shows the RMS delay spread distributions for all modeled environments. It is observed that histograms of RMS distributions overlap each other. For example, the histogram for RMS delay spread from CM1 is overlaid by those from CM 2 to CM 4. Given an RMS delay value from CM1(e.g. 20ns), the classified model is rarely recognized as the true class because the probability is overshadowed by higher probability of other classed.

It is also found that kurtosis is a poor feature for differentiating channels from different environments because the distributions from different environment are very close (as in Figure 4.6). Overall, the listed time domain parameters are insufficient in identifying all of the eight channel models.
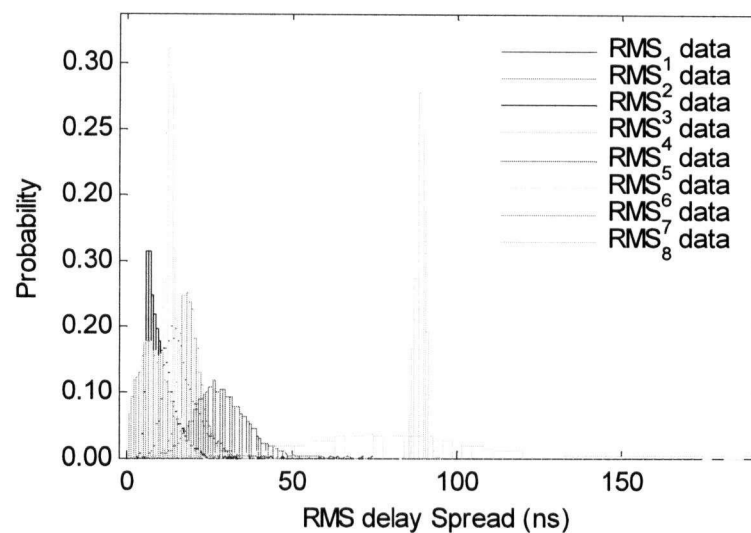
Figure 4.5 Distribution of RMS Delay Spread for CM 1-8.
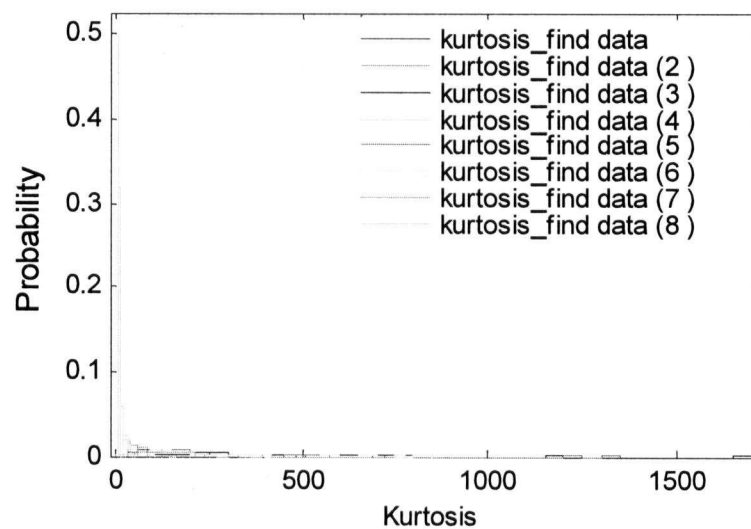


Figure 4.6 Distribution of Kurtosis for CM1-8.

Table 4.11 Comparison of AR-FD Attributes and Time Domain Attributes

| $C_i$ | Rate of correction classification (/100 samples) | | | |
| --- | --- | --- | --- | --- |
| | Type V | Time Domain Feature | | |
| | Poles + Initial Conditions +variance of driving noise m1 + m2 + (%) | RMS delay spread (%) | Excess delay (%) | Kurtosis (%) |
| 1. Res LOS | 60 | 8 | 11 | 0 |
| 2. Res NLOS | 96 | 53 | 26 | 7 |
| 3. Off LOS | 94 | 62 | 69 | 0 |
| 4. Off NLOS | 86 | 44 | 67 | 96 |
| 5. Out LOS | 61 | 66 | 54 | 0 |
| 6 Out NLOS | 52 | 81 | 83 | 52 |
| 7 Ind LOS | 61 | 37 | 22 | 20 |
| 8 Ind NLOS | 100 | 99 | 0 | 0 |
| CCR | 76.25 | 56.25 | 41.5 | 21.86 |

## 4.4.4 Classification with measured aircraft data

For channel propagation problems, very often the environment to be characterized is unconventional or unfamiliar. Comparison and similarities drawn between the new environment and existing channel models would help system designers deploying wireless system in unfamiliar environment. Aircraft environment is different from conventional environments in the following sense: i) geometry of the aircraft cabin is short tunnel like, enclosed by metallic reflectors ii) high density of obstacles (seats) in a conventional commercial aircraft suggests severe propagation conditions in such environment.

The input of the classifier in this case consists of 352 samples of attributes derived from channel responses measured in a mid-size airliner 737-200. The detailed description of measurement data can be found in [19]. The frequency span for the measurement is from 3.0 to 10.6 GHz. Depending on transmit and receive antenna locations, measured channel responses include both LOS and NLOS paths. The confusion matrix in Table 4.7 shows classification result of the type V classifier proposed in previous session. It labels the aircraft as office NLOS 56% of the time. 11% of time it labels the aircraft as residential LOS channels; 16% of the time it labels aircraft as industrial LOS. Figure 4.7 shows the classification result for type II and type V classifier. Both classifiers recognize the channel as office NLOS more than half of the time and identify industrial LOS as its major competitor. These results are anticipated because the aircraft environment consists two main parts physically: metallic reflectors of the aircraft cabin, and a high density of seats. The metallic reflectors can also be found in industrial environment because massive storage of machineries. If LOS path exists, the aircraft cabin and the seats both contribute to the multipath components in the channel. For NLOS paths, the scatterings from passenger seats dominate; thus, the classifier finds NLOS aircraft channels most close to office NLOS. Through these classifying results, we can expect the aircraft channel will behave most likely as the office NLOS channels due to the following reasons: i) in

practice, LOS paths are most likely obstructed by passengers or luggage; NLOS paths thus dominate in aircraft environment ii) dimension of mid-size airliner is most close to office environment. For larger airliners, similar results would hold because cabins can be divided into subsections.

Table 4.12 Confusion Matrices for the Type V Classifier with Aircraft Data

| Classified as | Res LOS | Res NLOS | Office LOS | Office NLOS | Outdoor LOS | Outdoor NLOS | Indust LOS | Indust NLOS |
|---|---|---|---|---|---|---|---|---|
| Aircraft data | 12 | 6 | 0 | 58 | 11 | 0 | 13 | 0 |
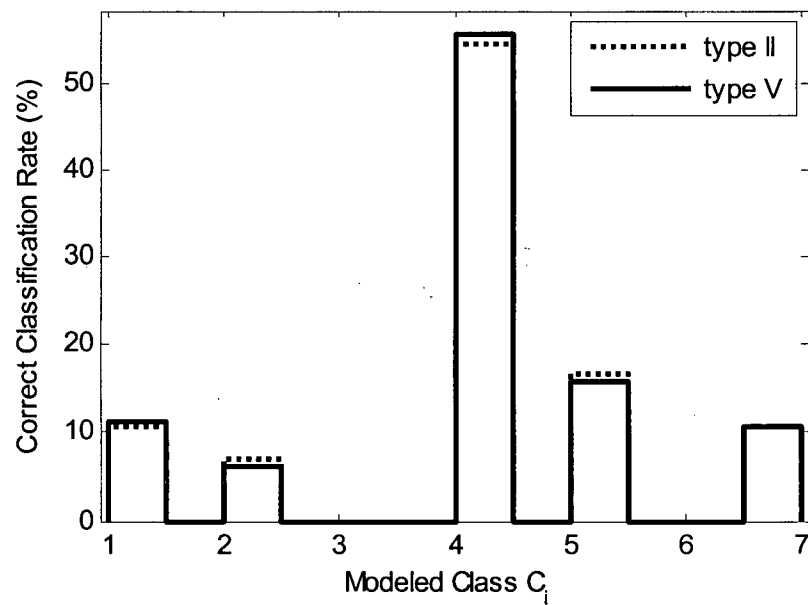


Figure 4.7 Classification Rate for Aircraft Channel as Standard Channel Models

## 4.5 Conclusion

In this paper, we devised a new UWB channel classifier which takes channel responses as inputs and predict a channel model which measured data belong to. Attributes of the channel classifier are AR-FD model parameters extracted from snapshots of UWB complex frequency response. We show that our maximum likelihood classifier with Naïve Bayesian assumption can achieve correct classification rate as high as 77.38% with 8 dimension attributes (Type II classifier) and 75% with 9 dimension attributes (Type III classifier). The drawback of the classifier is that it has a worst classified scenario which the correct classification rate is low and the winning class has a major competitor. An improvement is demonstrated by adding two auxiliary parameters, namely the first and second moment of pole, to the 9 attribute classifier. An average classification rate of 76.25% is obtained through the proposed 11 dimensional classifier (Type V classifier) and the effect of major competitor is diminished. The 11 dimension attribute classifier is used to compare unconventional aircraft channels with existing channel models; the result shows aircraft channel is most close to office NLOS channels. For LOS channels found in aircraft environment, industrial LOS seems to be the closest match.

# Bibliography

[1]  S. J. Howard, and K. Pahlavan, "Autoregressive Modeling of Wide-Band Indoor Propagation," *IEEE Trans. Commun*, vol. 40, no. 9, pp. 1540-1552, Sep. 1992

[2]  S. S. Ghassemzadeh, R. Jana, C.W. Rice, W. Turin, and V. Tarokh, "Measurement and Modeling of an Ultra-Wide Bandwidth Indoor Channel," *IEEE Trans. Commun*, vol. 52, no. 10, pp. 1786-1796, Oct. 2004

[3]  N. Xin and D. G. Michelson, "Frequency Domain Analysis of IEEE 802.15.4a Channel Models," *IEEE WCNC 2007 March*, pp 2058-2062

[4]  L. M. Correia and R. Prasad, " An overview of wireless broadband communications," *IEEE Commun. Mag.*, pp. 28-33, Jan. 1997

[5]  I. Rish, "An Empirical Study of the Naïve Bayes Classifier," IJCAI-01 Workshop on Empirical Methods in AI, 2001

[6]  T. M. Mitchell, "Generative and Discriminative Classifiers: Naïve Bayes and Logistic Regression", Machine Learning, McGraw Hill, 1997

[7]  A. K. Jain, R. W. Duln and J. Mao, "Statistical Pattern Recognition: A Review," *IEEE Trans. Pattern Anal. Mach. Intell.*, vol. 22, no. 1, Jan. 2000

[8]  J. Suzuki, "On Strong Consistency of Model Selection in Classification," *IEEE Trans. on Inf. Theory*, vol. 52, no. 11, pp. 4767-4774, Nov. 2006

[9]  I. Guvenc, CC. Chong, and F. Watanabe, "NLOS Identification and Mitigation for UWB Localization Systems," *IEEE WCNC 2007 Proceedings*, Hongkong, March

[10]  A.F. Molisch, K. Balakrishnan, D. Cassioli, CC. Chong, S. Emanmi, A. Fort, F. Karedal, J. Kunisch, H. Schantz, U. Schuster, and K. Siwiak., "IEEE 802.15.4a channel model - final report," IEEE P802. 15-04/662r0-SG4a

[11]  A. F. Molisch, "Ultrawideband Propagation Channels-Theory, Measurement, and Modeling," *IEEE Trans. Veh. Technol.*, vol. 54, no.5, pp. 1528-1545, Sep. 2005

[12]  A. Alvarez, G. Valera, M. Lobeira, R. Torres, and J. L. Garcia, " New Channel Impulse Response Model for UWB Indoor System Simulations," *IEEE VTC*, vol. 1. 22-25, pp.1-5, Spring 2003

[13] J. Kunisch and J. Pamp, " Measurement Results and Modeling Aspects for the UWB Radio Channel," *IEEE Conference on Ultra Wideband Systems and Technologies*, pp.19-23, 2002

[14] G. Morrison, and M. Fattouche, "Super-Resolution Modeling of the Indoor Radio Propagation Channel," *IEEE Trans. Veh. Technol.*, vol.47, no. 2, pp. 649-657, May 1998

[15] P. Hoeher, S. Kaiser and P. Robertson, "Two-dimensional Pilot-symbol-aided Channel Estimation by Wiener Filtering," *Proceedings of ICASSP*, vol. 3, pp. 1845-1848, 1997

[16] S. Kaiser and W.A. Krzymien, "Asynchronous Spread Spectrum Multi-Carrier Multiple Access Systems with Pilot Symbol Aided Channel Estimation," *IEEE VTC*, vol. 5, pp.19-22, Fall 1999

[17] A. A. M. Saleh, and R.A. Valenzuela, "Statistical Model for Indoor Multipath Propagation," *IEEE J. Sel. Areas Commun*, vol. SAC-5, no. 2, pp. 128-137, February 1987

[18] S. L. Marple Jr., "Digital Spectral Analysis with Applications" Prentice-Hall, pp.229, 1987

[19] J. Chuang, N. Xin, H. Huang, S. Chui and D. G. Michelson, "UWB Radiowave Propagation within the Passenger Cabin of a Boeing 737-200 Aircraft," *IEEE VTC*, 2007 April, pp. 496-500

[20] C. W. Anderson, E. A. Stolz, and S. Shamsunder, "Multivariate Autoregressive Models for Classification of Spontaneous Electroencephalographic Signals during Mental Tasks," *IEEE Trans. Biomed. Eng.*, vol. 45, no. 3, March 1998, pp 277-286

[21] L. Xu, A. Krzyzak, and C. Y. Suen, "Methods of Combining Multiple Classifiers and Their Applications to Handwriting Recognition," *IEEE Trans. Syst., Man, Cybern.*, vol. 22, no. 3, May/June 1992, pp. 418-435

# Chapter 5

# Conclusions and Recommendations

## 5.1 Conclusion

This work has been concerned with modeling of UWB channels in different environment using autoregressive frequency domain approach. Specifically, this work makes the following three major contributions.

First, we have modeled UWB channels in different environment based on a vast database of CIR provided in 4a. We have shown the AR-FD technique can model all 4a documented channels with reasonable accuracy. Compared to classic time domain modeling, the AR-FD model proposed in this work uses fewer parameters. We have compared RMS delay spreads obtained from 4a model and those obtained from AR-FD model. The result shows AR-FD generated channels are reasonably close to 4a channel. This AR-FD technique is powerful in comparing channels from different environments. Thus, in chapter 3, we have applied the AR-FD technique to measured channel frequency response in aircraft environment. We have shown that LOS channels in aircraft environment are similar to those found in industrial environment. On the other hand, NLOS channels in aircraft environment are most close to those found in office environment. This result is further proved in chapter 4, in which we proposed an AR-FD parameter based classifier. The Naïve Bayesian classifier makes use of distribution of AR-FD parameters. For untrained data, an average classification rate of 76.25% is obtained through the proposed 11 dimensional classifier.

## 5.2 Future Challenge and Recommendation

In our proposed AR-FD modeling technique, the modeling database is from 4a channel impulse response generator. For industrial environment in particular, the shape of the power delay profile from 4a generator does not quite match with its quoted source where the measurement and model was originally outlined. Our analysis shows the pole locations are very condense in two regions. Further measurements in industrial environment are necessary to prove the validity of the 4a industrial model. We modeled aircraft environment with aggregated LOS and NLOS data. For future work, the test setup should clearly be divided into LOS and NLOS scenario. Then, the model would better reflect the propagation environment and it would be easier to process.

# Appendix A

AR Yule-Walker normal equations step-by-step derivation

$$H(f_n) = -\sum_{k=1}^{p} a_k H(f_{n-k}) + U(f_n) \tag{A1}$$

Multiply (A1) by $H^*(f_{n-m})$

$$E\{H(f_n)H^*(f_{n-m})\} = -\sum_{k=1}^{p} a_k E\{H(f_{n-k})H^*(f_{n-m})\} + E\{U(f_n)H^*(f_{n-m})\} \tag{A2}$$

$$R_{HH}(f_m) = -\sum_{k=1}^{p} a_k R_{HH}(f_{m-k}) + R_{UH}(f_m) \tag{A3}$$

where

$$R_{UH}(f_m) = \begin{cases} 0 & for \;\; m > 0 \\ \rho_w & for \;\; m = 0 \\ \rho_w H^*(-f_m) & for \;\; m < 0 \end{cases} \tag{A4}$$

Substitute (A4) into (A3)

$$R_{HH}(f_m) = \begin{cases} -\sum_{k=1}^{p} a_k R_{HH}(f_{m-k}) & for \;\; m > 0 \\ -\sum_{k=1}^{p} a_k R_{HH}(f_{-k}) + \rho_w & for \;\; m = 0 \\ R_{HH}{}^*(f_{-m}) & for \;\; m < 0 \end{cases} \tag{A5}$$

Evaluate for $0 \le m \le p$

$$\begin{bmatrix} R_{HH}(0) & R_{HH}(-1) & \cdots & R_{HH}(-p) \\ R_{HH}(1) & R_{HH}(0) & \cdots & R_{HH}(-p+1) \\ \vdots & \vdots & \ddots & \vdots \\ R_{HH}(p) & R_{HH}(p-1) & \cdots & R_{HH}(0) \end{bmatrix} \begin{bmatrix} 1 \\ a_1 \\ \vdots \\ a_p \end{bmatrix} = \begin{bmatrix} \rho_w \\ 0 \\ \vdots \\ 0 \end{bmatrix} \tag{A6}$$

# Appendix B

### Correlation Matrix between Parameters (CM1)

| $\rho$ | $\lvert p_1 \rvert$ | $\lvert p_2 \rvert$ | $\angle p_1$ | $\angle p_2$ | $u_0$ | $\mathrm{Re}\{H_1\}$ | $\mathrm{Re}\{H_2\}$ | $\mathrm{Im}\{H_1\}$ | $\mathrm{Im}\{H_1\}$ |
|---|---|---|---|---|---|---|---|---|---|
| $\lvert p_1 \rvert$ | 1.0000 | 0.2384 | 0.5595 | 0.2039 | -0.6622 | -0.0259 | -0.0307 | -0.0115 | -0.0031 |
| $\lvert p_2 \rvert$ | 0.2384 | 1.0000 | 0.0902 | 0.4616 | -0.4757 | 0.0030 | 0.0021 | 0.0017 | 0.0001 |
| $\angle p_1$ | 0.5595 | 0.0902 | 1.0000 | -0.0924 | -0.3443 | -0.0254 | -0.0297 | -0.0174 | -0.0089 |
| $\angle p_2$ | 0.2039 | 0.4616 | -0.0924 | 1.0000 | -0.6859 | 0.0128 | 0.0078 | 0.0019 | 0.0086 |
| $u_0$ | -0.6622 | -0.4757 | -0.3443 | -0.6859 | 1.0000 | 0.0103 | 0.0175 | 0.0083 | -0.0025 |
| $\mathrm{Re}\{H_1\}$ | -0.0259 | 0.0030 | -0.0254 | 0.0128 | 0.0103 | 1.0000 | 0.9267 | 0.0060 | -0.1905 |
| $\mathrm{Re}\{H_2\}$ | -0.0307 | 0.0021 | -0.0297 | 0.0078 | 0.0175 | 0.9267 | 1.0000 | 0.2022 | 0.0065 |
| $\mathrm{Im}\{H_1\}$ | -0.0115 | 0.0017 | -0.0174 | 0.0019 | 0.0083 | 0.0060 | 0.2022 | 1.0000 | 0.9281 |
| $\mathrm{Im}\{H_1\}$ | -0.0031 | 0.0001 | -0.0089 | 0.0086 | -0.0025 | -0.1905 | 0.0065 | 0.9281 | 1.0000 |

### Correlation Matrix between Parameters (CM2)

| $\rho$ | $\lvert p_1 \rvert$ | $\lvert p_2 \rvert$ | $\angle p_1$ | $\angle p_2$ | $u_0$ | $\mathrm{Re}\{H_1\}$ | $\mathrm{Re}\{H_2\}$ | $\mathrm{Im}\{H_1\}$ | $\mathrm{Im}\{H_1\}$ |
|---|---|---|---|---|---|---|---|---|---|
| $\lvert p_1 \rvert$ | 1.0000 | 0.1706 | 0.3701 | 0.0999 | -0.7613 | -0.0061 | 0.0147 | 0.0174 | 0.0183 |
| $\lvert p_2 \rvert$ | 0.1706 | 1.0000 | 0.1617 | 0.1988 | -0.2489 | -0.0042 | 0.0100 | 0.0085 | 0.0186 |
| $\angle p_1$ | 0.3701 | 0.1617 | 1.0000 | 0.5656 | -0.2570 | -0.0031 | 0.0180 | 0.0264 | 0.0197 |
| $\angle p_2$ | 0.0999 | 0.1988 | 0.5656 | 1.0000 | -0.3932 | -0.0113 | 0.0089 | 0.0162 | 0.0075 |
| $u_0$ | -0.7613 | -0.2489 | -0.2570 | -0.3932 | 1.0000 | 0.0002 | -0.0134 | -0.0160 | -0.0155 |
| $\mathrm{Re}\{H_1\}$ | -0.0061 | -0.0042 | -0.0031 | -0.0113 | 0.0002 | 1.0000 | 0.7257 | -0.0050 | -0.5200 |
| $\mathrm{Re}\{H_2\}$ | 0.0147 | 0.0100 | 0.0180 | 0.0089 | -0.0134 | 0.7257 | 1.0000 | 0.5074 | -0.0107 |
| $\mathrm{Im}\{H_1\}$ | 0.0174 | 0.0085 | 0.0264 | 0.0162 | -0.0160 | -0.0050 | 0.5074 | 1.0000 | 0.7223 |
| $\mathrm{Im}\{H_1\}$ | 0.0183 | 0.0186 | 0.0197 | 0.0075 | -0.0155 | -0.5200 | -0.0107 | 0.7223 | 1.0000 |

## Correlation Matrix between Parameters (CM3)

| $\rho$ | $|p_1|$ | $|p_2|$ | $\angle p_1$ | $\angle p_2$ | $u_0$ | $Re\{H_1\}$ | $Re\{H_2\}$ | $Im\{H_1\}$ | $Im\{H_1\}$ |
|---|---|---|---|---|---|---|---|---|---|
| $|p_1|$ | 1.0000 | 0.0949 | 0.3569 | -0.3148 | -0.4137 | -0.0218 | -0.0229 | -0.0041 | -0.0003 |
| $|p_2|$ | 0.0949 | 1.0000 | -0.0132 | -0.2446 | -0.4350 | -0.0117 | -0.0112 | 0.0064 | 0.0068 |
| $\angle p_1$ | 0.3569 | -0.0132 | 1.0000 | -0.0248 | -0.2219 | -0.0117 | -0.0136 | -0.0029 | -0.0007 |
| $\angle p_2$ | -0.3148 | -0.2446 | -0.0248 | 1.0000 | -0.3342 | -0.0029 | -0.0015 | 0.0117 | 0.0116 |
| $u_0$ | -0.4137 | -0.4350 | -0.2219 | -0.3342 | 1.0000 | 0.0396 | 0.0385 | -0.0240 | -0.0274 |
| $Re\{H_1\}$ | -0.0218 | -0.0117 | -0.0117 | -0.0029 | 0.0396 | 1.0000 | 0.9956 | 0.0076 | -0.0495 |
| $Re\{H_2\}$ | -0.0229 | -0.0112 | -0.0136 | -0.0015 | 0.0385 | 0.9956 | 1.0000 | 0.0638 | 0.0066 |
| $Im\{H_1\}$ | -0.0041 | 0.0064 | -0.0029 | 0.0117 | -0.0240 | 0.0076 | 0.0638 | 1.0000 | 0.9955 |
| $Im\{H_1\}$ | -0.0003 | 0.0068 | -0.0007 | 0.0116 | -0.0274 | -0.0495 | 0.0066 | 0.9955 | 1.0000 |

## Correlation Matrix between Parameters (CM4)

| $\rho$ | $|p_1|$ | $|p_2|$ | $\angle p_1$ | $\angle p_2$ | $u_0$ | $Re\{H_1\}$ | $Re\{H_2\}$ | $Im\{H_1\}$ | $Im\{H_1\}$ |
|---|---|---|---|---|---|---|---|---|---|
| $|p_1|$ | 1.0000 | 0.1752 | 0.5410 | 0.1155 | -0.7195 | -0.0041 | 0.0000 | 0.0048 | 0.0079 |
| $|p_2|$ | 0.1752 | 1.0000 | 0.2370 | 0.2987 | -0.3214 | 0.0061 | 0.0175 | 0.0207 | 0.0122 |
| $\angle p_1$ | 0.5410 | 0.2370 | 1.0000 | 0.0951 | -0.3339 | 0.0093 | 0.0100 | 0.0100 | -0.0041 |
| $\angle p_2$ | 0.1155 | 0.2987 | 0.0951 | 1.0000 | -0.5974 | -0.0121 | -0.0029 | 0.0186 | 0.0225 |
| $u_0$ | -0.7195 | -0.3214 | -0.3339 | -0.5974 | 1.0000 | 0.0039 | -0.0063 | -0.0281 | -0.0223 |
| $Re\{H_1\}$ | -0.0041 | 0.0061 | 0.0093 | -0.0121 | 0.0039 | 1.0000 | 0.7381 | -0.0078 | -0.4916 |
| $Re\{H_2\}$ | 0.0000 | 0.0175 | 0.0100 | -0.0029 | -0.0063 | 0.7381 | 1.0000 | 0.4872 | 0.0041 |
| $Im\{H_1\}$ | 0.0048 | 0.0207 | 0.0100 | 0.0186 | -0.0281 | -0.0078 | 0.4872 | 1.0000 | 0.7429 |
| $Im\{H_1\}$ | 0.0079 | 0.0122 | -0.0041 | 0.0225 | -0.0223 | -0.4916 | 0.0041 | 0.7429 | 1.0000 |

## Correlation Matrix between Parameters (CM5)

| $\rho$ | $|p_1|$ | $|p_2|$ | $\angle p_1$ | $\angle p_2$ | $u_0$ | $\mathrm{Re}\{H_1\}$ | $\mathrm{Re}\{H_2\}$ | $\mathrm{Im}\{H_1\}$ | $\mathrm{Im}\{H_1\}$ |
|---|---|---|---|---|---|---|---|---|---|
| $|p_1|$ | 1.0000 | 0.1664 | 0.5814 | -0.0723 | -0.6476 | 0.0072 | -0.0051 | -0.0141 | -0.0077 |
| $|p_2|$ | 0.1664 | 1.0000 | 0.2672 | 0.3484 | -0.3512 | -0.0084 | -0.0114 | -0.0265 | -0.0253 |
| $\angle p_1$ | 0.5814 | 0.2672 | 1.0000 | -0.0159 | -0.3130 | -0.0018 | -0.0093 | -0.0094 | -0.0030 |
| $\angle p_2$ | -0.0723 | 0.3484 | -0.0159 | 1.0000 | -0.5111 | 0.0004 | -0.0109 | -0.0333 | -0.0320 |
| $u_0$ | -0.6476 | -0.3512 | -0.3130 | -0.5111 | 1.0000 | -0.0200 | 0.0034 | 0.0459 | 0.0437 |
| $\mathrm{Re}\{H_1\}$ | 0.0072 | -0.0084 | -0.0018 | 0.0004 | -0.0200 | 1.0000 | 0.9316 | -0.0235 | -0.2262 |
| $\mathrm{Re}\{H_2\}$ | -0.0051 | -0.0114 | -0.0093 | -0.0109 | 0.0034 | 0.9316 | 1.0000 | 0.1868 | -0.0166 |
| $\mathrm{Im}\{H_1\}$ | -0.0141 | -0.0265 | -0.0094 | -0.0333 | 0.0459 | -0.0235 | 0.1868 | 1.0000 | 0.9343 |
| $\mathrm{Im}\{H_1\}$ | -0.0077 | -0.0253 | -0.0030 | -0.0320 | 0.0437 | -0.2262 | -0.0166 | 0.9343 | 1.0000 |

## Correlation Matrix between Parameters (CM6)

| $\rho$ | $|p_1|$ | $|p_2|$ | $\angle p_1$ | $\angle p_2$ | $u_0$ | $\mathrm{Re}\{H_1\}$ | $\mathrm{Re}\{H_2\}$ | $\mathrm{Im}\{H_1\}$ | $\mathrm{Im}\{H_1\}$ |
|---|---|---|---|---|---|---|---|---|---|
| $|p_1|$ | 1.0000 | 0.4977 | 0.2279 | 0.2618 | -0.7665 | 0.0130 | 0.0049 | 0.0031 | -0.0088 |
| $|p_2|$ | 0.4977 | 1.0000 | 0.1639 | 0.4577 | -0.6511 | -0.0066 | -0.0083 | -0.0030 | 0.0012 |
| $\angle p_1$ | 0.2279 | 0.1639 | 1.0000 | 0.3925 | -0.1655 | -0.0041 | -0.0083 | -0.0063 | 0.0075 |
| $\angle p_2$ | 0.2618 | 0.4577 | 0.3925 | 1.0000 | -0.5114 | 0.0053 | -0.0032 | 0.0010 | 0.0081 |
| $u_0$ | -0.7665 | -0.6511 | -0.1655 | -0.5114 | 1.0000 | -0.0070 | -0.0078 | -0.0056 | 0.0027 |
| $\mathrm{Re}\{H_1\}$ | 0.0130 | -0.0066 | -0.0041 | 0.0053 | -0.0070 | 1.0000 | 0.6774 | -0.0024 | -0.5027 |
| $\mathrm{Re}\{H_2\}$ | 0.0049 | -0.0083 | -0.0083 | -0.0032 | -0.0078 | 0.6774 | 1.0000 | 0.5245 | 0.0229 |
| $\mathrm{Im}\{H_1\}$ | 0.0031 | -0.0030 | -0.0063 | 0.0010 | -0.0056 | -0.0024 | 0.5245 | 1.0000 | 0.6959 |
| $\mathrm{Im}\{H_1\}$ | -0.0088 | 0.0012 | 0.0075 | 0.0081 | 0.0027 | -0.5027 | 0.0229 | 0.6959 | 1.0000 |

Correlation Matrix between Parameters (CM7)

| $\rho$ | $|p_1|$ | $|p_2|$ | $\angle p_1$ | $\angle p_2$ | $u_0$ | $\mathrm{Re}\{H_1\}$ | $\mathrm{Re}\{H_2\}$ | $\mathrm{Im}\{H_1\}$ | $\mathrm{Im}\{H_1\}$ |
|---|---|---|---|---|---|---|---|---|---|
| $|p_1|$ | 1.0000 | -0.1365 | 0.5805 | 0.0175 | -0.6548 | 0.0088 | 0.0065 | -0.0032 | 0.0069 |
| $|p_2|$ | -0.1365 | 1.0000 | -0.1057 | 0.1123 | 0.0069 | -0.0078 | -0.0092 | -0.0069 | -0.0084 |
| $\angle p_1$ | 0.5805 | -0.1057 | 1.0000 | 0.0817 | -0.2639 | 0.0178 | 0.0168 | -0.0081 | -0.0031 |
| $\angle p_2$ | 0.0175 | 0.1123 | 0.0817 | 1.0000 | -0.3768 | -0.0118 | -0.0154 | 0.0034 | 0.0084 |
| $u_0$ | -0.6548 | 0.0069 | -0.2639 | -0.3768 | 1.0000 | -0.0022 | -0.0011 | -0.0053 | -0.0154 |
| $\mathrm{Re}\{H_1\}$ | 0.0088 | -0.0078 | 0.0178 | -0.0118 | -0.0022 | 1.0000 | 0.9434 | -0.0056 | -0.1460 |
| $\mathrm{Re}\{H_2\}$ | 0.0065 | -0.0092 | 0.0168 | -0.0154 | -0.0011 | 0.9434 | 1.0000 | 0.1340 | -0.0048 |
| $\mathrm{Im}\{H_1\}$ | -0.0032 | -0.0069 | -0.0081 | 0.0034 | -0.0053 | -0.0056 | 0.1340 | 1.0000 | 0.9439 |
| $\mathrm{Im}\{H_1\}$ | 0.0069 | -0.0084 | -0.0031 | 0.0084 | -0.0154 | -0.1460 | -0.0048 | 0.9439 | 1.0000 |

Correlation Matrix between Parameters (CM8)

| $\rho$ | $|p_1|$ | $|p_2|$ | $\angle p_1$ | $\angle p_2$ | $u_0$ | $\mathrm{Re}\{H_1\}$ | $\mathrm{Re}\{H_2\}$ | $\mathrm{Im}\{H_1\}$ | $\mathrm{Im}\{H_1\}$ |
|---|---|---|---|---|---|---|---|---|---|
| $|p_1|$ | 1.0000 | 0.1695 | 0.3035 | -0.2795 | -0.6700 | -0.0003 | 0.0015 | 0.0130 | 0.0225 |
| $|p_2|$ | 0.1695 | 1.0000 | 0.3645 | 0.1393 | -0.1736 | -0.0110 | -0.0034 | 0.0165 | 0.0155 |
| $\angle p_1$ | 0.3035 | 0.3645 | 1.0000 | 0.2756 | -0.0400 | 0.0058 | 0.0021 | 0.0031 | 0.0055 |
| $\angle p_2$ | -0.2795 | 0.1393 | 0.2756 | 1.0000 | -0.3812 | 0.0222 | -0.0005 | -0.0041 | -0.0152 |
| $u_0$ | -0.6700 | -0.1736 | -0.0400 | -0.3812 | 1.0000 | -0.0152 | 0.0000 | -0.0094 | -0.0085 |
| $\mathrm{Re}\{H_1\}$ | -0.0003 | -0.0110 | 0.0058 | 0.0222 | -0.0152 | 1.0000 | 0.6108 | 0.0351 | -0.5755 |
| $\mathrm{Re}\{H_2\}$ | 0.0015 | -0.0034 | 0.0021 | -0.0005 | 0.0000 | 0.6108 | 1.0000 | 0.5931 | -0.0163 |
| $\mathrm{Im}\{H_1\}$ | 0.0130 | 0.0165 | 0.0031 | -0.0041 | -0.0094 | 0.0351 | 0.5931 | 1.0000 | 0.5788 |
| $\mathrm{Im}\{H_1\}$ | 0.0225 | 0.0155 | 0.0055 | -0.0152 | -0.0085 | -0.5755 | -0.0163 | 0.5788 | 1.0000 |